

# Investigation of LPIN1 and its Substrate, Phosphatidic Acid, as Modifiers of Niemann-Pick Type C disease

by  
Liam Sargison

A thesis submitted to the Victoria University of Wellington in  
fulfilment of the requirements for the degree of Master of  
Biomedical Science

Victoria University of Wellington

2016

## Abstract

Niemann-Pick type C (NP-C) disease is a neurodegenerative disease with a typically paediatric onset, for which no satisfactory cure is available. Inheritance of two dysfunctional copies of either cholesterol transport gene NPC1 or NPC2 perpetrates substantial accumulation of sterols and secondary lipids within the lysosome, eventuating in devastating and progressive visceral and neurological symptoms. Although the disease is ostensibly monogenic, there is an impressive diversity among sufferers of the disease in regards to onset of disease, specific symptoms imposed and prognosis. Recently, genetic modifiers of the NP-C disease have been reported in several models, which have improved understanding of the disease and identified new targets for treatment. Accordingly, the relevance of the LPIN1 gene and the phosphatidic acid phosphatase activity of its enzyme, were investigated for their ability to modify the NP-C phenotype in a fibroblast and mouse model. Treatment of NP-C fibroblasts with inhibition of phosphatidic acid-generating enzymes DGK and PLD was ineffective in reducing the lysosomal accumulation of cholesterol. Likewise, *Npc1<sup>-/-</sup>Lpin1<sup>-/-</sup>* mice were largely indistinguishable from *Npc1<sup>-/-</sup>*, *Lpin1<sup>-/-</sup>* and wild-type mice at P0 for brain and liver lipid profiles, cerebellar histology and liver autophagy.

## **Acknowledgements**

Foremost, Dr Andrew Munkacsi, thank you so much for giving me such a diverse and interesting project. I will always be grateful. Dr Peter Pfeffer, your advice shaped this project in a big way, and I regret not getting more of your advice. Dr Karen Reue, thanks for sending those mice from all the way across the Pacific. I couldn't have done it without them. Thanks to all the awesome people at Chemgen and throughout the school, it's been a great time. Natalie Hammond, at least half of my thesis is based in what you taught me, I am extremely grateful. Rosemary Heathcott, for getting me started in tissue culture, thank you. Dinidu Senanayake thanks for teaching me how to OPERA, and for all your sage advice. Rosine Cyuzuzo, thanks for helping me look after the mice, and for giving me tips about the microtome. Mum and Dad, thanks for being so caring, supportive, and interested. Thank you for growing me up capable of achieving this. Love you. and Mint, thank you for being the light at the end of this tunnel.

# Table of Contents

<b>Abstract</b>	1
<b>Acknowledgements</b>	2
<b>Table of Contents</b>	3
<b>List of Figures</b>	6
<b>List of Tables</b>	8
<b>Abbreviations</b>	9
<b>Chapter 1. Literature Review</b>	12
1.1 Niemann-Pick type C disease.....	12
1.1.1 History and classification.....	12
1.1.2 Clinical progression.....	14
1.1.3 Diagnosis.....	17
1.1.4 Molecular basis.....	19
1.1.5 Cholesterol homeostasis.....	20
1.1.6 Biochemical basis.....	21
1.2 Autophagy.....	22
1.3 Pharmacological modifiers.....	25
1.4 Genetic modifiers.....	26
1.4.1 Modifiers identified in mammalian cells.....	26
1.4.2 Modifiers identified in yeast cells.....	27
1.4.3 Lipin genes as candidate modifiers of NPC disease.....	28
1.5 Aims and hypotheses.....	30
<b>Chapter 2. Investigation of the therapeutic efficacy of targeting lipin to treat NPC disease</b>	<b>31</b>
2.1 Introduction.....	31
2.2 Methods.....	32
2.2.1 Mammalian tissue culture.....	32
2.2.2.1 Inhibition of DGK and PLD in fibroblasts.....	32

2.2.2.2 Filipin staining of unesterified cholesterol.....	32
2.2.2.3 OPERA imaging.....	33
2.2.2.4 Cell Profiler filipin quantification.....	33
2.2.2.4.1 Image conversion.....	33
2.2.2.4.2 Cell Profiler pipeline.....	33
2.2.3 Mouse Husbandry .....	36
2.2.4 Genotype determination.....	37
2.2.5 Weights.....	40
2.2.6 Collection of neonatal tissue.....	40
2.2.7 Western blot analysis.....	40
2.2.7.1 Protein extraction.....	40
2.2.7.2 Protein quantification.....	41
2.2.7.3 Protein Preparation and denaturation.....	41
2.2.7.4 SDS-PAGE electrophoresis.....	42
2.2.7.5 Membrane transfer.....	43
2.2.7.6 LC3 membrane probing.....	43
2.2.7.7 Actin membrane probing.....	43
2.2.7.8 Imaging and analysis.....	44
2.2.8 Histology.....	44
2.2.8.1 Tissue processing.....	44
2.2.8.2 Embedding.....	45
2.2.8.3 Microtome.....	46
2.2.8.4 Hematoxylin and Eosin staining.....	46
2.2.6 Lipid extraction.....	46

2.2.7 Lipidomic analysis.....	47
2.2.9 Statistical analyses.....	49
2.3 Results.....	50
2.3.1 Inhibition of diacylglycerol kinase does not ameliorate accumulation of unesterified cholesterol in NPC patient fibroblasts.....	50
2.3.2 Inhibition of phospholipase D does not ameliorate accumulation of unesterified cholesterol in NPC patient fibroblasts.....	52
2.3.3 <i>Npc1</i> <sup>-/-</sup> <i>Lpin1</i> <sup>-/-</sup> mice were generated by crossing <i>Npc1</i> <sup>+/-</sup> and <i>Lpin1</i> <sup>+/-</sup> mice.....	54
2.3.4 <i>Npc1</i> <sup>-/-</sup> <i>Lpin1</i> <sup>-/-</sup> mice are recovered at expected Mendelian ratios.....	56
2.3.4.1 Effect of <i>Npc1</i> <sup>-/-</sup> and <i>Lpin1</i> <sup>-/-</sup> conditions on birth weight.....	57
2.3.5 Autophagy is not disrupted in <i>Npc1</i> <sup>-/-</sup> <i>Lpin1</i> <sup>-/-</sup> mice.....	58
2.3.6 Brain pathology is not disrupted in <i>Npc1</i> <sup>-/-</sup> <i>Lpin1</i> <sup>-/-</sup> mice.....	61
2.3.7 Sterol homeostasis in the liver of <i>Npc1</i> <sup>-/-</sup> <i>Lpin1</i> <sup>-/-</sup> mice mimics the <i>Npc1</i> <sup>-/-</sup> mouse.....	63
2.3.8 Sterol homeostasis in the brain of <i>Npc1</i> <sup>-/-</sup> <i>Lpin1</i> <sup>-/-</sup> mice is indistinguishable from <i>Npc1</i> <sup>-/-</sup> and <i>Lpin1</i> <sup>-/-</sup> mice.....	65
2.3.9 Sphingolipid homeostasis is not altered by <i>Lpin1</i> deletion in <i>Npc1</i> <sup>-/-</sup> mice in the liver...67	
2.3.10 Sphingolipid homeostasis is not altered by <i>Lpin1</i> deletion in <i>Npc1</i> <sup>-/-</sup> mice in the brain.71	
2.3.11 Phospholipid homeostasis is regulated unexpectedly in the liver of <i>Npc1</i> <sup>-/-</sup> <i>Lpin1</i> <sup>-/-</sup> mice .....	76
2.3.12 Phospholipid homeostasis (is/is not) disrupted in the brain of <i>Npc1</i> <sup>-/-</sup> <i>Lpin1</i> <sup>-/-</sup> mice.....	84
2.5 Discussion.....	92

## Chapter 3. References

96

## List of Figures

Figure 1: A French cohort of NP-C patients.....	16
Figure 2: A breakdown of NP-C disease.....	18
Figure 3: Macroautophagy and endocytosis converge at the amphisome.....	24
Figure 4: The synthetic lethal interaction of <i>ncr1Δ</i> and <i>pah1Δ</i> .....	28
Figure 5: Representative images of fibroblasts under four conditions.....	50
Figure 6: R59022 treatments do not reduce cholesterol storage according to filipin staining. ....	51
Figure 7: Representative images of fibroblasts under four conditions.....	52
Figure 8: FIPI treatments do not reduce cholesterol storage according to filipin staining. ....	53
Figure 9: Amplified bands against 1kb+ ladder. ....	55
Figure 10: <i>Npc1</i> <sup>-/-</sup> mice have a lower birth weight to littermates. ....	57
Figure 11: Bulk LC3 levels not influenced by genotype. ....	59
Figure 12: Cerebellum is intact in <i>Npc1</i> <sup>-/-</sup> <i>Lpin1</i> <sup>-/-</sup> mouse.....	60
Figure 13: Free cholesterol is increased in <i>NPC1</i> <sup>-/-</sup> and <i>NPC1</i> <sup>-/-</sup> <i>LPIN1</i> <sup>-/-</sup> mouse liver.....	62
Figure 14: Cholesterol-ester is reduced in <i>NPC1</i> <sup>-/-</sup> and <i>NPC1</i> <sup>-/-</sup> <i>LPIN1</i> <sup>-/-</sup> mouse liver.....	63
Figure 15: Free cholesterol abundance in mouse brain is unaffected by deletion of <i>NPC1</i> and <i>LPIN1</i> .....	64
Figure 16: Cholesterol-ester is reduced in <i>NPC1</i> <sup>-/-</sup> and <i>LPIN1</i> <sup>-/-</sup> mice.....	65
Figure 17: Among sphingolipids, LacCer increases 15-fold in the <i>NPC1</i> <sup>-/-</sup> mouse liver. ....	66
Figure 18: Deletion of <i>LPIN1</i> <sup>-/-</sup> in mouse does not modify liver sphingolipid profile. ....	67
Figure 19: Among sphingolipids, LacCer is increased 15-fold in the <i>NPC1</i> <sup>-/-</sup> <i>LPIN1</i> <sup>-/-</sup> mouse liver.....	68
Figure 20: Loss of <i>Npc1</i> results in 15-fold increase in LacCer in mouse liver, <i>Lpin1</i> loss does not modify lactosylceramide profile.....	69

Figure 21: Sphingolipid profile not significantly altered by loss of <i>Npc1</i> in mouse brain.....	70
Figure 22: Among sphingolipids, sulfatide is modestly reduced in the <i>Lpin1</i> <sup>-/-</sup> mouse brain.....	71
Figure 23: SM and MhCer increased in <i>Npc1</i> <sup>-/-</sup> <i>Lpin1</i> <sup>-/-</sup> mouse brain.....	72
Figure 24: MhCer accumulates in the <i>Npc1</i> <sup>-/-</sup> <i>Lpin1</i> <sup>-/-</sup> mouse brain. ....	73
Figure 25: LacCer accumulates with loss of <i>Npc1</i> , which is not modified by loss of <i>Lpin1</i> in mouse brain.....	74
Figure 26: PS and PG reduced in <i>Npc1</i> <sup>-/-</sup> mouse liver.....	75
Figure 27: Abundance of investigated phospholipids unaltered by deletion of <i>Lpin1</i> in mouse liver.....	76
Figure 28: PE and PG reduced in <i>Npc1</i> <sup>-/-</sup> <i>Lpin1</i> <sup>-/-</sup> mouse liver. ....	77
Figure 29: Mouse liver profile of PE and variations.....	78
Figure 30: Mouse liver profile of PC and variations. ....	79
Figure 31: Mouse liver profile of PS and variations. ....	80
Figure 32: Mouse liver profile of PI and LPI. ....	81
Figure 33: Mouse liver profile of PG and variations.....	82
Figure 34: Phospholipid profile of <i>Npc1</i> <sup>-/-</sup> mouse brain similar to wild-type.....	83
Figure 35: Measured phospholipids not affected by deletion of <i>Lpin1</i> in mouse brain.....	84
Figure 36: PI reduced in <i>Npc1</i> <sup>-/-</sup> <i>Lpin1</i> <sup>-/-</sup> mouse brain.....	85
Figure 37: Mouse brain profile of PE and variations.....	85
Figure 38: Mouse brain profile of PC and variations.....	86
Figure 39: Mouse brain profile of PS and variations.....	87
Figure 40: Mouse brain profile of PI and LPI.....	88
Figure 41: Profile of PG and variations.....	89



## List of tables

Table 1: Cell profiler pipeline.....	34
Table 2: Possible breeding outcomes from crossing mice heterozygous for both deletion alleles.....	37
Table 3: Primers used for mouse genotypes.....	38
Table 4: PCR reaction reagents.....	38
Table 5: Cycling conditions used for all PCRs.....	39
Table 6: Protein denaturation reagents.....	41
Table 7: 15% separating gel.....	42
Table 8: 4% stacking gel.....	42
Table 9: Tissue processor protocol.....	45
Table 10: Staining procedure for H&E histology.....	46
Table 11: Standards used in lipidomic analysis.....	48
Table 12: Chi squared test: Pup genotype ratios.....	56

## Abbreviations

AC	Acyl Carnitine
AcylPG	Acyl Phosphatidylglycerol
AKT	Protein Kinase B
APS	Ammonium Persulfate
ATG	Autophagy Gene
BBB	Blood Brain Barrier
BCA	Bicinchoninic Acid
BMP	Bis(monoacylglycero)phosphate
CE	Cholesterol Ester
Cer	Ceramide
CST	Sulfatide Synthesis Enzyme
DG	Diacylglycerol
dhCer	Dihydroceramide
dhSM	Dihydrosphingomyelin
DKO	Double Knock Out
DMEM	Dulbecco's Minimum Essential Media
DMSO	Dimethyl Sulfoxide
EAF1	ELL-Associated Factor 1
ER	Endoplasmic Reticulum
FC	Free Cholesterol
FFA	Free Fatty Acid
GB3	Globotriaosylceramide
GM2	Disialotetrahexosylganglioside
GM3	Monosialodihexosylganglioside
HDAC	Histone deacetylase
HMG-R	HMG-CoA reductase
HPB-CD	Hydroxypropyl- $\beta$ -cyclodextrin
HPLC	High Performance Liquid Chromatography

INSIG1	Insulin induced gene 1
KO	Knock-out
LacCer	Lactosylceramide
LacCer	Lactosylceramide
LC3-I	Light Chain 3
LDL	Low Density Lipoprotein
LPC	Lysophosphatidylcholine
LPCE	Ether lysophosphatidylcholine
LPE	Lysophosphatidylethanolamine
LPep	Plasmogen Lysophosphatidylethanolamine
LPI	Lysophosphatidylinositol
LPS	Lysophosphatidylserine
MAPT	Microtubule-Associated Protein Tau
MG	Monoacylglycerol
MHCer	Monohexosylceramide
mTOR	Mechanistic Target Of Rapamycin
NAPE	N-Acyl Phosphatidylethanolamine
NAPS	N-Acyl Phosphatidylserine
NP-C	Niemann-Pick type C
NSer	N-Acyl Serine
P0	0 days post-partum
P14	14 days post-patum
PA	Phosphatidic acid
PAH1	Phosphatidic Acid Hydrolase
PAP	Phosphatidic Acid Phosphatase
PBS	Phosphate Buffered Saline
PC	Phosphatidylcholine
PCe	Ether phosphatidylcholine
PCR	Polymerase Chain Reaction
PE	Phosphatidylethanolamine

PEp	Plasmalogen phosphatidylethanolamine
PFA	Paraformaldehyde
PG	Phosphatidylglycerol
PI	Phosphatidylinositol
PLD	Phospholipase D
PPAR $\alpha$	Peroxisome Proliferator-Activated Receptor Alpha
PS	Phosphatidylserine
PVDF	Polyvinylidene Difluoride
RAB9	Ras-related protein 9
RIPA buffer	Radioimmunoprecipitation Assay Buffer
rTth	Thermus thermophilus
S1P	Sphingosine-1-Phosphate
S2P	Sphingosine-2-Phosphate
SAHA	Suberoylanilide Hydroxamic Acid
SCAP	SREBP cleavage activating protein
SDS	Sodium dodecyl sulfate
SM	Sphingomyelin
SNARE	SNAP receptor
SRE	Sterol Regulatory Element
SREBP	Sterol regulatory element-binding protein
Sulf	Sulfatide
TAG	Triacylglycerol
TEMED	Tetramethylethylenediamine
VSGP	Vertical Supranuclear Gaze Palsy
WT	Wild-Type

## **Chapter 1. Literature Review**

### **1.1 Niemann-Pick type C disease**

#### **1.1.1 History and classification**

Albert Niemann first observed and described symptoms of hepatosplenomegaly in an infant in 1914, and this infant succumbed to neurodegeneration at 18 months of age. In the 1920's, Niemann and prolific histologist Ludwig Pick studied this patient and associated symptoms in greater breadth and detail, and provided distinctions from Gaucher's Disease, another lysosome storage disease with similar manifestations. The eponym 'Niemann-Pick Disease' is used in recognition of these seminal studies.

In 1934, sphingomyelin was identified as a notable lipid accumulation in the liver of Niemann-Pick Disease sufferers (Brady, Kanfer, Mock, & Fredrickson, 1966). In 1958, Niemann-Pick Disease was categorised into four types: A,B,C and D (Crocker, 1961). All forms of this disease could be characterised by sphingomyelin accumulation and presence of foam cells, however age of onset and severity of symptoms regarding the central nervous system were variable. More specifically, sphingomyelinase deficiency was identified in 1966 as the cause of Niemann-Pick type A, the classic infantile form of Niemann-Pick disease (Brady et al., 1966). In 1991, the clinically distinct Niemann-Pick type B was also found to be the result of a dysfunctional sphingomyelinase gene. Intermediate forms of Niemann-Pick type A and B, named types E and F, have also been proposed from exiguous cases (Schneider, Pentchev, Hibbert, Sawitsky, & Brady, 1978; Terry, Sperry, & Brodoff, 1954). These forms, disparate in presentation, also arise from deficiency in the sphingomyelin cleavage gene, but are clinically distinct from Niemann-Pick types C and D.

In 1979, Roscoe Brady at the National Institutes of Health received tissue from a mouse colony with a recessive lipid storage disorder (Peter G Pentchev, 2004). Investigating these tissues and finding lipid and enzyme anomalies resembling human Gaucher and Niemann-Pick

Diseases, there was hope to use these mice as a model to elucidate some therapy for the better characterised Niemann-Pick type A. In 1984, these mice, when fed a high cholesterol diet, were found to have livers with a lysosomal accumulation of unesterified cholesterol. Ensuing enzymology of these mice and their cultured fibroblasts found accumulation that was not the result of reduced activity of cholesterol esterification by acyl-CoA cholesterol acyltransferase and was thus expected to be irregular storage of the sterol in the lysosome (P. G. Pentchev et al., 1984).

By comparing the lipid profile of these mice to repositories of human cell lines of various lipidoses, Pentchev and colleagues were able to identify human Niemann-Pick type C disease as most resembling the cholesterol storage phenotype of this murine disorder (P G Pentchev et al., 1986; P G Pentchev et al., 1985). Human chromosome 18, when introduced to these mice, corrected their cholesterol build-up, suggesting the location of a gene responsible for Niemann-Pick type C disease (Kurimasa, Ohno, & Oshimura, 1993). Subsequent positional cloning refined the location of the gene from chromosome-wide to within a 1 centimorgan area (Carstea et al., 1993). Here the Niemann-Pick type C gene (*NPC1*) was finally identified by positional cloning methods (Carstea et al., 1997; Gu et al., 1997). With this finding, Niemann-Pick type C (NP-C) was confirmed to be genetically distinct from types A and B. The *Npc1*<sup>-/-</sup> mouse model, so indispensable in these discoveries, remains useful and relevant in the study of NP-C disease, alongside the more recently developed missense mutant *Npc1*<sup>nmf164</sup> mouse model (M. E. Lopez, Klein, Dimbil, & Scott, 2011; Maue et al., 2012).

The Nova Scotian form of Niemann Pick Disease (Niemann-Pick type D) is notable for being reported exclusively in the direct descendants of the Nova Scotian couple Joseph and Marie Muise born in 1679 and 1684, respectively (Winsor & Welch, 1978). In 1998, Niemann-Pick type D was found to be caused by a non-synonymous point mutation in *NPC1*, reclassifying the disease as an allelic variant of NP-C disease (Greer et al., 1998).

During the hunt for the gene underlying Niemann-Pick type C disease, somatic cell hybridisation experiments in patient fibroblasts identified a minor group of NP-C cases to which the disease-causing mutation did not map to the 18<sup>th</sup> chromosome. This observation indicated that two genes that might be individually capable of imparting NP-C disease (Vanier, Duthel, Rodriguez-Lafrasse, Pentchev, & Carstea, 1996). This alternative agent for NP-C was identified in 2000 in the *HEI* gene, now more frequently referred to as *NPC2* (Naureckiene et al., 2000). Niemann-Pick type C disease can therefore be sub-categorised by its genetic origin (*i.e.*, mutations in *NPC1* or *NPC2*). As *NPC1* mutations constitute ~95% of NP-C cases, this is the primary focus of this rare disease (Vanier, 2010).

### **1.1.2 Clinical progression**

It is an unfortunate fact that in most countries a considerable portion of early victims of NP-C disease are undiagnosed or misdiagnosed, therefore it is difficult to accurately predict the true incidence of the disease. Considering varied estimates from reported cases in Australia (Meikle, Hopwood, Clague, & Carey, 1999) and multiple Western European Countries (Pinto et al., 2004; Vanier & Millat, 2003), a minimal incidence of 1 per 120,000 live births has been suggested (Vanier, 2010). Two founder effect situations have been identified in North America of populations with atypical incidence of NP-C disease, one being the aforementioned Nova Scotian isolate (Greer et al., 1998) and the other located in Southern Colorado (Millat et al., 1999).

Although the median age of onset in NP-C disease is below ten years of age (Meikle et al., 1999), the disease has a variable age of onset, leading professionals to designate four forms of NP-C disease based on age of onset. These are Early Infantile (from neonatal to 2 years old), Late Infantile (from 2-6 years old), Juvenile (from 6-15 years old), and Adolescent/Adult (greater than 15 years old) (Vanier, 2010).

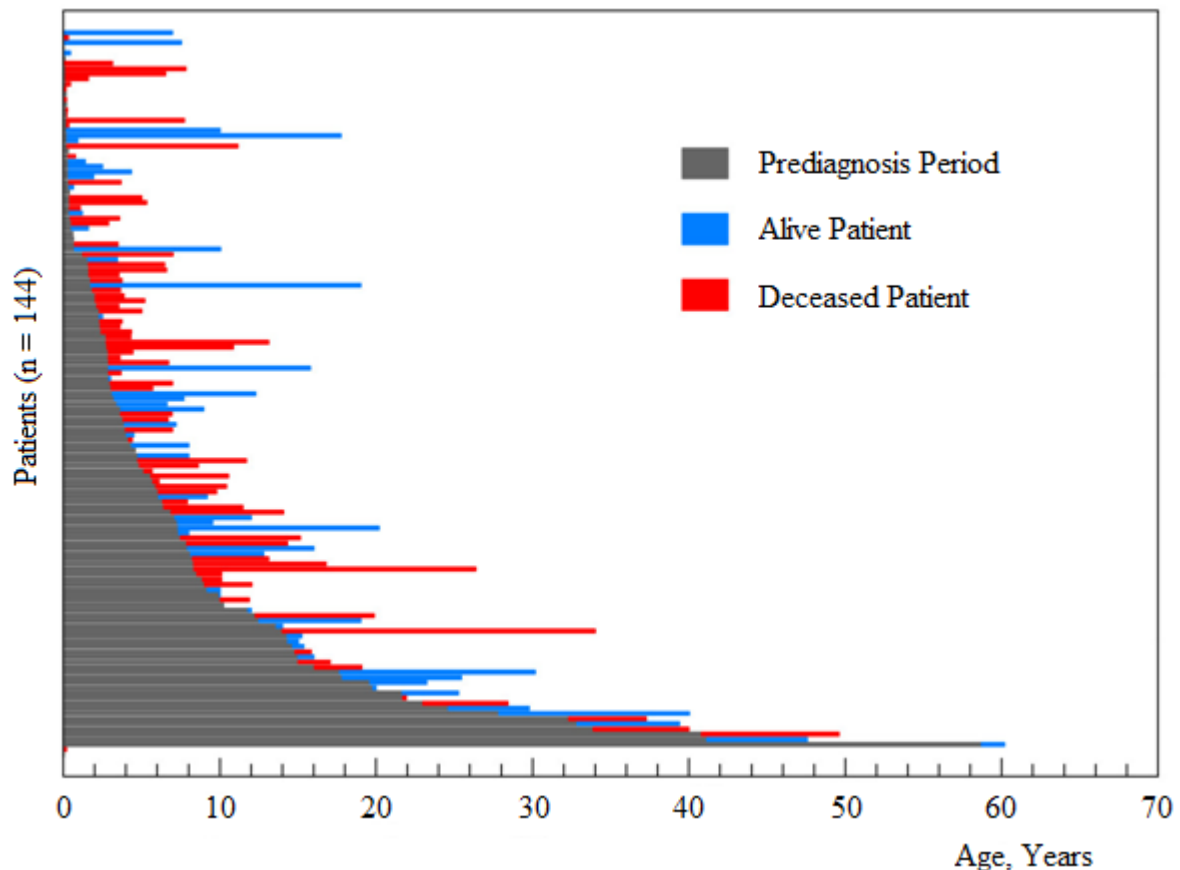


**Figure 1:** A French cohort of NP-C patients, revealing the diversity in age of onset and prognosis after diagnosis. Figure adapted from Vanier (2010).

The age of onset affects which symptoms are likely to present as well as which organs are most severely afflicted. The younger the age of onset, the more severe the defect in the spleen and liver. Neonatal NP-C sufferers experience symptoms unique to their age group such as fetalis and ascites (Surmeli-Onay et al., 2013). Early Infantile patients are typically checked in to the hospital with jaundice and often not immediately diagnosed. The prognosis for these individuals is poor; it is rare for patients to survive beyond 5 years of age and often perish in a matter of months (R. Yang et al., 2015).

Late infantile cases also present first with hepatosplenomegaly or splenomegaly. Neurologic involvement of the disease is seen in language delays and ataxia that results in clumsiness and dysphagia, which usually progresses until gastrostomy is necessary. In many

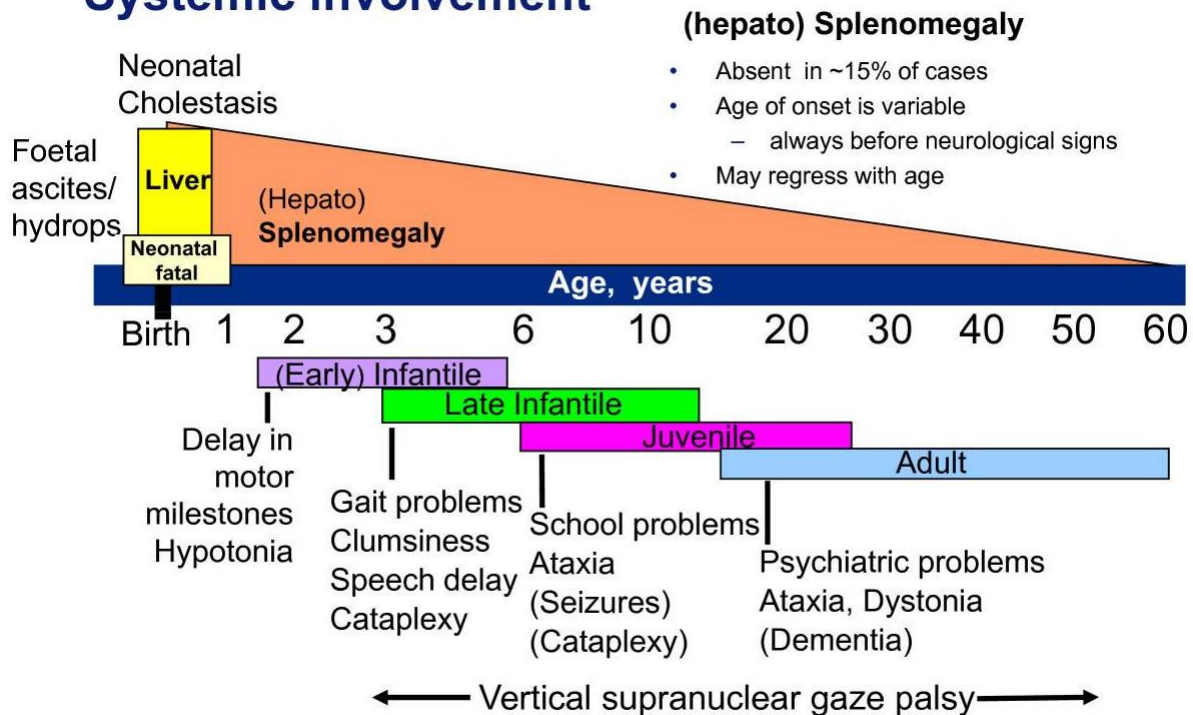


cases, seizures are experienced of which the severity varies. The majority of these individuals will not live into their teenage years (Imrie, Heptinstall, Knight, & Strong, 2015).

In the juvenile period, patients tend not to experience hepatomegaly, rather just an enlargement of the spleen, this is often less pronounced than in earlier onset NP-C, and may resolve somewhat before any onset of neurological symptoms. In fact, a minority of juvenile onset patients lack detectible organomegaly. One of the most regular neurological symptoms is Vertical Supranuclear Gaze Palsy (VSGP), which is an inability to vertically rotate the eyes to shift gaze, instead the individual must resort to adjustment of the entire head (Solomon, Winkelman, Zee, Gray, & Büttner-Ennever, 2005). Other symptoms include cataplexy, which may involve narcolepsy, and subtler presentations such as attention issues and trouble with writing. Individuals suffer seizures as well as progressive dysphagia and dysarthria, as in late infantile cases. The lifespan of these individuals is varied, and some will live until their 30s (Wraith et al., 2009).

In many cases of adolescent and adult onset of NP-C disease, splenomegaly is minor or undetectable. Symptoms of juvenile onset patients are generally experienced by adult onset individuals as well, however often present in a milder form (Vanier, 2010). From onset of neurological and psychiatric symptoms, disease development may be gradual, but is often rapid (Anheim et al., 2014). Formal diagnosis is often preceded with a swathe of psychiatric upsets such as paranoid delusions, hallucinations (auditory or visual), and occasionally bipolar disorder or obsessive compulsive disorders (Wouters, De Meirleir, Campforts, & Lampo, 2014). The development, rarity and red herring symptoms suggest that this form of NP-C disease is underreported. Further complicating matters, there have been three instances where individuals over the age of 50 have been diagnosed with a purely visceral-manifesting form of NP-C disease (Dvorakova et al., 2006). These cases are striking as their symptoms are antipodal to the typical phenotype of their age group.

## Systemic involvement



## Neurological involvement

**Figure 2:** Age of onset can be segmented into 5 categories, for each of which symptoms vary in incidence and severity. NP-C symptoms are described as systemic, neurological and psychiatric, and the involvement of these forms generally shifts with age of onset. Adapted from Vanier (2010).

### 1.1.3 Diagnosis

Due to the diverse nature of NP-C disease and the plethora of other diseases that share symptoms, diagnosis of NP-C can be challenging and protracted. A recently developed diagnosis tool is the NP-C Suspicion Index (Patterson et al., 2012; Wijburg et al., 2012). The index was developed by retrospective examination of both confirmed NP-C patients, as well as individuals confirmed not to have NP-C while displaying some common symptoms associated with NP-C disease. The index is a system where symptoms from three categories (visceral, neurological and psychiatric) are assigned a point score based on their correlation to NP-C disease. This is a useful tool for healthcare providers to decide the likelihood their patient

has NP-C disease and thus request the appropriate follow-up for further diagnosis. If a patient scores low on the Suspicion Index, then other potential diseases should be eliminated as possibilities.

Filipin, a fluorescent stain that binds unesterified cholesterol, is the current gold standard for the diagnosis of NP-C disease. It was first used in NP-C cells in 1986 (Kruth et al., 1986). NP-C patient fibroblasts stained with filipin reveal brightly fluorescing vesicles, mostly clustered around the nucleus (Vanier & Latour, 2015). Of NP-C cases investigated, 85% will show the classical form of NP-C and exhibit a classical filipin phenotype for NP-C. However some cases of NP-C disease will not show this “classical” phenotype, and may present an “intermediate” or “variant” phenotype, which may be more difficult to declare as NP-C positive. These “intermediate” and “variant” forms are correlated with specific NP-C alleles, including when these exist as compound heterozygotes with “classical” NP-C alleles (Millat et al., 2001; Sun et al., 2001). This heterogeneity in accumulation of unesterified cholesterol reflects the broad spectrums of onset, symptoms and prognosis in this disease.

Confoundingly, there are some reports of other diseases giving a positive result for the filipin test. MEGDEL syndrome, Smith-Lemli-Optiz syndrome and Tangier disease all have been reported to produce cholesterol profiles that may be interpreted as “variant” forms of NP-C (Platt et al., 2014; Sechi et al., 2014; Wortmann et al., 2012). To affirm a filipin diagnosis (especially for non-classical presentation), other assays are available. An assay for the rate of LDL-induced cholesterol esterification in NPC patient fibroblasts is a common supporting test (Wraith et al., 2009). Light microscope examination of liver biopsy is a historic, highly documented technique, although distinguishing NP-C from other lipidoses can be problematic (Elleder et al., 1984). Given there are potential caveats in each diagnostic tool, DNA sequencing of NPC1 and NPC2 should be the final test when there is strong evidence that a patient has NP-C disease (Alobaidy, 2015).

Antenatal diagnosis can be achieved for pregnancies in families with a history of NP-C. Amniocentesis and chorionic villus sampling have both been successfully used to acquire samples for filipin analysis, of which the latter method is recommended. Successful diagnosis relies on the foetus displaying a classical filipin phenotype, which means 15-20% of fetal NP-C cases will be missed by this diagnosis (Vanier et al., 1992; Wraith et al., 2009).

#### **1.1.4 Molecular basis**

The NPC1 protein is encoded by the *NPC1* gene on chromosome 18 (Carstea et al., 1997). The 1278-amino acid protein consists of 13 transmembrane helices which span membranes of lysosomes or late endosomes (Higgins, Davies, Chen, & Ioannou, 1999). The protein contains a sterol-sensing domain with homology to domains in HMG-R and SREBP Cleavage Activating Protein (SCAP), two important cholesterol homeostatic proteins (Davies & Ioannou, 2000). The N-terminal domain of the protein binds cholesterol with high affinity (Infante et al., 2008).

The *NPC2* gene, also known as *HE1*, exists on chromosome 14, and encodes a much smaller protein of 132 amino acids that resides in the lumen of the late endosome/lysosome (Naureckiene et al., 2000). NPC2 also binds cholesterol but in the reverse origin: while NPC1 binds the 3-hydroxyl end of the cholesterol molecule, NPC2 binds to the isooctyl side chain portion of cholesterol (Kwon et al., 2009).

Murine gene deletion studies of *NPC1* and *NPC2* indicated these two proteins have a non-redundant and cooperative function. Indeed, NPC1 and NPC2 proteins bind cholesterol from opposite orientation for the direct passing of the ligand from one protein to the other, with NPC2 collecting cholesterol from the lysosomal lumen, handing it off to NPC1, and NPC1 transporting cholesterol across the membrane (Kwon et al., 2009; Sleat et al., 2004).

#### **1.1.5 Cholesterol homeostasis**

Core to the regulation of intracellular cholesterol management are the Sterol Regulatory Element Binding Proteins encoded by *SREBP1* and *SREBP2*. Inactive SREBPs reside in the membrane of the endoplasmic reticulum. However the N-terminal domain, if cleaved from the rest of the protein, will translocate to the nucleus, and by binding to specific Sterol Regulatory Element (SRE) sequences, will behave as a transcription factor for a multitude of genes responsible for cholesterol synthesis and cellular endocytosis of cholesterol (J. M. Lopez, Bennett, Sanchez, Rosenfeld, & Osborne, 1996; Sato et al., 1994; Shimano et al., 1996; X. Wang, Sato, Brown, Hua, & Goldstein, 1994; J. Yang, Sato, Goldstein, & Brown, 1994). This liberation of the transcription factor domain (nuclear SREBP) is achieved by two cleavage events mediated by SCAP, the SREBP Cleavage Activating Protein (Cheng et al., 1999; Sakai et al., 1998). Formation of the SCAP/SREBP complex enables activation of the S1P protease which performs the first cleavage, which bares the second cleavage site, actioned by the S2P protease (Sakai et al., 1998). This SREBP activation process is regulated by cholesterol. ER cholesterol may bind the SCAP/SREBP complex and enable its binding to INSIG1, another membrane-bound protein. This prevents the cleavage events that lead to release of nuclear SREBP (Radhakrishnan, Sun, Kwon, Brown, & Goldstein, 2004). This negative feedback mechanism prevents further cholesterol production when the ER has sufficient cholesterol, and the SCAP/SCREBP inhibition is lost when sterol abundance dwindles.

This cholesterol regulation machinery is dependent on sterol sensing. This end product inhibition is effective regardless of cholesterol origin; whether by cellular uptake of dietary LDL (Low Density Lipoprotein) or cholesterol biosynthesis, SCAP/SREBP activity is kept in check. Loss of function of the sterol sensing domain of SCAP was observed in Chinese Hamster Ovary (CHO) cells and resulted in levels of nuclear SREBP ten times greater than in cell lines capable of regulation (Hua, Nohturfft, Goldstein, & Brown, 1996). In the same year, Shimano and colleagues generated a mouse overexpressing a truncated form of SREBP1a

containing purely the soluble transcription factor (Shimano et al., 1996). These mice experienced a 5-fold increase in hepatic cholesterol production and a 25-fold increase in fatty acid biosynthesis, as this truncated SREBP was immune to any regulation. A consequence of unrelenting transcription of SREBP targeted genes was a two to four-fold increase in liver mass.

NPC1 has an important role in cholesterol homeostasis and is transcriptionally upregulated in cells with inhibited cholesterol biosynthesis or cells cultured in cholesterol deficient media. This was credited to SREBPs binding SRE sequences in the *NPC1* promoter region (Gévry, Schoonjans, Guay, & Murphy, 2008). LDL receptors too are a SREBP regulated agent for the cholesterol management, specifically endocytosis of extracellular LDL. These populate the outer cellular membrane and facilitate endocytosis of LDL units. LDL derived cholesterol will be eventually transported out of the late endosome or lysosome by the NPC1 and NPC2 proteins, or be retained within these organelles (Goldstein & Brown, 1987).

#### **1.1.6 Biochemical basis**

In NP-C disease, loss of function of both copies of either the *NPC1* or *NPC2* gene prevents or severely limits egress of LDL-cholesterol from the late endosome/lysosome. This cholesterol is retained from the rest of the cell and cannot be accessed, and does not interact with the SREBP/SCAP complexes in the ER (P G Pentchev et al., 1987). The consequence of this is LDL-receptors are not downregulated nor biosynthesis of cholesterol is stemmed, and cholesterol accumulates in the late endosome/lysosome. Secondary to this defect, a multitude of other lipid species also accumulate, which vary appreciably between visceral organs and the brain (Vanier, 2015; Vanier & Millat, 2003; Walkley & Vanier, 2009). The specific mechanisms behind non-cholesterol accumulations are not well understood.

In the spleen and liver, unesterified cholesterol accumulation is prominent and detectible even *in utero*. A variety of glycosphingolipids will also accumulate (Vanier, 1983). Interestingly, sphingomyelin accumulation is particularly pronounced in the human spleen, while mice instead accumulate sphingomyelin in the liver (Sleat et al., 2004). Since the human liver experiences a reasonable increase in free sphingoid bases, a higher sphingosine:sphinganine ratio would be expected.

Cholesterol does not accumulate in the brain, however some displacement in cholesterol distribution has been reported with cholesterol accumulating at the central cell soma and being sparse along the axons (Karten, Vance, Campenot, & Vance, 2002). The blood-brain-barrier restricts cholesterol used by the brain to that which is locally synthesised (Morell & Jurevics, 1996), which may limit the degree to which cholesterol might accumulate. Gangliosides GM2 and GM3 accumulate in the brain, and obvious storage of these glycosphingolipids can occur very early in classic and severe forms of the disease (e.g., GM2 and GM3 accumulate slowly from the second year of life in classically presenting individuals (Zervas, Dobrenis, & Walkley, 2001)).

## **1.2 Autophagy**

The lysosome is an organelle central to macroautophagy, and failure of the NPC1 and NPC2 proteins is detrimental to this cellular process. Macroautophagy, usually referred to simply as autophagy, is a broad spectrum system that clears impaired organelles and protein aggregates, as well as a resource scavenger system in starvation conditions (Ravikumar et al., 2010). Autophagy can be driven either by mTOR-dependant or mTOR-independent mechanisms, but in either case a prodigious recruitment and interaction of proteins drive the production of a double-membrane phagophore engulfing targets such as mitochondria and protein aggregates and thus generating an autophagosome (Sarkar, 2013). Cargo encapsulated

within an autophagosome will be degraded by lysosomal fusion. This degradative process can converge with the endosome, where autophagosomes and endosomes pool contents as an amphisome before fusion with the lysosome and degradation of cargo (Berg, Fengsrud, Strømhaug, Berg, & Seglen, 1998; Tooze et al., 1990).

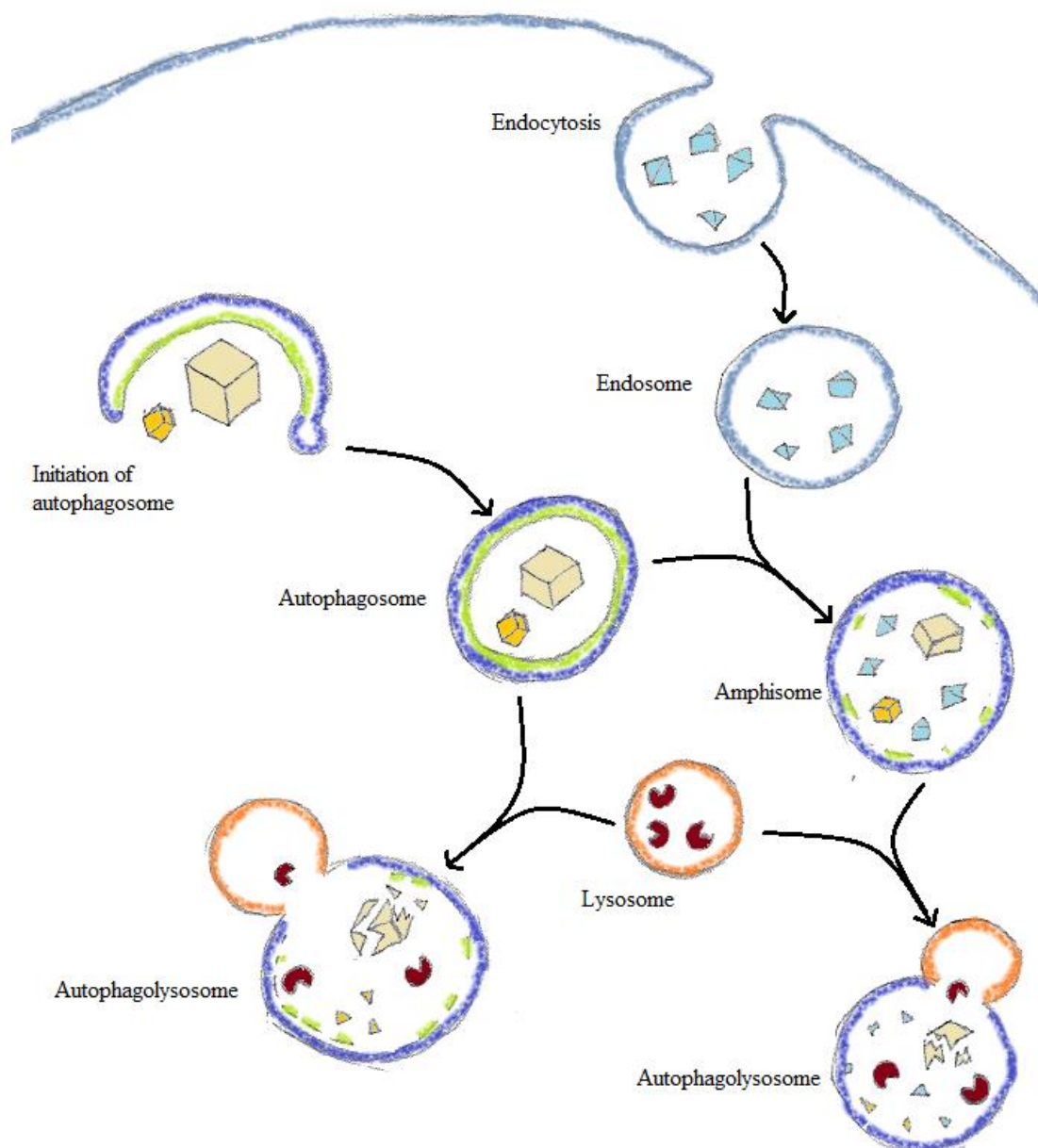


**Figure 3:** Macroautophagy and endocytosis converge at the amphisome. Both intracellular and extracellular cargo is ultimately trafficked to the lysosome for degradation. Adapted from Klionsky *et al.* (2014).

*In vitro* experiments identified autophagy having a key role in free fatty acid (FFA) extraction from lipid droplets (Singh et al., 2009). The inhibition of autophagy reduced markers



for triacylglycerol (TAG) hydrolysis to FFA and also increased levels of cellular TAG storage. Starvation conditions will increase both cellular uptake of TAG via lipid droplets, and lipolysis of TAG to generate FFA to satisfy energy requirements (Finn & Dice, 2006). *In vivo* mouse studies identified that autophagy inhibition results in a dramatic accumulation in TAG in starvation conditions, as upregulated TAG uptake far outstrips hydrolysis.

Autophagy blockage alone induces a progressively neurodegenerative condition in mice, including vulnerability of otherwise healthy neurons to unchecked protein aggregations (Hara et al., 2006). Specifically, Purkinje cells suffer axonal swelling and deterioration when autophagy was prevented by deletion of autophagy gene *ATG7* (Komatsu et al., 2007).

NP-C cells experience an increase in Beclin-1 (mTOR independent) mediated autophagy (Pacheco, Kunkel, & Lieberman, 2007). However autophagy is delayed or flawed resulting in an accumulation of autophagy machinery, there are three current suggestions as to the crux of the issue. Either accumulating lipids are rendering lysosomal proteases ineffective (Elrick & Lieberman, 2013), or that there is a failure in SNARE recruitment, stymieing fusion of the late endosome and the autophagosome (Sarkar et al., 2013). Impaired lysosome function from lipid accumulation has also been associated with cathepsin D levels (Liao et al., 2007). The lysosomal enzyme cathepsin D has been observed to accumulate particularly in cells in the cerebellum, a location primarily affected in NP-C disease. Leakage of cathepsin D and other lysosomal proteins from accumulated autophagic organelles is also expected to be a contributing factor to neural cell death.

### 1.3 Pharmacological modifiers

NP-C currently has no definitive cure as the current pharmacological practice is largely palliative. As dysphagia progresses, NP-C sufferers generally switch to diets of softened, thickened food that is easier to swallow, and commonly gastrostomy when the individual is incapable of swallowing (Patterson et al., 2012). The diverse manifestations of NP-C disease often result in the individual being prescribed an assortment of compounds. Anti-epileptics can be prescribed to control seizures, anticholinergic drugs for dystonia, and tricyclic antidepressants for cataplexy (Alobaidy, 2015).

The glycosphingolipid synthesis inhibitor miglustat has been approved internationally for the treatment of NP-C disease. First approved for Gaucher's disease, miglustat has also been proven to be beneficial in NP-C disease slowing progression of neurological symptoms including dysphagia and deterioration in gait and motor scores (Patterson, Vecchio, Prady, Abel, & Wraith, 2007). This is the first non-palliative pharmacological that has had a positive effect on NP-C patients, in particular the juvenile onset subset. Miglustat has also been shown to stall the onset of neurological symptoms in individuals with exclusively visceral presentation, or those genetically identified before any disease onset (Di Rocco, Dardis, Madeo, Barone, & Fiumara, 2012). Miglustat cannot stall symptoms indefinitely nor will it provide much treatment for the visceral aspects of the disease.

Hydroxypropyl-  $\beta$ -cyclodextrin (HPB-CD) has also been investigated as a potential NP-C therapeutic, with disease progression delayed in mice treated at P7 (Davidson et al., 2009). However, beyond formation of the blood brain barrier (BBB), the therapeutic properties of HPB-CD were reduced. In a phase 0 clinical trial, pharmacokinetic parameters of cyclodextrin were investigated in a 6 year old girl and the treatment was deemed not toxic (Y. Tanaka et al., 2015). Two patients were treated with twice or thrice-weekly infusions of 2 g/kg of HPB-CD,

and these individuals experienced some minor resolution of hepatosplenomegaly and at best transient neurological benefits (Matsuo et al., 2013).

## **1.4 Genetic modifiers**

### **1.4.1 Modifiers identified in mammalian cells**

RAB9, a ras-like GTPase, regulates vesicular transport between the late endosome and the trans Golgi network (Lombardi et al., 1993). It was discovered that overexpression of *RAB9* amplified transport of lactosylceramide (LacCer) in human fibroblasts, and posited as a potential avenue for NP-C treatment (Choudhury et al., 2002). Elsewhere, NP-C patient fibroblasts had been transfected with a telomerase expression vector that drove overexpression of *RAB9*. A striking reversal of the NP-C filipin phenotype was observed in these cells, suggesting a depletion of cholesterol from typically over-laden lysosomes (Walter, Davies, & Ioannou, 2003). *RAB9* overexpression was then shown to increase life expectancy of the *Npc1*<sup>-/-</sup> mouse (Kaptzan et al., 2009).

The microtubule-binding protein tau also imparts a protective role in NP-C, and deletion of the tau gene *MAPT* has a devastating effect on the disease severity of the *Npc1*<sup>-/-</sup> mouse (Pacheco, Elrick, & Lieberman, 2009). Loss of *MAPT* resulted in failure to induce autophagy, as evidenced by reduction in both LC3-I (a cytosolic marker for autophagy induction) and LC3-II (a marker for the autophagosome interior). Furthermore, proteolysis was reduced in *MAPT* siRNA treated fibroblasts (Pacheco et al., 2009).

Likewise, the Protein Kinase B (AKT) serine/threonine kinase had reduced the abundance of the NPC1 protein. *AKT* was identified as an inducer of NPC1 protein degradation, in an investigation of cancer cell lines overexpressing *AKT* (Du et al., 2015). Interestingly, *AKT* upregulates mTOR and mediates the ubiquitination and degradation of the NPC1 protein via the misfolded protein machinery.

### 1.4.2 Modifiers identified in yeast cells

In order to identify genetic modifiers of the *NPC1* gene in an unbiased manner, our group utilised NCR1, the yeast ortholog of *NPC1*. They conducted a genome-wide analysis of 4,800 double deletion mutant strains wherein each strain was deficient for NCR1 and each of 4,800 non-essential genes. These strains were grown both in regular conditions and in an anaerobic environment that disabled the oxygen-dependent process of yeast sterol biosynthesis. It was determined that 13 non-essential genes were synthetic lethal with NCR1 only in the anaerobic condition (Munkacsı et al., 2011). These genes therefore had some role of mitigating the sterol deprivation effect of loss of the NCR1 transporter, which was crucial to survival in a yeast that couldn't manufacture its own sterol. The most notable of these genes to date was EAF1.

Investigation of the histone acetylase EAF1 led to the identification of the histone deacetylase inhibitor drug SAHA (also known as Vorinostat) as a promising candidate for the treatment of NP-C disease. SAHA reduced filipin accumulation and improved LacCer trafficking in NP-C patient fibroblasts (Munkacsı et al., 2011). Currently, clinical trials are underway to determine the efficacy of SAHA in humans.

### 1.4.3 Lipin genes as candidate modifiers of NPC disease

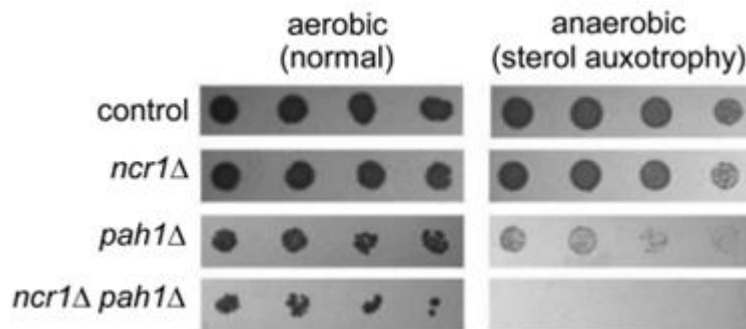


**Figure 4:** The synthetic lethal interaction of *ncr1*Δ and *pah1*Δ is conditional on the yeasts inability to manufacture its own sterol. Figure adapted from Munkacsy *et al.* (2011).

The yeast gene *PAH1* gene was also identified in the aforementioned anaerobic yeast screen. *PAH1* has three human orthologs in *LPIN1*, *LPIN2*, and *LPIN3*. *LPIN1*, as with the *NPC1* gene, was discovered thanks to investigation of a BALB/c mouse strain that had acquired a lipodystrophy. The mutant murine *LPIN1* gene has suffered a rearrangement in the gene, with a significant length of the gene orientated in reverse, with some portion near the rearrangement deleted (Péterfy, Phan, Xu, & Reue, 2001). The *LPIN* proteins are magnesium-dependant phosphatidate phosphatase (PAP1) enzymes that convert phosphatidic acid (PA) to diacylglycerol (DAG) and inorganic phosphate. *LPIN1* is the most potent PAP1 enzyme of the lipins, with about 4 times greater activity than *LPIN2*, and 5 times greater activity than *LPIN3* (Donkor, Sariahmetoglu, Dewald, Brindley, & Reue, 2007). Beyond activity, the three lipins differ in their expression between different organs, with *LPIN1* being the predominant lipin species present in adipose tissue, skeletal muscle, and the brain, *LPIN2* is the major lipin of the cerebellum, and the three lipins are fairly evenly expressed in the liver, kidney and bone (Csaki *et al.*, 2013; Donkor *et al.*, 2007).

Impairment of PAP activity has several implications, but explicitly the accumulation of the enzyme's substrate PA and deficiency of its product DAG. Accumulation of PA in the

murine brain has an adverse effect on both initial myelination in development, as well as for the maintenance of already mature myelin (Nadra et al., 2008). Therefore, PA accumulation will generate a progressive neuropathy, whether myelinating Schwann Cells are in development, or fully matured at onset of PA dysregulation.

To mitigate the lipid imbalance imparted by PAP knockdown, a reciprocal downregulation of enzymes participating in PA metabolism might be considered. The Diacylglycerol Kinase (DGK) enzyme operates antagonistically to PAP enzymes in that it mediates conversion of DAG into PA. Conversely, accumulation of PA can be constrained by inhibition of Phospholipase D (PLD), which catalyses the conversion of Phosphatidylcholine (PC) to PA.

Aside of its PAP activity, Lipin-1 also promotes expression of PPAR $\alpha$ , which plays a key role in liver lipid metabolism (Finck et al., 2006). Nuclear LPIN-1 will inhibit expression of SREBP genes, but when phosphorylated by mTORC1 will not locate to the nucleus (Peterson et al., 2011). *LPIN-1* has also been shown to have a critical role in autophagy of damaged mitochondria, with a deficiency in *LPIN-1* resulting in an increase in irregular and ineffective mitochondria (Zhang, Verity, & Reue, 2014). *LPIN-1* deficient mice treated with statins were seen to suffer a profound myopathy and cellular increases in ceramide, FFA and PA compared to untreated Lipin-1 deficient mice. This is striking as statins, which inhibit cholesterol synthesis pathway enzyme HMG-CoA reductase, seem to induce a similar affect to *NPC1* deficiency.

## 1.5 Aims and hypotheses

Considering the literature and recent research by our group, an interesting relationship has been identified between the yeast NCR1 and PAH1 genes. The overall aim of this thesis is to further test these findings in yeast and determine the relevance of the *LPIN-1* interaction as a therapeutic target in human and mouse models of NP-C disease. Specifically, the aims are the following:

1. To investigate the therapeutic potential of DGK inhibition in NP-C patient fibroblasts.
2. To investigate the therapeutic potential of PLD inhibition in NP-C patient fibroblasts.
3. To investigate the impact of deletion of both *NPC1* and *LPIN-1* in the *Npc1<sup>-/-</sup> Lpin1<sup>-/-</sup>* mouse.

It is hypothesised that by inhibition of DGK or PLD, NP-C patient fibroblasts will have a somewhat reduced disease severity detectable by a change in cholesterol accumulation in a filipin assay. Likewise, it is expected that the deletion of *Lpin1* will exacerbate disease severity in the *Npc1<sup>-/-</sup>* mouse.

## **Chapter 2. Investigation of the therapeutic efficacy of targeting lipin to treat NPC disease**

### **2.1 Introduction**

Niemann-Pick type C is a fatal lysosomal storage disorder with both visceral and neurological manifestations. The disease has a recessive mode of inheritance, requiring both chromosomal copies of either NPC1 or NPC2 dysfunctional to impart disease. Although the disease is extremely heterogeneous in initiation and course, onset of disease is in most cases pediatric, and prognosis is predominantly poor, with half of individuals succumbing to the disease before the age of 20 (Vanier, 2010). Currently, there is no satisfactory cure for this disease (Madra & Sturley, 2010).

The NPC1 and NPC2 proteins function to transport cholesterol from the late endosome and lysosome, of which the salient repercussion is collapse of the capacity to regulate cellular cholesterol, with inappropriate transcriptional upregulation of cholesterol synthesis and uptake (Kwon et al., 2009; Munkacsı, Pentchev, & Sturley, 2009). Secondarily, a more intricate imbalance of a plethora of other cellular lipids is experienced, the mechanisms of which are poorly understood (Vanier, 2015).

Although the disease is prescribed by loss of a single gene, it is expected that several genes may modify which symptoms present, severity of symptoms, and age of onset of disease. Further, the most successful mitigative therapy to date, miglustat, does not target the cholesterol homeostasis machinery (Anheim et al., 2014). The identification of a conditional synthetic lethal interaction between the yeast orthologs of Npc1 and Lpin1 genes (Munkacsı et al., 2011) warranted further investigation of their mammalian orthologs.



## **2.2 Methods**

### **2.2.1 Mammalian tissue culture**

The NP-C patient fibroblast cell line GM03123 (Coriell) was derived from a 9-year-old female Western European donor. The donor was a compound heterozygote; one allele contained a missense 709C>T mutation, the other a missense 3182T>C mutation. The control cell line GM09503 (Coriell) was derived from a 10-year-old male European donor. These cell lines were maintained in 75 cm<sup>2</sup> flasks, with Dulbecco's Minimum Essential Media (DMEM) (Thermo Fisher) supplemented with 10% Fetal Calf Serum, 2 uM Glutamax (Thermo Fisher) and 100 units/mL penicillin/streptomycin antibiotic (Thermo Fisher). Flasks were kept within an incubator at 37°C with 5% CO<sub>2</sub>. Flasks were passaged prior to being 90% confluent. To achieve passage, medium was removed and replaced with 1 ml TrypLE (Thermo Fisher) and incubated at 37°C for 4 min or until the majority of cells were no longer adherent. These would be centrifuged in media for 4 min at 300 g, and pellet was resuspended in 1 ml fresh media. Generally, 20% of this would seed the new flask. Then 10 µl of trypsinised cells were mixed with 10 µl trypan blue, and 10 µl of this was counted using a haemocytometer to approximate cell density. Fibroblasts were diluted with fresh media to 1x10<sup>4</sup> cells per 100 µl of solution. Next 100 µl of media was added to wells of a 96 well plate and given 24 hours for cells to adhere to each well. Compounds were administered by replacing media with fresh media containing compound.

#### **2.2.2.1 Inhibition of DGK and PLD in fibroblasts**

Fibroblasts, adherent in 96 well plates (2.2.1) would be treated by replacement of media with compound containing media. DGK inhibitor R59022 (Sigma) and PLD inhibitor FIPI (Sigma) were used. To ensure solubility, both R59022 and FIPI were dissolved in dimethyl sulfoxide (DMSO), and media was added to reduce the concentration of DMSO to 0.5%.

Untreated control wells were also given 0.5% DMSO media. Fibroblasts were incubated for 48 hours to reach confluence before filipin visualisation.

#### **2.2.2.2 Filipin staining of unesterified cholesterol**

Filipin is notoriously light sensitive, so utmost care should be taken to avoid photobleaching before imaging. Using aspirator, media was removed from cells and cells were washed three times with 1x PBS (pH 7.4). Then 100 µl 1.5% Paraformaldehyde (PFA) (Sigma) was added to each well for 20 min and washed three times with 1x PBS. PBS was then replaced with 100 µl of 50µg/ml Filipin (Sigma) dissolved in 1xPBS and incubated for 45 min. After this, another three washes of 1x PBS was performed and the plate was ready for imaging.

#### **2.2.2.3 OPERA imaging**

The OPERA spinning-disk confocal microscope (Perkin Elmer) was used to visualise filipin-stained fibroblasts. This machine is ideal as the nature of this variety of microscope allows for informative images to be taken with consistent and minimal light exposure to the cells. To visualise filipin, the 405 nm laser was used with 20x objective. Once focused, images were taken, 3 z-stacks 1 µm apart, in 5 non-adjacent sites per well with an exposure of 3 s per image.

#### **2.2.2.4 Cell Profiler filipin quantification**

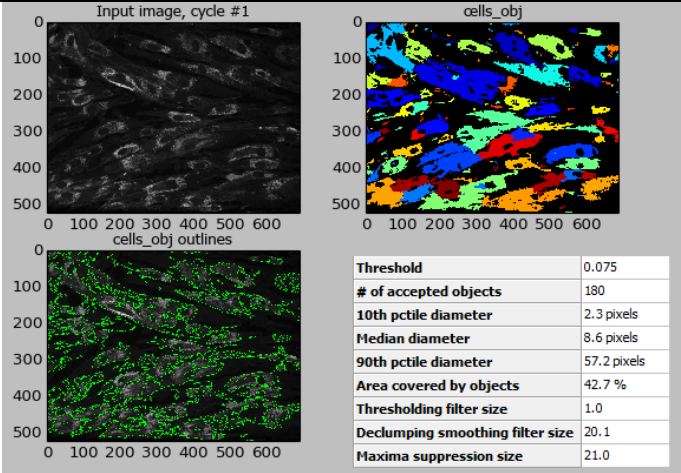
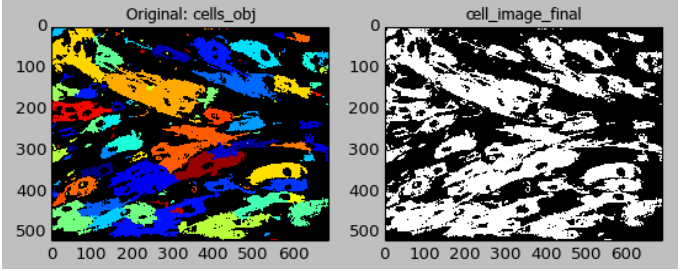
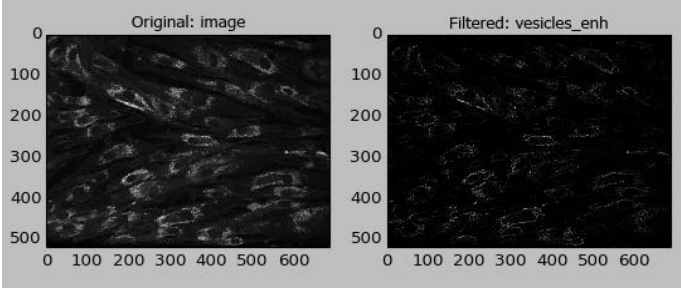
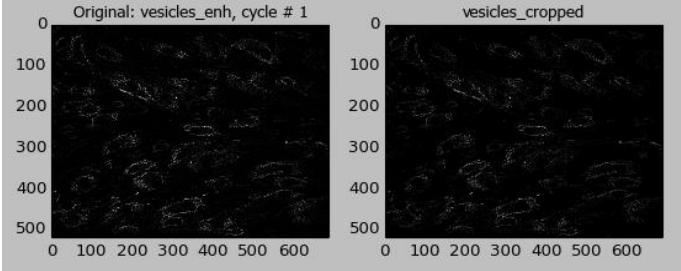
##### **2.2.2.4.1 Image conversion**

Images were produced by the OPERA as .flex file types. ImageJ was used to separate individual images from .flex files to .tiff format.

##### **2.2.2.4.2 Cell Profiler pipeline**

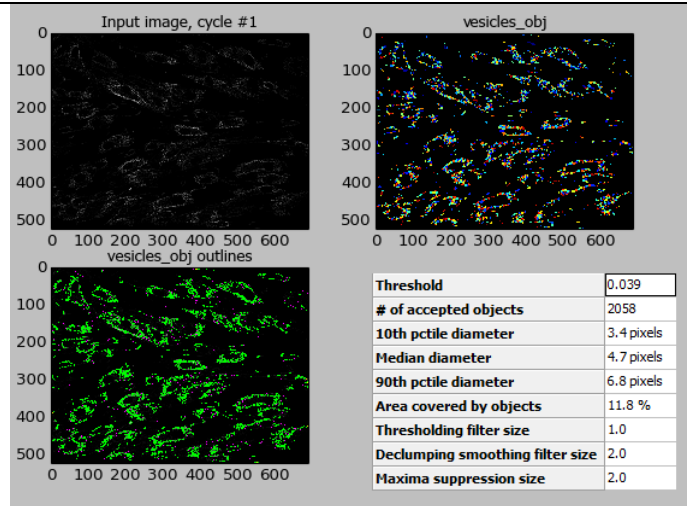
The pipeline (Table 1) was adapted from an example Speckle counting pipeline from the CellProfiler website: <http://cellprofiler.org/examples.html#Speckles>

**Table 1:** Cell profiler pipeline

Module name and description	Example image																		
<p><b>IdentifyPrimaryObjects</b></p> <p>Identified objects based on size and intensity threshold rules. Each cell was identified as an object.</p>	 <table border="1"> <tbody> <tr> <td>Threshold</td><td>0.075</td></tr> <tr> <td># of accepted objects</td><td>180</td></tr> <tr> <td>10th pctile diameter</td><td>2.3 pixels</td></tr> <tr> <td>Median diameter</td><td>8.6 pixels</td></tr> <tr> <td>90th pctile diameter</td><td>57.2 pixels</td></tr> <tr> <td>Area covered by objects</td><td>42.7 %</td></tr> <tr> <td>Thresholding filter size</td><td>1.0</td></tr> <tr> <td>Declumping smoothing filter size</td><td>20.1</td></tr> <tr> <td>Maxima suppression size</td><td>21.0</td></tr> </tbody> </table>	Threshold	0.075	# of accepted objects	180	10th pctile diameter	2.3 pixels	Median diameter	8.6 pixels	90th pctile diameter	57.2 pixels	Area covered by objects	42.7 %	Thresholding filter size	1.0	Declumping smoothing filter size	20.1	Maxima suppression size	21.0
Threshold	0.075																		
# of accepted objects	180																		
10th pctile diameter	2.3 pixels																		
Median diameter	8.6 pixels																		
90th pctile diameter	57.2 pixels																		
Area covered by objects	42.7 %																		
Thresholding filter size	1.0																		
Declumping smoothing filter size	20.1																		
Maxima suppression size	21.0																		
<p><b>ConvertObjectsToImage</b></p> <p>Converted identified objects in previous module to a binary image. Objects were black pixels and non-objects were white pixels.</p>																			
<p><b>EnhanceOrSuppressFeatures</b></p> <p>Identified “Speckles” features in image.</p>																			
<p><b>Crop</b></p> <p>Produced cropped image only containing identified “Speckles”, which were points of high intensity filipin fluorescence.</p>																			

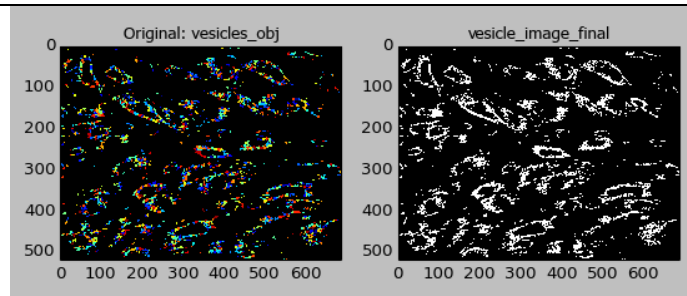
### IdentifyPrimaryObjects

Identified objects from cropped image.



### ConvertObjectsToImage

Converted objects identified from cropped image into a binary image.



### MeasureImageAreaOccupied

Measured number of black pixels in images representing cells and images representing fluorescent vesicles.

Objects or Image	Area Occupied	Perimeter	Total Area
cell_image_final	152760	32750	357760
vesicle_image_final	42075	27102	357760

### CalculateMath

Divided the pixel count of fluorescent vesicles by pixel count of cells.

Measurement name	Measurement type	Result
vesicle_percentage_area	Image	0.28

### ExportToSpreadsheet

Stored values as a .csv (Comma-separated values) file.

### 2.2.3 Mouse Husbandry

Animal research was conducted in compliance with Victoria University Animal Ethics Committee. Mice were kept in 1145T00SU-V cages (Techniplast) with dimensions 365x156x132mm. The mouse room operated under a 12 h light/dark cycle. Feed (Diet 86, Sharpes Stockfeed) and water were accessible *ab libitum* and bedding (Fort Richards) was replaced weekly. Sterile shredded paper was included in each cage as nesting material.

The colony was established with 6 *Npc1*<sup>+/-</sup> *Lpin1*<sup>+/-</sup> mice (3 male, 3 female) in the BALB/c background gratefully received from Dr Karen Reue at the David Geffen School of Medicine at the University of California at Los Angeles. With the intention of generating mice homozygous for both NPC1 and LIPIN1 knockout (KO) alleles and appropriate controls, mice heterozygous for each KO allele were selected as breeders. Breeding cages were set up with 1 male and 1 female breeder, and females were plug checked to predict the day of birth. Assuming Mendelian ratios are observed, we would expect to see 1 in 16 mice born as *Npc1*<sup>-/-</sup> *Lpin1*<sup>-/-</sup> (Table 2).

**Table 2:** Possible breeding outcomes from crossing mice heterozygous for both deletion alleles

	NPC1 WT LIPIN1 WT	NPC1 WT LIPIN1 KO	NPC1 KO LIPIN1 WT	NPC1 KO LIPIN1 KO
NPC1 WT LIPIN1 WT	NPC1+/+ LIPIN1+/+	NPC1+/+ LIPIN1+/-	NPC1+/- LIPIN1+/+	NPC1+/- LIPIN1+/-
NPC1 WT LIPIN1 KO	NPC1+/+ LIPIN1+/-	NPC1+/+ LIPIN1-/-	NPC1+/- LIPIN1+/-	NPC1+/- LIPIN1 -/-
NPC1 KO LIPIN1 WT	NPC1+/- LIPIN1+/+	NPC1+/- LIPIN1+/-	NPC1-/- LIPIN1+/+	NPC1-/- LIPIN1+/-
NPC1 KO LIPIN1 KO	NPC1+/- LIPIN1+/-	NPC1+/- LIPIN1 -/-	NPC1-/- LIPIN1+/-	NPC1-/- LIPIN1-/-

## 2.2.4 Genotype determination

All animals were genotyped at 14 days of age (P14). Each mouse was ear-tagged and had a 2 mm tail tip removed by razor blade. Genomic DNA of tail tips was extracted in 1.5 ml microfuge tubes. The tail tip was suspended in 300 µl of 50 mM NaOH and placed in a 98°C heat block for 50 min. Tubes were vortexed for 15 sec and 30 µl of 1M Tris (pH 8) was added. This was centrifuged at 16,000x g for 6 min. The supernatant was used for PCR analysis. For each mouse, four genotype PCRs were required.

**Table 3:** Primers used for mouse genotypes

Allele to check	Forward Primer	Reverse Primer
NPC1 Wild Type Allele	CTGTAGCTCATCTGCCATCG	TCTCACAGCCACAAGCTTCC
NPC1 Knock Out Allele	TGAGCCCAAGCATAACTTCC	GGTGCTGGACAGCCAAGTA
LIPIN1 Wild Type Allele	GGGGAGTCCGTGGATTGCA	CAGATGCACACATTCAGCCAGT
LIPIN1 Knock Out Allele	CTGATCGTTGTCAGTCTCT	GAGAGATGCAGCTGCGTCA

**Table 4:** PCR reaction reagents

Reagent	Volume per reaction (ul)
ddH <sub>2</sub> O	17.375
10x PCR Buffer (Roche)	2.5
dNTPs (2.5mM) (Sigma)	2
Forward Primer (10μM) (Macrogen)	1
Reverse Primer (10μM) (Macrogen)	1
rTth polymerase (Roche)	0.125
DNA	1
Total Volume	25

**Table 5:** Cycling conditions used for all PCRs

Temperature (°C)	Time (min)	
94	3:00	
94	0:40	x 20
63  ( less 0.5°C/cycle)	1:00	
72	1:00	
92	0:40	x 16
53	1:00	
72	1:00  (gain 0:05/cycle)	
10	(HOLD)	

PCR products were loaded on a 1% agarose gel in 1x TBE and 0.005% Ethidium Bromide. 1Kb+ ladder (Life Technologies) was loaded alongside PCR products to distinguish size of product. The gel was electrophoresed at 90 V in 1x TBE running buffer and visualised under 365 nm UV light.



### **2.2.5 Weights**

All animals were weighed weekly from P14 within a plastic box on an electronic scales.

### **2.2.6 Collection of neonatal tissue**

Mice were weighed and beheaded with sharp scissors at P0. The body was immediately placed in a dish containing 1x PBS. A further coronal cut was made to the back of the head (just behind the ears) to reveal the foramen magnum. Using the scissors, cuts of a few millimetres were made from the foramen magnum along the skull sagittally and in either transverse direction. Using the flat edge of the scissors, careful pressure was applied to the base of the snout, and the brain was gently ejected from the skull. The brain was separated into two hemispheres, with one immediately immersed in 70% ethanol cooled by dry ice and the other hemisphere was rinsed in 1x PBS and immersed in 1.5% PFA. Holding the abdominal wall with fine tissue forceps, the abdominal cavity was gently opened. By cutting the portal vessels, the liver was removed from the animal as a single piece. From there, lobes were separated with care and either immersed in dry ice-cooled ethanol or 1.5% PFA. Finally, the tail was removed for genotyping as in **2.2.4**. Organ samples in 1.5% PFA were put on a rocker at 4°C for 24 hours, then washed and stored in 70% ethanol.

### **2.2.7 Western blot analysis**

#### **2.2.7.1 Protein extraction**

Each organ sample was immersed in 200 µl of ice cold RIPA buffer (Sigma) containing protease inhibitor cocktail (Roche). Using a Z359971 electric homogeniser tool (Sigma) with replaceable plastic dounces, samples were homogenised by 20-30 slow plunges. Homogenate was then incubated on ice for 30 min and centrifuged for 30 min at 16,000 xg at 4°C. The upper phase was pipetted off and stored at -80°C.

### 2.2.7.2 Protein quantification

Protein extracts were quantified by the Pierce BCA Protein Assay Kit (Thermo Fisher) following the manufacturer protocol. Protein samples were diluted 4-fold with ddH<sub>2</sub>O. Change in opacity was measured by the EnSpire<sup>®</sup> 2300 Multimode Reader (Perkin Elmer) at 600 nm.

### 2.2.7.3 Protein Preparation and denaturation

Protein samples were diluted with ddH<sub>2</sub>O to 2.4 µg/µl and prepared for denaturation as follows:

**Table 6:** Protein denaturation reagents

Reagent	Volume (µl)
Protein sample	42
5x Laemmli buffer	12
β-mercaptoethanol (Sigma)	6
Total	60

Laemmli buffer consists of 60 mM Tris-Cl pH 6.8 (Formedium), 2% sodium dodecyl sulfate (SDS) (Invitrogen), 10% glycerol (Invitrogen) and 0.01% bromophenol blue (Sigma). Samples were then vortexed for 15 sec and centrifuged for 30 sec at 2,600 xg, and then incubated at 37°C for 10 min. If not used immediately, samples were stored at -80°C.

#### 2.2.7.4 SDS-PAGE electrophoresis

Separation of proteins was achieved by a two-part gel produced by sequential casting.

Each gel was given 1 hr to set.

**Table 7:** 15% separating gel

Reagent	Volume
1.5M Tris pH 6.8	5 ml
30% acrylamide (Bio-Rad)	10
ddH <sub>2</sub> O	4.69 ml
10% SDS	200 µl
10% ammonium persulfate (APS) (Sigma)	100 µl
Tetramethylethylenediamine (TEMED) (Sigma)	10 µl

**Table 8:** 4% stacking gel

Reagent	Volume
0.5M Tris pH 6.8	2.5 ml
30% acrylamide (Bio-Rad)	1.3 ml
ddH <sub>2</sub> O	6.1 ml
10% SDS	100 µl
10% ammonium persulfate (APS) (Sigma)	50 µl
Tetramethylethylenediamine (TEMED) (Sigma)	10 µl

The gel tank was filled with room temperature 1x SDS running buffer. 25 µl of protein sample was added to lanes with 2 µl of Dual Color ladder (Bio-Rad) added to leftmost and rightmost lanes. Running buffer was diluted from 10x stock (10 g SDS powder (Thermo Fisher), 30.3 g Tris, 144 g Glycine (Life Technologies) dissolved in ddH<sub>2</sub>O made up to 1L). Gel was run for 1 hr 45 minutes at 120 V.

#### **2.2.7.5 Membrane transfer**

Proteins were transferred from the acrylamide gel to a 0.2 µm pore size polyvinylidene difluoride (PVDF) membrane (Bio-Rad) using Bio-Rad transfer equipment. Membrane was normalised in methanol for 2 min and rinsed in transfer buffer. Transfer buffer was produced from 3.03 g Tris, 14.4 g Glycine, and 200 ml Methanol made up to 1L in ddH<sub>2</sub>O and chilled to 4°C. Transfer was run with an ice block at room temperature for 2 hr 15 min at 40 V.

#### **2.2.7.6 LC3 membrane probing**

Membrane containing transferred protein was blocked with 1x PBS with 1% trim milk powder at 4°C for 30 min, and then washed with 1x PBS without milk three times for 10 min. The primary antibody rabbit polyclonal anti-LC3 (Novus Biologicals) was diluted 1:1000 in 1x PBS with 1% trim milk powder and incubated with the membrane rocking overnight for 15-18 hr at 4°C. Membrane was then washed with 1x PBS three times for 10 min, and incubated with secondary goat anti-rabbit Cy5 antibody (Millipore) at 1:1000 dilution in 1x PBS with 1% trim milk powder for 1.5 hr in a light protected container. Membrane was then washed in 1x PBS three times for 10 min.

#### **2.2.7.7 Actin membrane probing**

After probing for LC3, mouse anti-actin antibody (Sigma) dissolved 1:1000 in 1x PBS with 1% trim milk powder was used to probe the membrane. The membrane was put on a rocker in the primary antibody for 2 hr at 4°C. Membrane was then rinsed in 1x PBS three

times for 10 min. Membrane was then probed with secondary goat anti-mouse Cy5 antibody dissolved 1:1000 in 1x PBS with 1% trim milk powder on rocker at 4°C for 1 hr. Membrane was then washed in 1x PBS three times for 10 min.

#### **2.2.7.8 Imaging and analysis**

Probed proteins in membranes were visualised using the Typhoon FLA 9500 scanner (Fuji). Images were scanned using a 649 nm laser at 700 V and at a 50  $\mu\text{m}^2$  pixel size. Scanned images were quantified by densitometry software (ImageJ).

### **2.2.8 Histology**

#### **2.2.8.1 Tissue processing**

Tissues fixed in PFA and transferred to 70% ethanol in 2.2.6 were put in tissue cassettes (Thermo Fischer). The Leica TP1020 benchtop tissue processor, a 12 basket machine with automatic functions, was used to dehydrate the tissue and then infuse the samples with paraffin wax.

**Table 9:** Tissue processor protocol

Basket	Reagent	Time (hours:minutes)
1	70% Ethanol	2:00
2	80% Ethanol	1:30
3	95% Ethanol	1:00
4	95% Ethanol	1:00
5	Absolute Ethanol (Sigma)	1:30
6	Absolute Ethanol	1:15
7	Absolute Ethanol	1:10
8	Absolute Ethanol/Xylol (Sigma)	1:30
9	Xylol	1:00
10	Xylol	1:00
11	Paraffin Wax (Sigma)	1:30
12	Paraffin Wax under vacuum	2:00

### **2.2.8.2 Embedding**

Tissue cassettes were set in wax blocks using the Leica EG1160 automatic embedding system.

### 2.2.8.3 Microtome

Seven  $\mu\text{m}$  slices were produced from tissue blocks using a Leica RM2235 microtome. Slices were floated upon a 40°C water bath, caught on slides and left to air-dry.

### 2.2.8.4 Hematoxylin and Eosin staining

Slides were stained using Delafield's Hematoxylin (Sigma) using the following procedure:

**Table 10:** Staining procedure for H&E histology

Stain									
Reagent	Xylene	Xylene	100%	95%	75%	30%	ddH2O	Haematoxylin	
			EtOH	EtOH	EtOH	EtOH			
Time (h:min)	3:00	3:00	3:00	3:00	3:00	3:00	0:30	9:00	
Destain									
Reagent	Tap	Acid	70%	Eosin	95%	100%	100%	Xylene	Xylene
	H <sub>2</sub> O	alcohol	EtOH		EtOH	EtOH	EtOH		
Time (h:min)	10 dips	1 dip	2:00	0:20	2:00	3:00	3:00	3:00	3:00

### 2.2.9 Lipid extraction

Lipid was extracted as previously described (Bligh and Dyer, 1959). In brief, tissue was added to 500  $\mu\text{l}$  of chloroform:methanol (1:2) and homogenised using electric homogeniser

tool with replaceable plastic douncers. Homogenate was transferred to a new 1.5 ml tube containing 150 µl chloroform:methanol (1:2). 300 µl chloroform and 200 µl 1M KCl were added to the tube, vortexed for 30 sec, and incubated for 60 sec on ice. Vortex and incubation was repeated an additional two times. The tube was then centrifuged at 10,000 rpm at 4°C to separate phases. The lower (organic) phase was transferred to a fresh tube and stored on ice. To the remaining phases, another 400 µl of chloroform was added and vortex, incubation and centrifugation steps were repeated with a new organic phase pooled with the previously acquired organic phase. This pooled organic phase was dried using a speed vacuum. A layer of argon was then added to the dried lipids prior to lipidomic analyses.

#### **2.2.10 Lipidomic analysis.**

Lipidomic analysis was conducted as follows, in keeping with methods previously used (Chan et al, 2012).

Whole lipid extracts (2.2.6) were spiked with internal standards (Agilent) detailed below (Table 11). Glycerophospholipids and sphingolipids were separated by normal phase HPLC by Agilent Zorbax Rx-Sil column, and separation of sterol and glycerolipid species was performed by reverse-phase HPLC, utilising a Zorbax Eclipse XDB-C18 column (Agilent). Species were analysed by the Triple Quadrupole 3200 QTrap (Applied Biosystems). Multiple reaction monitoring was used to quantify lipids, and internal standards were used to identify peaks. Each lipid was quantified and normalized to total lipids for each sample.



**Table 11:** Standards used in lipidomic analysis.

Standard	Concentration (mg/ml)	Volume (µl)	Amount (µg)
Chol d7	5.0	100	500
Chol 24OH d7	1.0	50	50
C17:0 CE	1.0	20	20
C17 MG	0.1	40	4
DG 4ME	1.0	10	10
TG 50:0 d5	0.5	20	10
C17:0 Cer	2.5	20	50
C12:0 SM	2.0	75	150
C12:0 DHSM	2.0	40	80
C12:0 GalCer	2.0	20	40
C17:0 Sulf	1.0	30	30
C12:0 LacCer	1.0	10	10
C14:0 PA	0.5	10	5
C14:0 PC	10.0	50	500
C14:0 PE	10.0	25	250
C15:0 PG	0.2	10	2
C16:0 PI	1.0	100	100
C14:0 PS	10.0	10	100
C17:0 LPC	0.1	10	1
C14:0 lyso PE	0.1	10	1
C13:0 lyso PI	0.1	10	1
C14:0 LBPA	0.1	10	1
C14:0 sLBPA	0.1	10	1

### **2.2.11 Statistical analysis**

A chi-squared test was used to compare the genotypic proportions of mice born against the expected Medelian ratios. All other comparisons of quantified data were achieved by performing a two-tailed Student's t-test, under the assumption of equal variance in compared groups.

## 2.3 Results

### 2.3.1 Inhibition of diacylglycerol kinase does not ameliorate accumulation of unesterified cholesterol in NPC patient fibroblasts

Filipin is a fluorescent stain that binds unesterified cholesterol, and is the gold standard for diagnosis of NP-C in a clinical setting (Vanier & Latour, 2015). Filipin will accumulate in cholesterol-laden lysosomes in NP-C fibroblasts and is indicative of the cholesterol storage defect. Compounds ameliorative of the NP-C cholesterol storage phenotype will result in a stained cell more similar to the wild-type fibroblast (Fig. 6D). Precedent for this assay has been established with the HDAC inhibitor SAHA reducing filipin accumulation in NP-C patient fibroblasts (Munkacsı et al., 2011).

With the yeast homolog of the *Lpin1* gene being identified as potentially protective for NP-C severity, PA, the target of the LPIN1 enzyme, was targeted with the diacylglycerol kinase inhibitor R59022 (de Chaffoy de Courcelles, Roevens, & Van Belle, 1985). Concentrations between 10  $\mu$ M – 50  $\mu$ M have been used for the inhibition of DGK in a variety of cell types (Ford, Stemkowski, Light, & Smith, 2003; Sovadinova et al., 2015) and in fibroblasts a 10  $\mu$ M treatment was effective, albeit over a time interval (Camina, Casabiell, & Casanueva, 1999). To allow resolution of cholesterol accumulation (Munkacsı et al., 2011), a 24-hour treatment time was used and concentrations of 25  $\mu$ M and 50  $\mu$ M were used. From visual inspection (Fig. 6) and quantification (Fig. 7) of filipin staining of fibroblasts, DGK inhibition by R59022 was ineffective in reversing the NP-C phenotype.

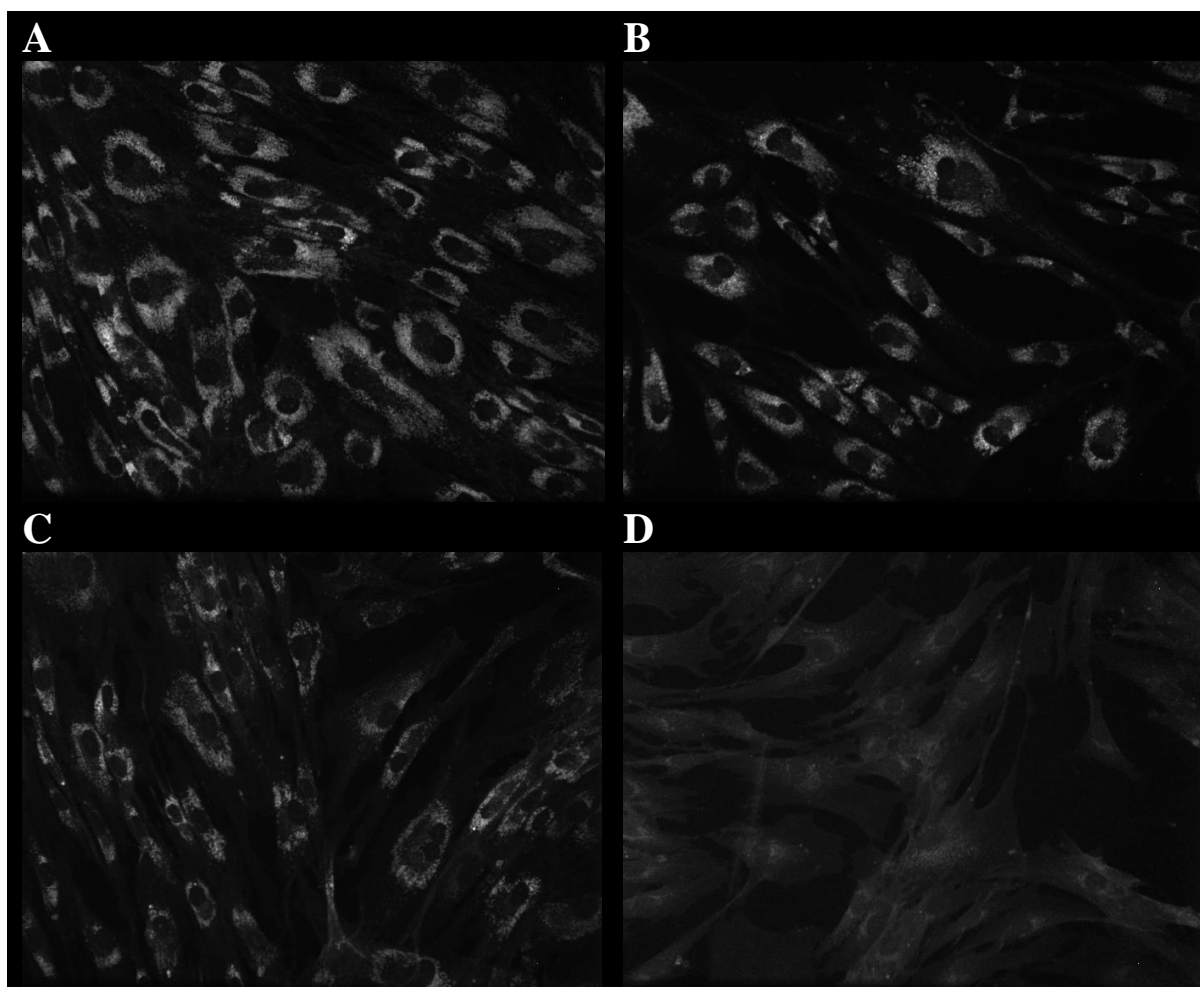


**Figure 5: Representative images of fibroblasts under four conditions. A.** NP-C fibroblast with 25  $\mu$ M R59022 **B.** NP-C fibroblast with 50  $\mu$ M R59022 **C.** Untreated control NP-C fibroblast **D.** Normal (healthy) untreated control fibroblast.

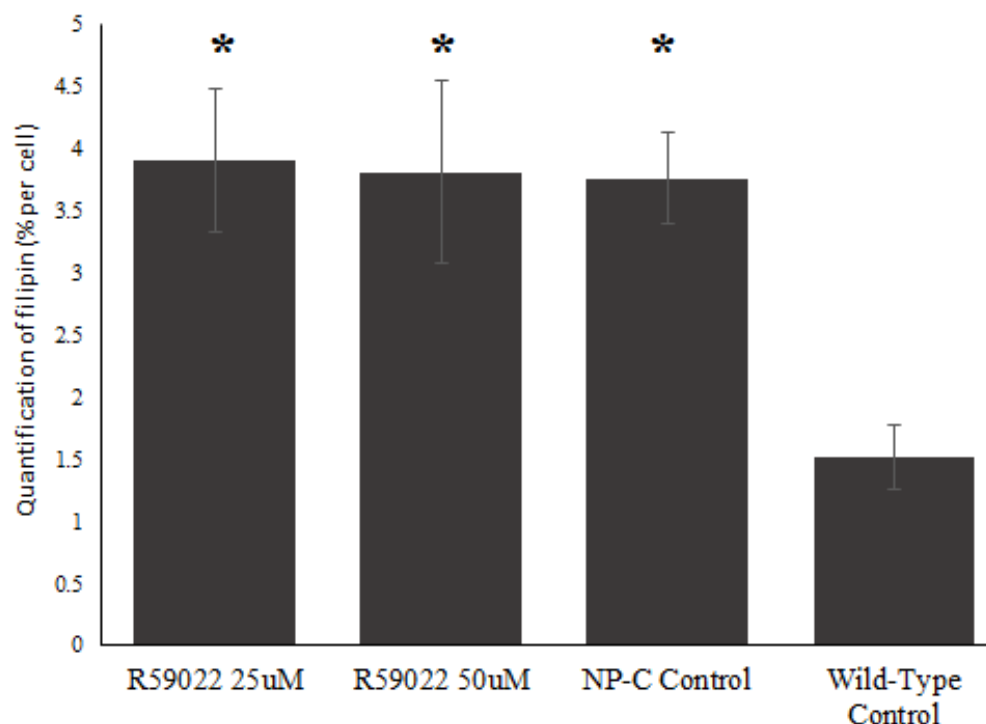


**Figure 6: R59022 treatments do not reduce cholesterol storage according to filipin staining.** Fibroblasts stained with filipin before OPERA microscopy. Filipin stain quantified by CellProfiler speckle counting pipeline. Error bars show standard error of normalised values. \* $p < 0.05$  Student's t-test against wild-type control group. Analysed images collected from 4 biological replicates, 12 clean images taken from each.

### 2.3.2 Inhibition of phospholipase D does not ameliorate accumulation of unesterified cholesterol in NPC patient fibroblasts

With the intent on targeting PA to ameliorate the filipin phenotype in NP-C fibroblasts as had previously been achieved with SAHA (Munkacsı et al., 2011), the phosphatidylcholine hydrolases PLD1 and PLD2 were inhibited using FIPI. FIPI is a potent inhibitor of PLD1/2, with an  $IC_{50}$  at 10 nM in CHO cells for PLD2, and an  $IC_{50}$  of 1 nM for PLD1 (Su et al., 2009). To inhibit PLD activity in the NP-C fibroblasts, concentrations of 20 nM and 40 nM FIPI were tested over a 24 hour time period. As with the R59022 mediated inhibition of DGK, by visual examination (Fig. 8) and digital quantification of filipin accumulation (Fig. 9), PLD inhibition was found to be not ameliorative, as least in so far as can be determined by lysosomal cholesterol storage.

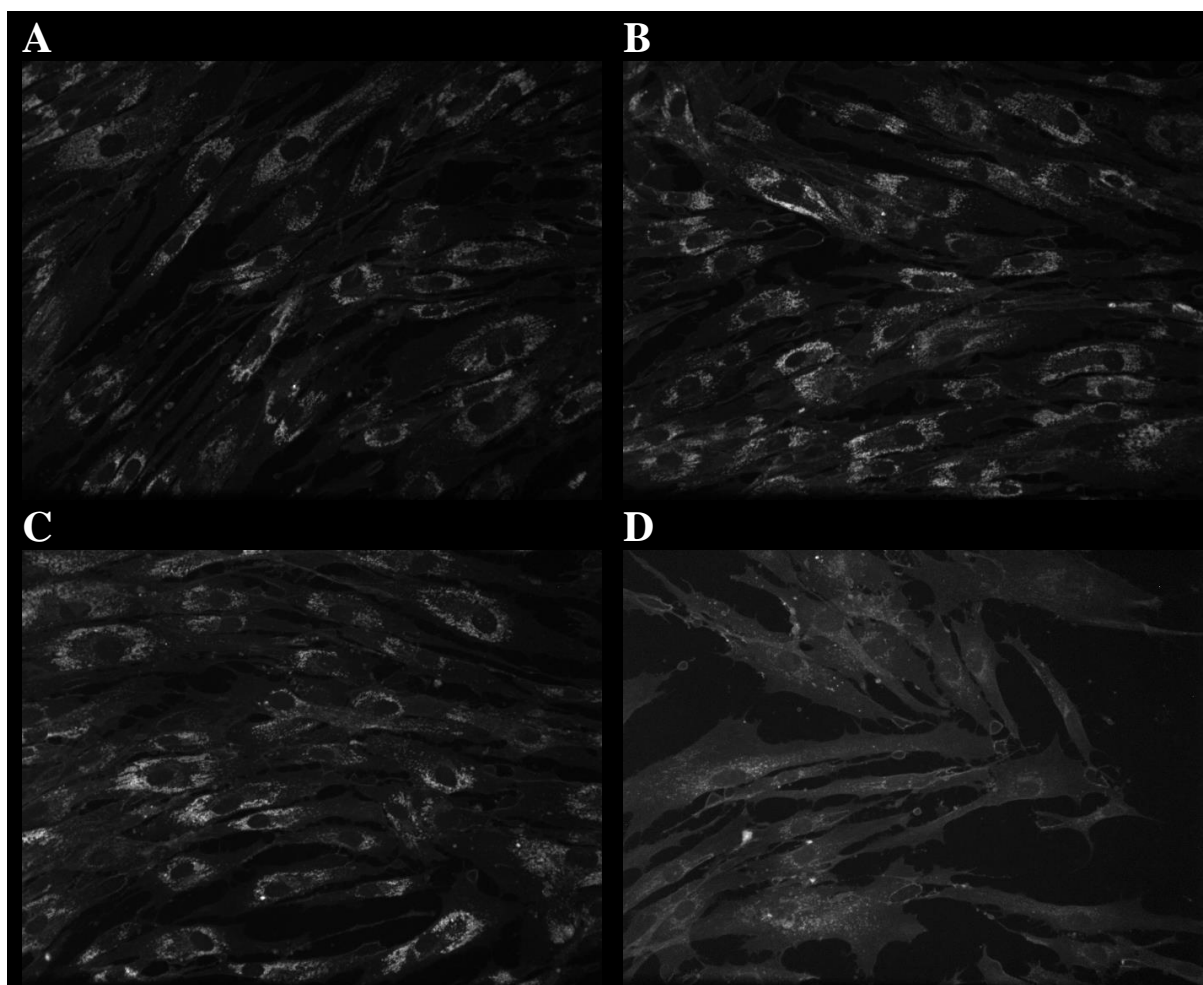


**Figure 7: Representative images of fibroblasts under four conditions. A.** NP-C fibroblast with 20 nM FIPI **B.** NP-C fibroblast with 40 nM FIPI **C.** Untreated control NP-C fibroblast **D.** Normal (healthy) untreated control fibroblast.

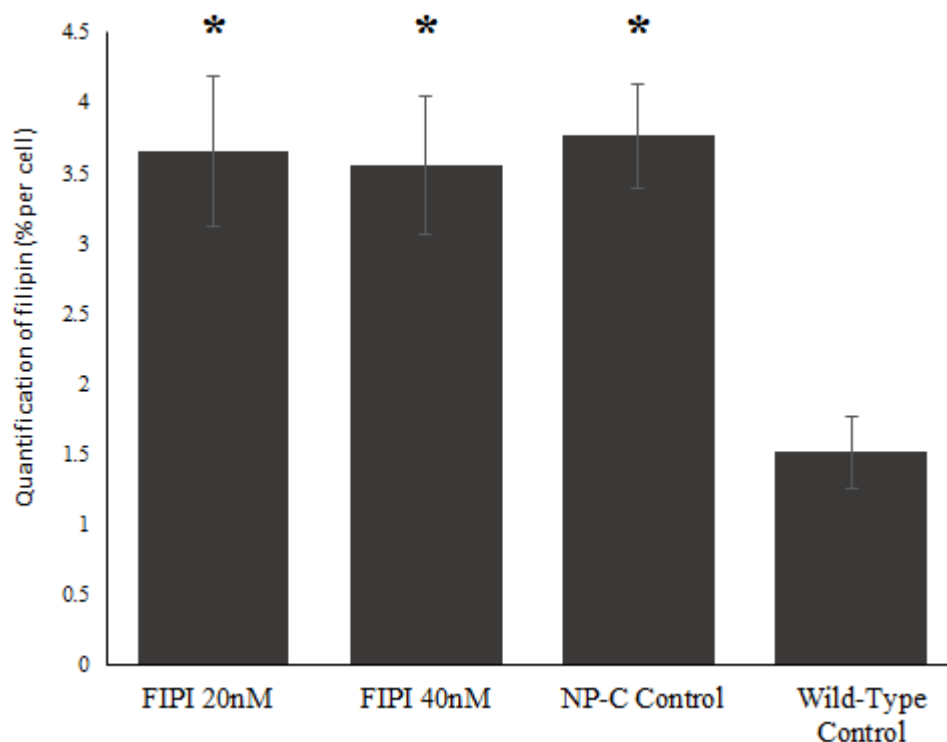


**Figure 8: FIPI treatments do not reduce cholesterol storage according to filipin staining.** Fibroblasts stained with filipin before OPERA microscopy. Filipin stain quantified by CellProfiler speckle counting pipeline. Error bars show standard error of normalised values. \* $p < 0.05$  Student's t-test against wild-type control group. Analysed images collected from 4 biological replicates, 12 clean images taken from each.

### 2.3.3 *Npc1*<sup>-/-</sup> *Lpin1*<sup>-/-</sup> mice were generated by crossing *Npc1*<sup>+/-</sup> and *Lpin1*<sup>+/-</sup> mice

As mice which lack copies of either *Npc1* or *Lpin1* are not capable of reproduction, mice which are heterozygous for each allele are the necessary genotype for the most efficient breeding regimen. Breeding cages were set up with one female and one male, purely to maximise the number of cages that could be established. Females were plug-checked so litters could be predicted ahead of time.

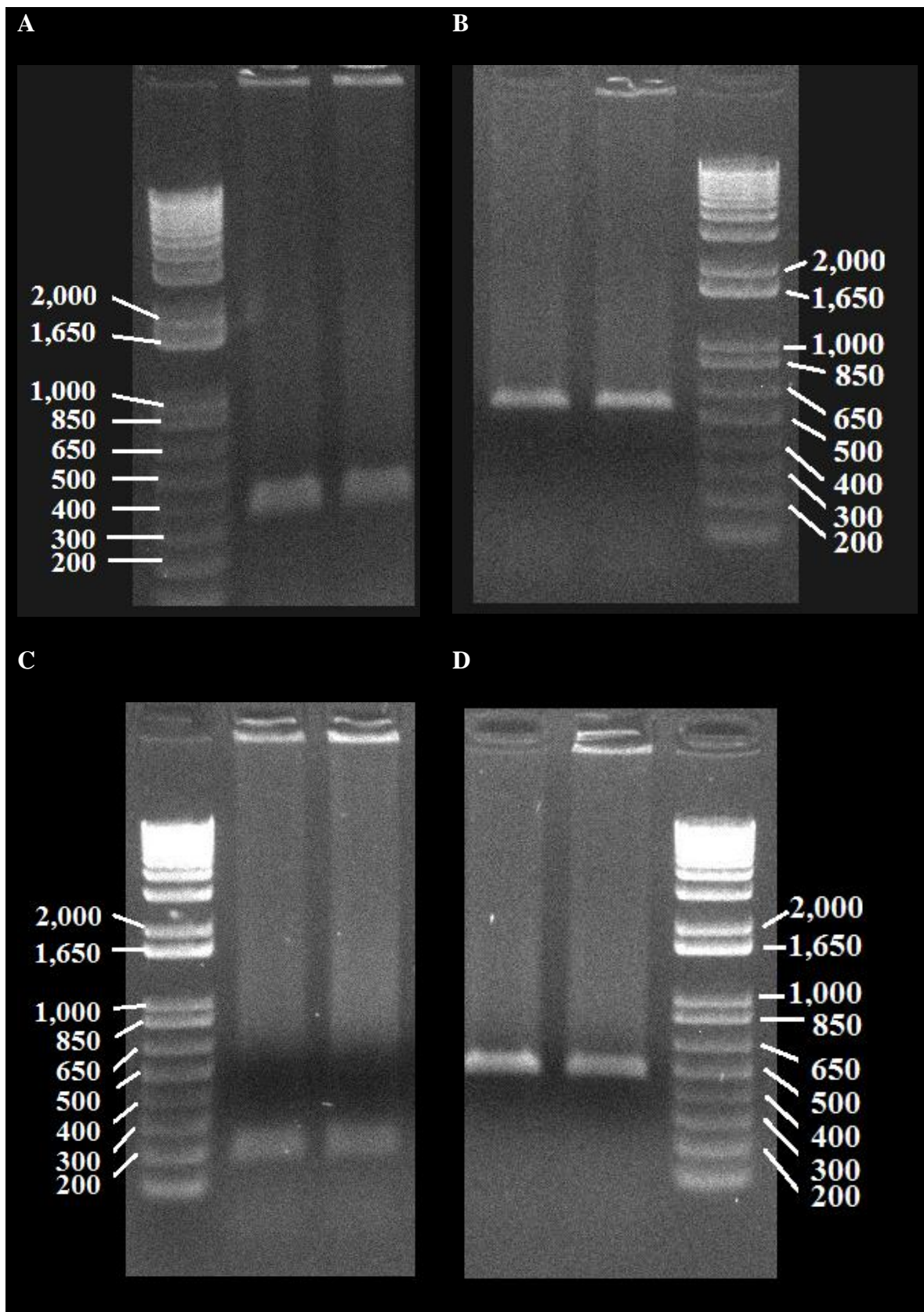


**Figure 9: Amplified bands against 1kb+ ladder.** Ladder band sizes shown in base pairs. **A.** *Npc1* wild-type allele at 400 bp. **B.** *Npc1* knock-out allele at 600 bp. **C.** *Lpin1* wild-type allele at 300 bp. **D.** *Lpin1* knock-out allele at 500 bp.



### 2.3.4 *Npc1*<sup>-/-</sup> *Lpin1*<sup>-/-</sup> mice are recovered at expected Mendelian ratios

Given both *Npc1*<sup>-/-</sup> mice and *Lpin1*<sup>-/-</sup> mice each exhibit fatty liver disease (Loftus et al., 1997; Péterfy et al., 2001) and that *Npc1*<sup>-/-</sup> mice only live 10-12 weeks compared to the normal lifespan of ~96 weeks, we hypothesized that *Npc1*<sup>-/-</sup>*Lpin1*<sup>-/-</sup> mice will have severe developmental defects. First we monitored viability at birth. If litters were produced with perfect Mendelian ratios, only 1 in 16 pups would be expected to be the *Npc1*<sup>-/-</sup>*Lpin1*<sup>-/-</sup> genotype. To test the hypothesis that the genotypic profile of the pups was proportional to the expected Mendelian ratio (suggested in Table 2), a chi square test was performed. With 9 degrees of freedom the threshold for statistical significance ( $p < 0.05$ ) is a chi square value of 16.92 (Pearson, 1900). With a chi square value of 5.79 we are unable to reject the hypothesis that the observed genotypes of mice born were proportional to expected as by Mendelian ratio.

**Table 12:** To challenge whether pups were being born at Mendelian ratios, a chi-squared test was performed. Expected values calculated by using a punnet square (Table 2). With 9 degrees of freedom, the chi-squared value of 5.79 does not register as significant.

Possible Genotype	Observed	Expected	Observed - Expected	(O-E) <sup>2</sup>	(O-E) <sup>2</sup> /E
N <sup>-/-</sup> L <sup>-/-</sup>	3	5.875	-2.875	8.265625	1.406915
N <sup>+/-</sup> L <sup>-/-</sup>	11	11.75	-0.75	0.5625	0.047872
N <sup>+/+</sup> L <sup>-/-</sup>	6	5.875	0.125	0.015625	0.00266
N <sup>-/-</sup> L <sup>+/-</sup>	10	11.75	-1.75	3.0625	0.260638
N <sup>+/-</sup> L <sup>+/-</sup>	23	23.5	-0.5	0.25	0.010638
N <sup>+/+</sup> L <sup>+/-</sup>	13	11.75	1.25	1.5625	0.132979
N <sup>-/-</sup> L <sup>+/+</sup>	4	5.875	-1.875	3.515625	0.598404
N <sup>+/-</sup> L <sup>+/+</sup>	18	11.75	6.25	39.0625	3.324468
N <sup>+/+</sup> L <sup>+/+</sup>	6	5.875	0.125	0.015625	0.00266
SUM	94	94	0		<b>5.787234</b>

#### 2.3.4.1 Effect of *Npc1*<sup>-/-</sup> and *Lpin1*<sup>-/-</sup> conditions on birth weight

The *Npc1*<sup>-/-</sup> mouse model, having a severely truncated version of the NPC1 protein, (Loftus et al., 1997) experienced a phenotype comparable to a severe onset form of human NPC, and will rarely live beyond 12 weeks. The *Npc1*<sup>-/-</sup>*Lpin1*<sup>-/-</sup> mouse suffers a course that has an earlier onset and induces a much earlier demise. This prompted investigation at the P0 time point, with the intention of identifying early markers and enable a greater breadth of understanding regarding the pathology of the *Npc1*-*Lpin1* interaction.

Prior to dissection described in 2.2.6, P0 mice were weighed as in 2.2.5. Due to the inability to dissect all pups at the same precise time point from their time of birth, and to account factors such as litter size and parent, all pup weights were normalised to the average pup weight in their litter. From a total of 94 pups, 19 pups of interest genotypes were compared (Fig. 11). The wild-type and *Lpin1*<sup>-/-</sup> mice weighed significantly more than the *Npc1*<sup>-/-</sup> mice, the wild-type mice on average 15% heavier. The *Npc1*<sup>-/-</sup>*Lpin1*<sup>-/-</sup> mice were also lighter on average than wild-type and *Lpin1*<sup>-/-</sup> mice, however among the three mice one was conspicuously heavier than the other two, which is evident in a standard error twice as large as any other group. It is suspected that with a larger sample size the weight disparity between wild-type and *Npc1*<sup>-/-</sup>*Lpin1*<sup>-/-</sup> mice would become statistically supported. Whether a greater sample size would identify a difference between the birth weight of *Npc1*<sup>-/-</sup> and *Npc1*<sup>-/-</sup>*Lpin1*<sup>-/-</sup> mice would be even more intriguing.

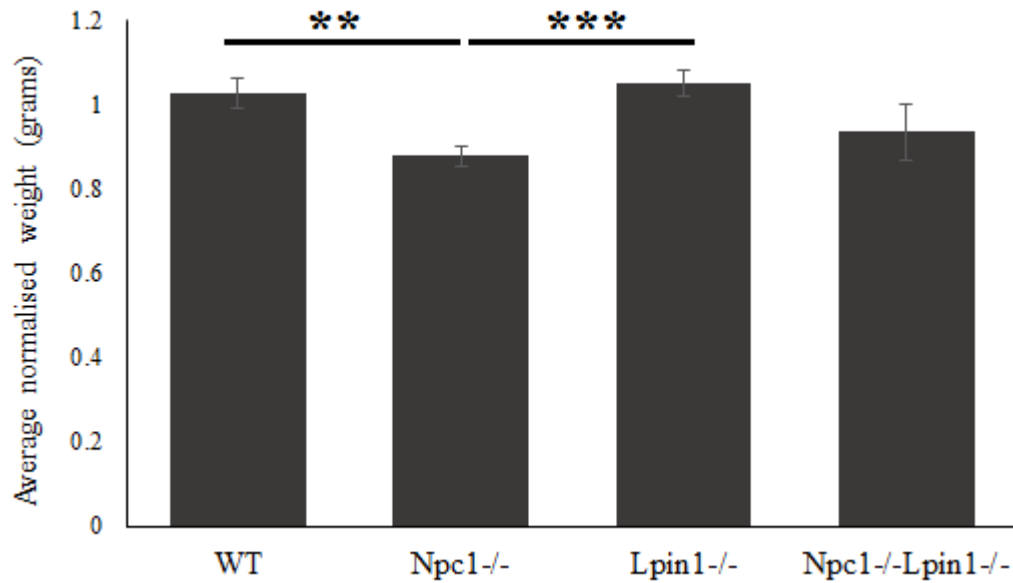


**Figure 10: *Npc1*<sup>-/-</sup> mice have a lower birth weight to littermates.** All mice normalised against the average weight of their litter before comparison. Error bars represent standard error. \*\*p<0.01, \*\*\*p<0.005 Student's t-test against indicated group. WT (Wild-Type) n=6, *Npc1*<sup>-/-</sup> n=4 *Lpin1*<sup>-/-</sup> n=6, DKO (Double Knock-out aka *Npc1*<sup>-/-</sup>*Lpin1*<sup>-/-</sup>) n=3 from 94 pups in 17 litters.

### 2.3.5 Autophagy is not disrupted in *Npc1*<sup>-/-</sup> *Lpin1*<sup>-/-</sup> mice

Autophagy has been observed to be crucial immediately after birth in the mouse model with neonates deficient in *ATG5*, a protein necessary for autophagosome formation, as these mice die within the first day of birth (Kuma et al., 2004). Disconnection of the neonate from placental nutrients initiates a state of immediate starvation before the first milk meal, and autophagy is a necessary means of nutrient scavenging between feeding (Medina, Vicario, Juanes, & Fernández, 1992). Loss of *Npc1* and *Lpin1*, genes that have wide-ranging effects on lipid metabolism and regulation, might leave a neonatal mouse pup especially vulnerable in times between milk-feeding. We hypothesized that *Npc1*<sup>-/-</sup>*Lpin1*<sup>-/-</sup> mice might struggle to compete for milk. A dysfunctional autophagy machinery would be devastating to an animal and contribute to premature demise.

Quantifying LC3-I and LC3-II protein is a core assay in the investigation of blockages in autophagic machinery (Daniel J Klionsky, Cuervo, & Seglen, 2007). Cytosolic LC3-I is upregulated for the induction of autophagy, while LC3-II, with the addition of a phosphatidylethanolamine group, resides within autophagic vesicles. We measured LC3 using Western blot in the four genotypes of interest at P0, and failed to achieve separation of the LC3-I and LC3-II proteins (Fig. 12A). Quantification of total LC3 from the P0 mouse liver has shown there is no statistical suggestion of autophagy differing in nature between the genotypes investigated here (Fig. 12B). It seems most likely that it is the LC3-I protein that has not been visualised, as it is more prone to denature and apocryphally, may not bind some LC3 antibodies as effectively (D. J. Klionsky et al., 2008). Regardless, increased autophagy flux or autophagy blockage will result in increased levels of either form of LC3, and this should be observable even if the more abundant LC3 species cannot be distinguished.

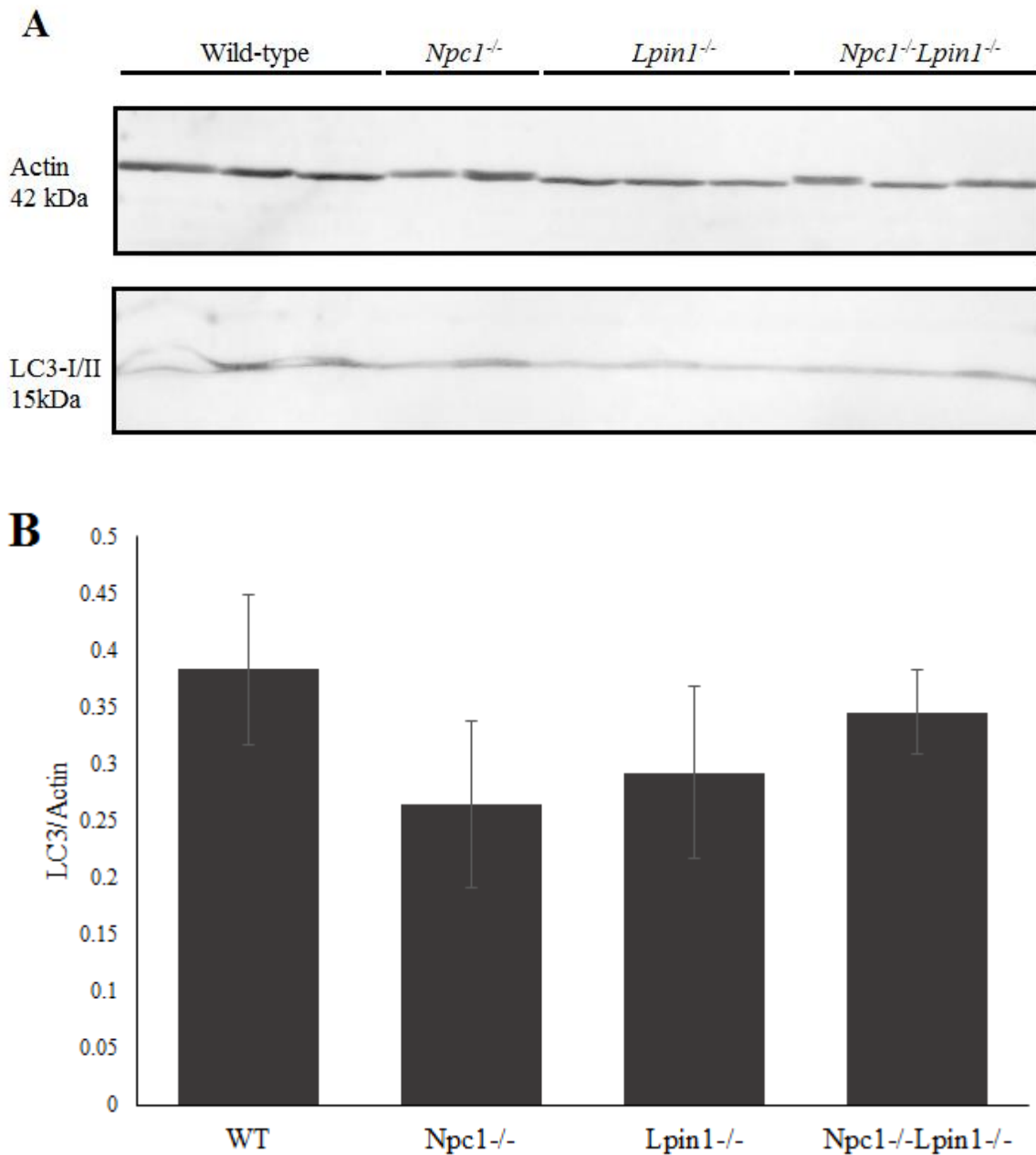
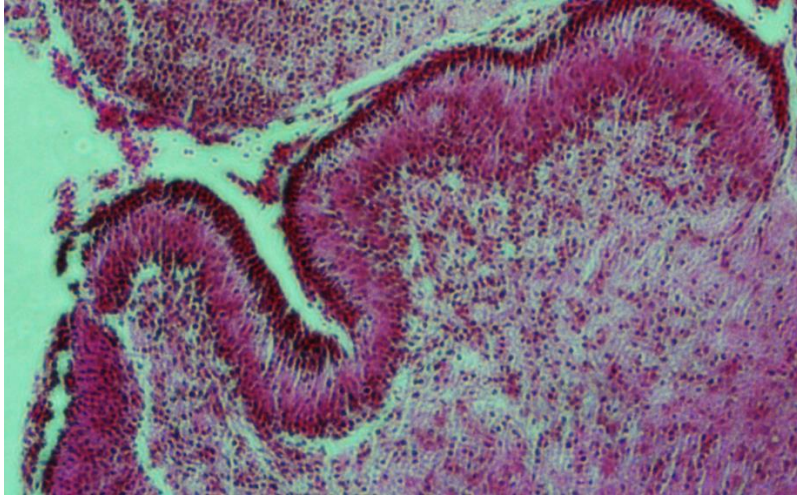


**Figure 11: Bulk LC3 levels not influenced by genotype.** **A.** LC3 protein examined by Western blot. Total protein extracted from P0 mouse liver. Proteins visualised by Cy5 fluorescent antibodies binding primary antibodies. **B.** Graph represents total LC3 signal normalised to actin signal as detected using the FIJI image analysis application. Each bar represents four blots, n=3 per genotype per blot, except for *Npc1*<sup>-/-</sup>, which is n=2. Error bars represent standard error.

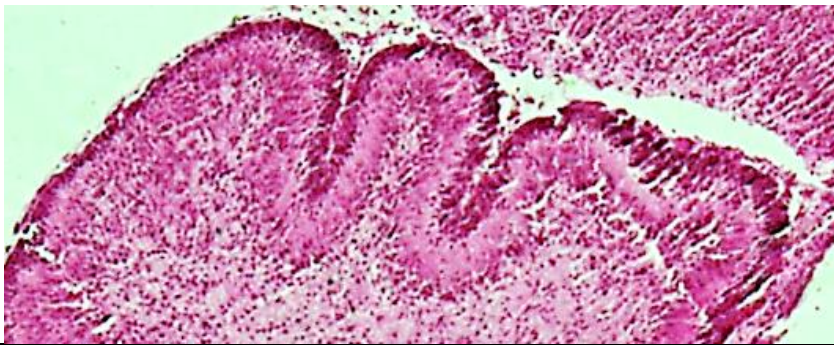
### 2.3.6 Brain pathology is not disrupted in *Npc1*<sup>-/-</sup> *Lpin1*<sup>-/-</sup> mice

The cerebellum is an organ particularly affected in NP-C disease, and is implicated in many early-onset neurodegenerative symptoms, such as hypotonia, dysphagia, and progressive loss of ambulatory skills (Vanier, 2010). Cerebellar dysfunction is just as relevant to disease progression in the mouse model of NP-C disease. For example, the Purkinje cells in the cerebellum are lost beginning from the 6<sup>th</sup> week of life in the *Npc1*<sup>-/-</sup> mouse until the 10<sup>th</sup> week (Higashi, Murayama, Pentchev, & Suzuki, 1993; J. Tanaka, Nakamura, & Mlyawaki, 1988). The cerebellum has not previously been investigated in the *Npc1*<sup>-/-</sup> mouse at P0. Here we conducted a histological analysis cerebellar cortex in the four genotypes. Cortex width and layer formation seems to be consistent between genotypes. Purkinje cells are not distinguishable. The *Npc1*<sup>-/-</sup>*Lpin1*<sup>-/-</sup> appears to have a less distinct granular layer.

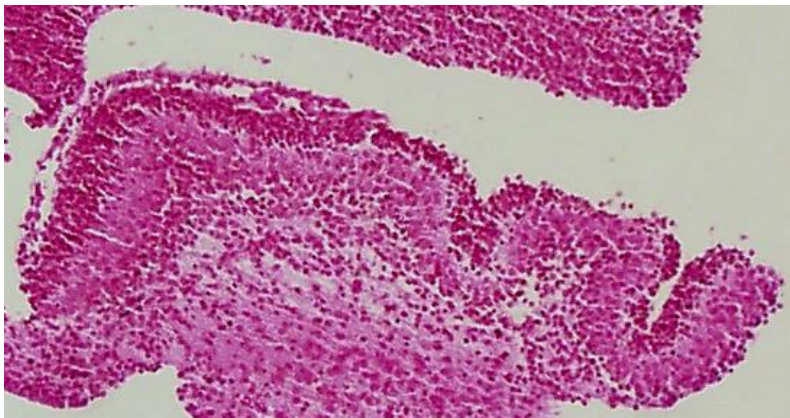
**A**



**B**



**C**



**D**

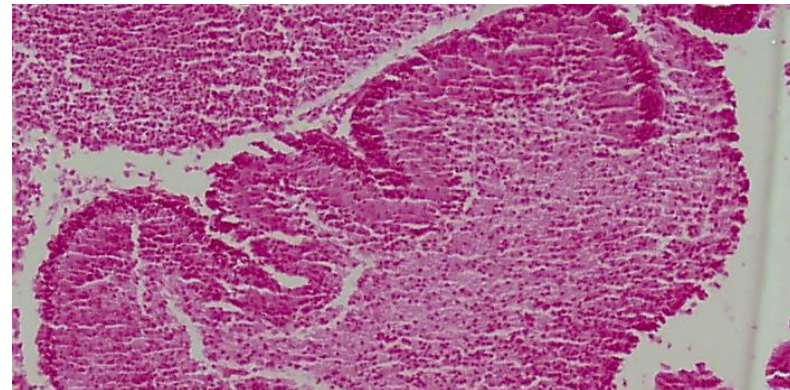


**Figure 12: Cerebellum is intact in *Npc1<sup>-/-</sup>Lpin1<sup>-/-</sup>* mouse.** A. Wild-type B. *Npc1<sup>-/-</sup>* C. *Lpin1<sup>-/-</sup>* D. *Npc1<sup>-/-</sup>Lpin1<sup>-/-</sup>*. Brain hemispheres were fixed in 1.5% paraformaldehyde immediately after dissection and kept in 70% ethanol until processing for microtome. Delafield's hematoxylin counterstained with eosin.

### **2.3.7 Sterol homeostasis in the liver of *Npc1<sup>-/-</sup> Lpin1<sup>-/-</sup>* mice mimics the *Npc1<sup>-/-</sup>* mouse**

Visceral accumulation of free cholesterol is a primary biochemical hallmark of NP-C disease, and in humans this occurs even before birth (Beltroy, Liu, Dietschy, & Turley, 2007). With the deletion of *Npc1* or *Lpin1* alone in mice, the P0 mouse does not harbour a cholesterol load statistically distinguishable from the wild-type (Fig. 14), albeit this may reflect the low sample size. Quantification of free cholesterol in the *Lpin1<sup>-/-</sup>* mouse fell short of significance from wild-type in a two-tailed t-test ( $p = 0.096$ ), however with a greater sample size a more resolute statistic might be observed, which is supported by the recent finding in *C. elegans* that *LPIN1* upregulates SREBP-1 independent of cholesterol (Smulan et al., 2016). In the mouse with both *Npc1* and *Lpin1* deleted, this double mutant is indistinguishable from the *Npc1* mutation alone (Fig. 14).



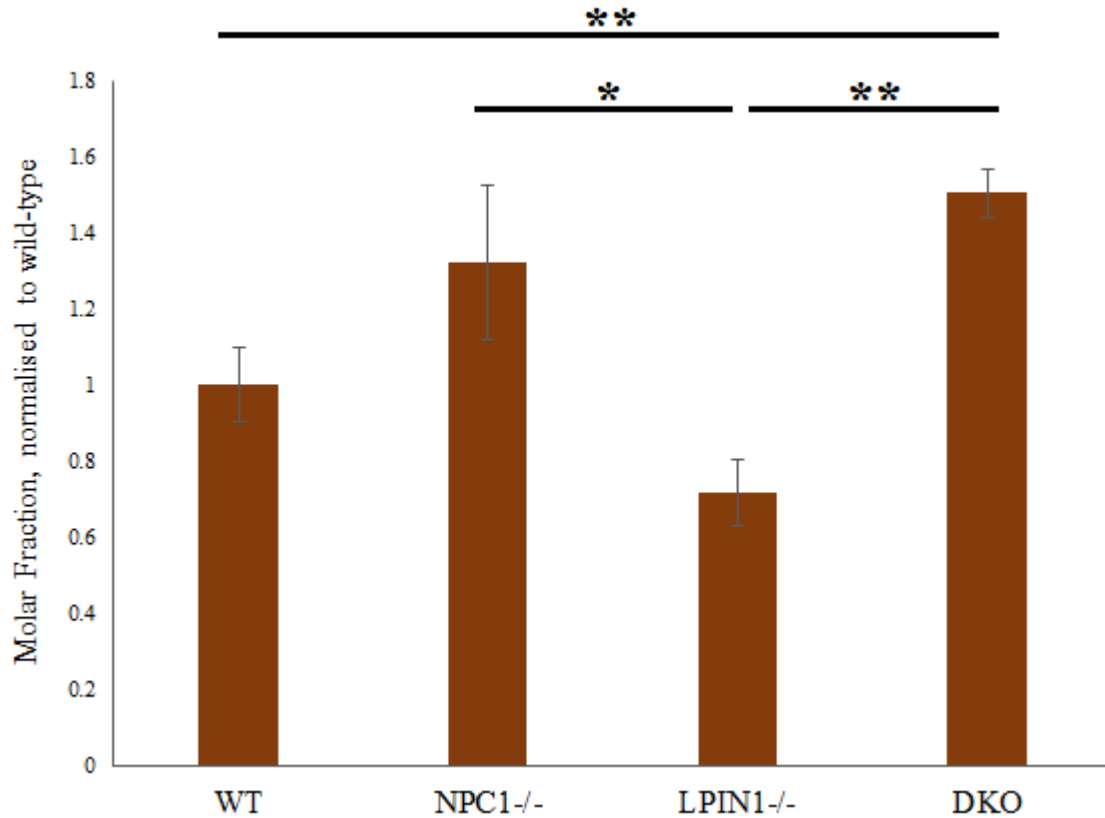


**Figure 13: Free cholesterol is increased in *NPC1*<sup>-/-</sup> and *NPC1*<sup>-/-</sup> *LPIN1*<sup>-/-</sup> mouse liver.** Free cholesterol separation and quantification by reverse-phase HPLC with Applied Biosystems Triple Quadrupole 3200 QTrap. Bars represent molar fraction of total lipid, normalised to the wild-type. Error bars show standard error of normalised values. WT (Wild-Type) n=3, *NPC1*<sup>-/-</sup> n=2 *LPIN1*<sup>-/-</sup> n=4, DKO (Double Knock-out aka *NPC1*<sup>-/-</sup>*LPIN1*<sup>-/-</sup>) n=4. \*p < 0.05; \*\*p<0.01 Student's t-test versus indicated group.

Contrasting the free cholesterol profile, cholesterol ester is significantly diminished in the *Npc1*<sup>-/-</sup> mouse liver compared to WT (Fig. 15). In agreement with the free cholesterol result, cholesterol ester levels in the *Npc1*<sup>-/-</sup>*Lpin1*<sup>-/-</sup> mice mimic the *Npc1*<sup>-/-</sup> mice. In regards to cholesterol ester quantification in the *Lpin1*<sup>-/-</sup> mouse verses wild-type, the Student's t-test returns 0.0510, again just shy of significance. The sterol defect imparted by *Lpin1* loss is therefore less pronounced and seemingly recessive to the *Npc1*<sup>-/-</sup> phenotype.

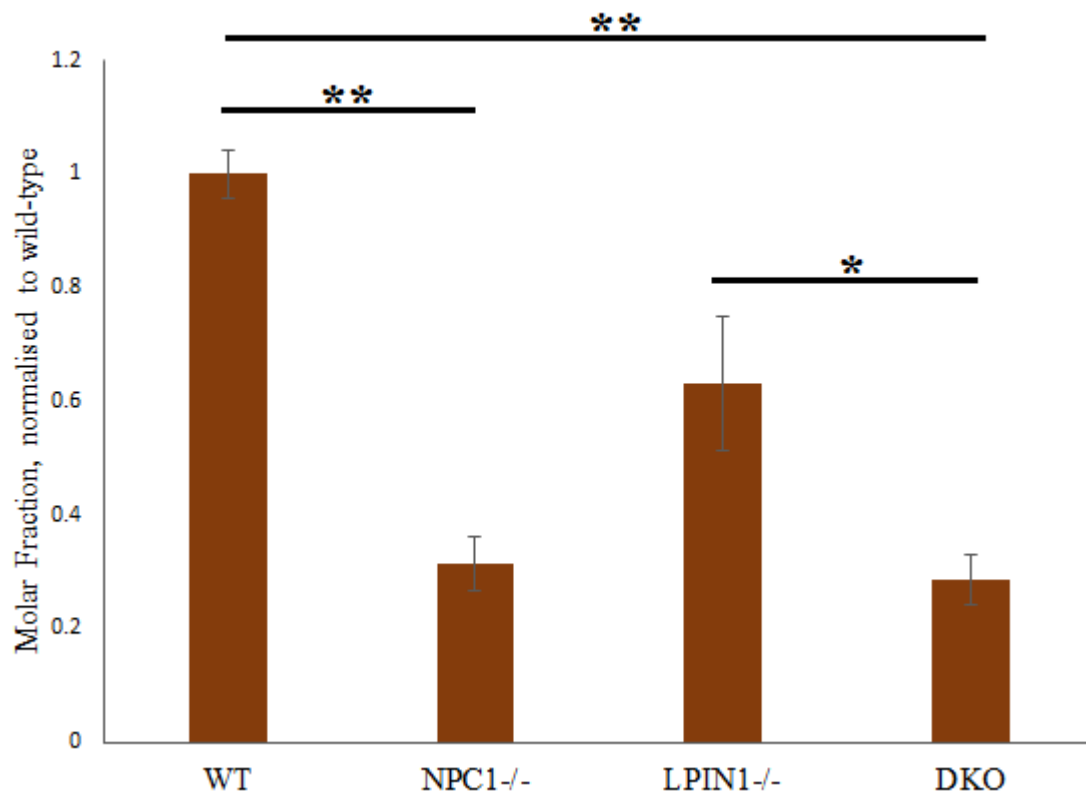


**Figure 14: Cholesterol ester is reduced in *NPC1*<sup>-/-</sup> and *NPC1*<sup>-/-</sup> *LPIN1*<sup>-/-</sup> mouse liver.** Cholesterol-ester quantification by reverse-phase HPLC with Applied Biosystems Triple Quadrupole 3200 QTrap. Bars represent molar fraction of total lipid, normalised to the wild-type. Error bars show standard error of normalised values. WT (Wild-Type) n=3, *Npc1*<sup>-/-</sup> n=2 *Lpin1*<sup>-/-</sup> n=4, DKO (Double Knock-out aka *Npc1*<sup>-/-</sup>*Lpin1*<sup>-/-</sup>) n=4. \*p < 0.05; \*\*p<0.01 Student's t-test versus indicated group.

### 2.3.8 Sterol homeostasis in the brain of *Npc1*<sup>-/-</sup> *Lpin1*<sup>-/-</sup> mice is indistinguishable from *Npc1*<sup>-/-</sup> and *Lpin1*<sup>-/-</sup> mice

As has been previously observed in the human brain in all stages and manifestations, the level of free cholesterol in the mouse brain is unaffected by loss of *Npc1* (Vanier, 2015). It also appears that *Lpin1* is not consequential to free cholesterol content in the neonate mouse brain.

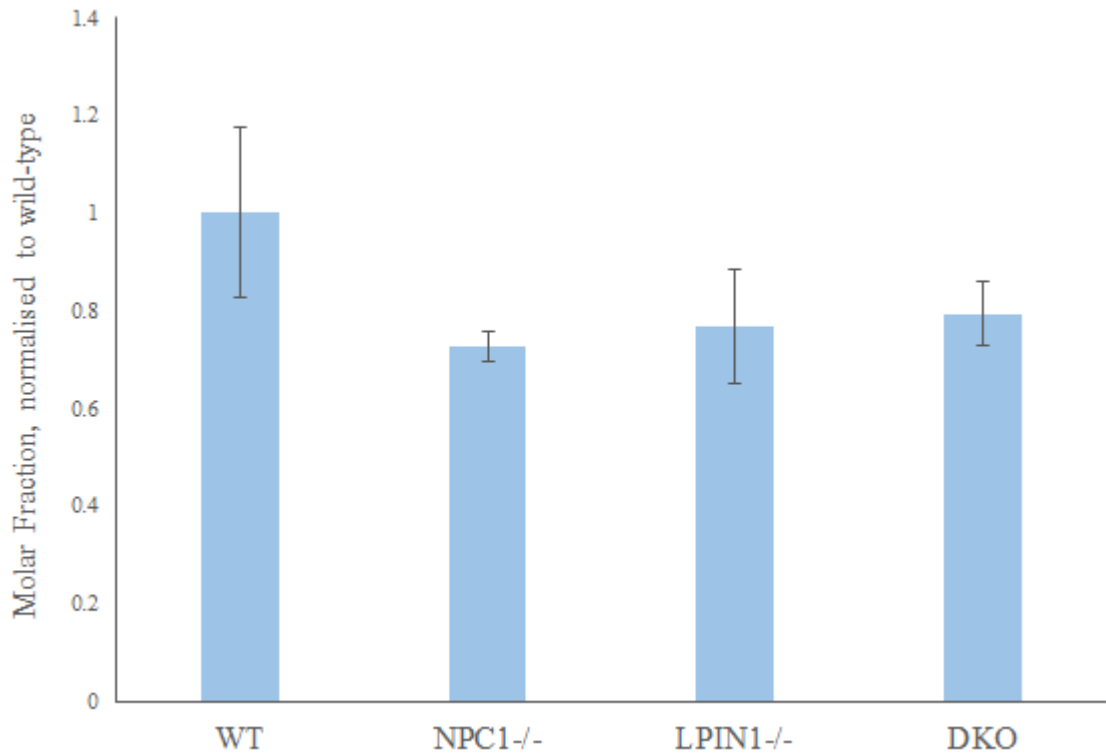


**Figure 15: Free cholesterol abundance in mouse brain is unaffected by deletion of *NPC1* and *LPIN1*.** Free cholesterol quantification by reverse-phase HPLC with Applied Biosystems Triple Quadrupole 3200 QTrap. Bars represent molar fraction of total lipid, normalised to the wild-type. Error bars show standard error of normalised values. WT (Wild-Type) n=3, *Npc1*<sup>-/-</sup> n=2, *Lpin1*<sup>-/-</sup> n=4, DKO (Double Knock-out aka *Npc1*<sup>-/-</sup>*Lpin1*<sup>-/-</sup>) n=4.

Cholesterol ester abundance is reduced in the *Npc1*<sup>-/-</sup>, *Lpin1*<sup>-/-</sup> and *Npc1*<sup>-/-</sup>*Lpin1*<sup>-/-</sup> mice compared to wild-type (Fig. 17). Unlike the systematic cholesterol supply, neural cholesterol is hypothesised to be supplied unesterified by glia-derived APOE, and so neural cholesterol ester is generated from endosomal cholesterol (Aquil et al., 2011) and this would require cholesterol efflux by NPC1.

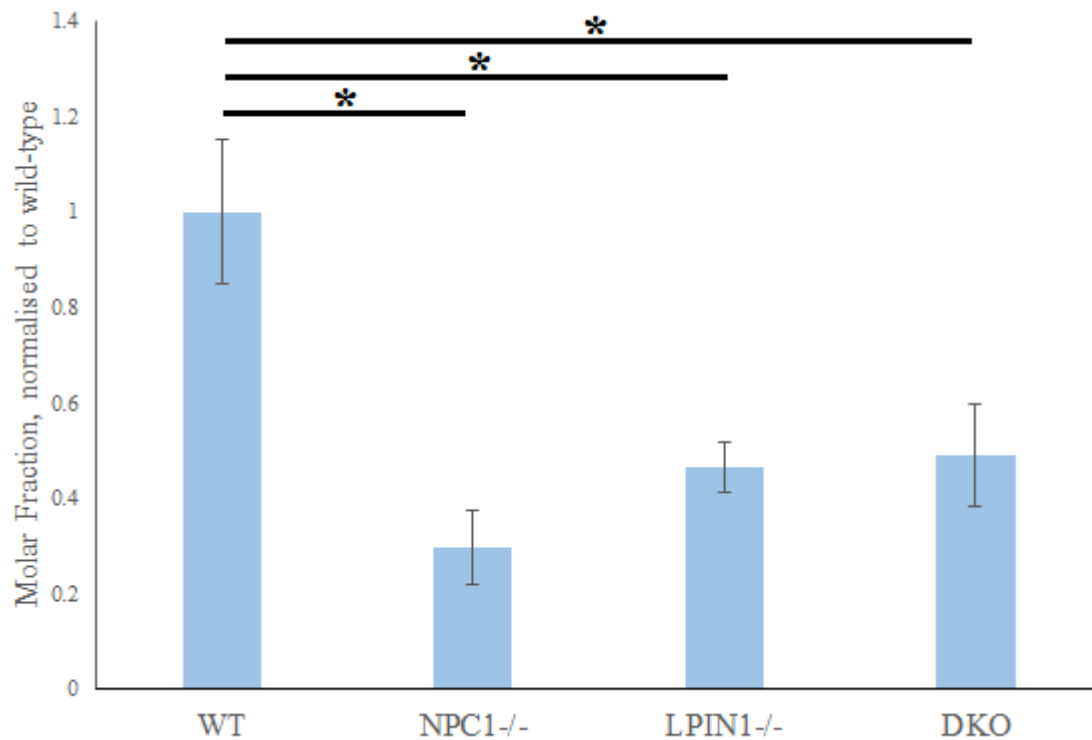


**Figure 16: Cholesterol ester is reduced in *NPC1*<sup>-/-</sup> and *LPIN1*<sup>-/-</sup> mice.** Cholesterol-ester quantification by reverse-phase HPLC with Applied Biosystems Triple Quadrupole 3200 QTrap. Bars represent molar fraction of total lipid, normalised to the wild-type. Error bars show standard error of normalised values. WT (Wild-Type) n=3, *NPC1*<sup>-/-</sup> n=2, *LPIN1*<sup>-/-</sup> n=4, DKO (Double Knock-out aka *NPC1*<sup>-/-</sup>*LPIN1*<sup>-/-</sup>) n=4. \*p < 0.05, Student's t-test versus indicated group.

### 2.3.9 Sphingolipid homeostasis is not altered by *Lpin1* deletion in the *Npc1*<sup>-/-</sup> mice in the liver

In the perinatal onset form on NP-C disease, sphingomyelin (SM) tends not to have begun accumulating, except in severe cases (Vanier, 1999). Here we see lactosylceramide (LacCer) is greatly increased in the liver of *Npc1*<sup>-/-</sup> mice (Fig. 18). It has been shown that oxidised-LDL-treated cells will over produce LacCer, which acts as a second messenger to various pathways and involving apoptosis and inflammation (Chatterjee & Pandey, 2008). Additional deletion of the *Lpin1* gene does not modify this prominent hepatic LacCer

accumulation (Fig. 20), and *Lpin1* deletion alone has no quantified effect on sphingolipids in the P0 liver (Fig.19).

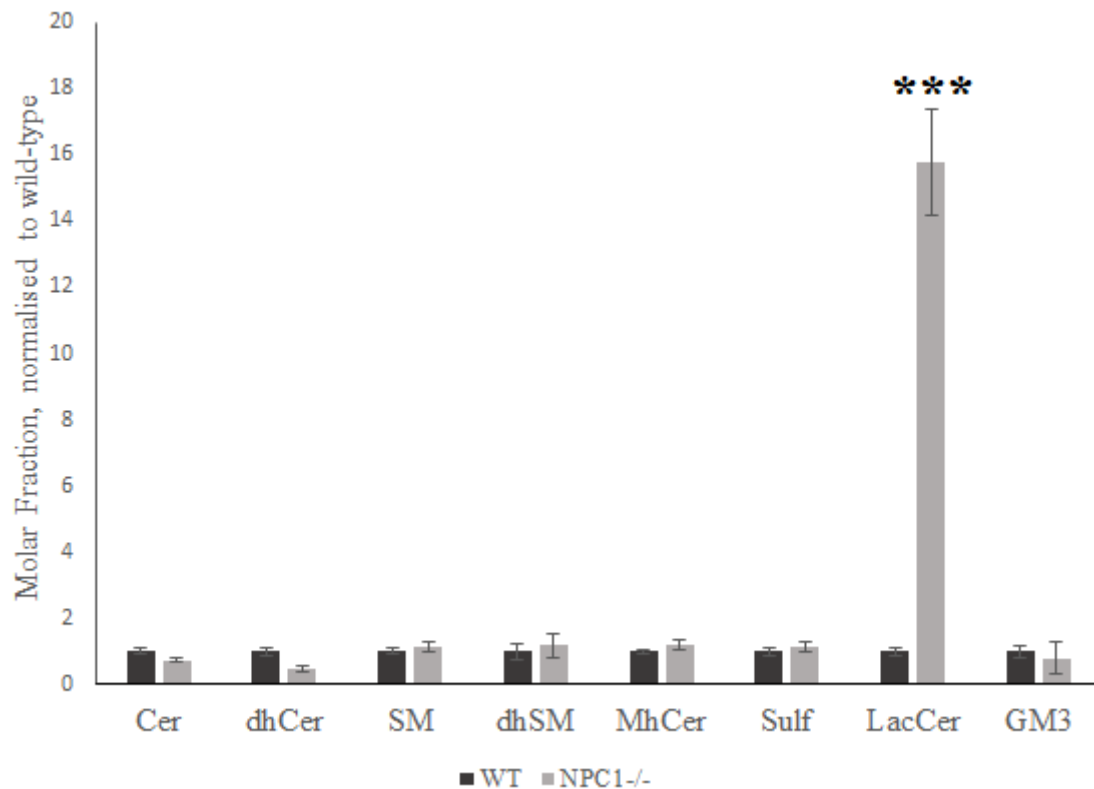


**Figure 17: Among sphingolipids, LacCer increases 15-fold in the *NPC1*<sup>-/-</sup> mouse liver.** Cer: ceramide, dhCer: dihydroceramide, SM: sphingomyelin dhSM: dihydrosphingomyelin Sulf: sulfatide, LacCer: lactosylceramide. Sphingolipid quantification by normal-phase HPLC with Applied Biosystems Triple Quadrupole 3200 QTrap . Bars represent molar fraction of total lipid, normalised to the wild-type. Error bars show standard error of normalised values. WT (Wild-Type) n=3, *NPC1*<sup>-/-</sup> n=2, *LPIN1*<sup>-/-</sup> n=4, DKO (Double Knock-out aka *NPC1*<sup>-/-</sup>*LPIN1*<sup>-/-</sup>) n=4. \*\*\*p<0.005, Student's t-test versus appropriate wild-type.

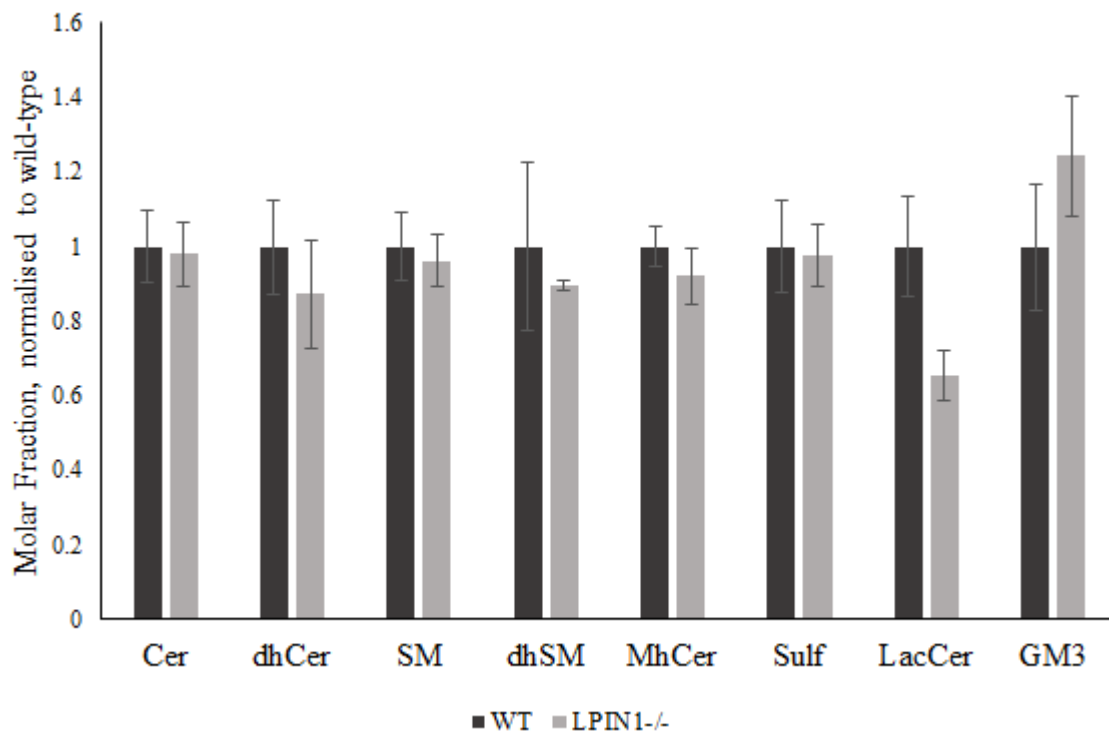


**Figure 18: Deletion of *LPIN1*<sup>-/-</sup> in mouse does not modify liver sphingolipid profile.** Cer: ceramide, dhCer: dihydroceramide, SM: sphingomyelin dhSM: dihydrosphingomyelin Sulf: sulfatide, LacCer: lactosylceramide. Sphingolipid quantification by normal-phase HPLC with Applied Biosystems Triple Quadrupole 3200 QTrap. Bars represent molar fraction of total lipid, normalised to the wild-type. Error bars show standard error of normalised values. WT (Wild-Type) n=3, *NPC1*<sup>-/-</sup> n=2 *LPIN1*<sup>-/-</sup> n=4, DKO (Double Knock-out aka *NPC1*<sup>-/-</sup>*LPIN1*<sup>-/-</sup>) n=4.

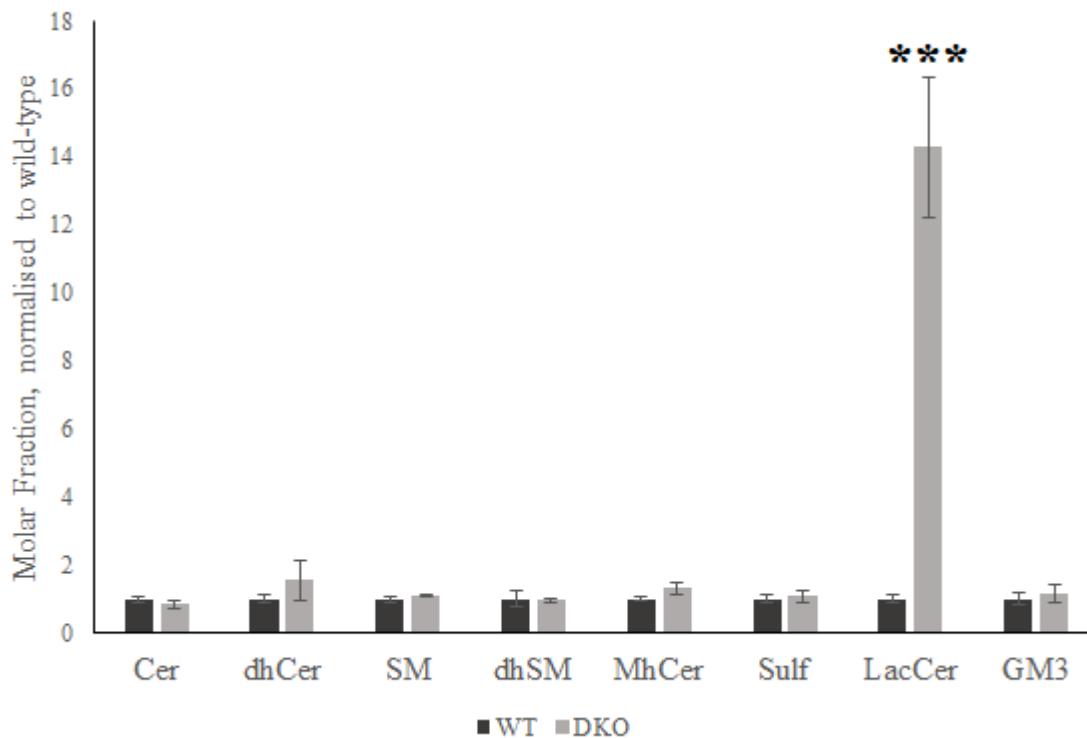


**Figure 19: Among sphingolipids, LacCer is increased 15-fold in the *NPCI<sup>-/-</sup>LPINI<sup>-/-</sup>* mouse liver.** Cer: ceramide, dhCer: dihydroceramide, SM: sphingomyelin dhSM: dihydrosphingomyelin Sulf: sulfatide, LacCer: lactosylceramide. Sphingolipid quantification by normal-phase HPLC with Applied Biosystems Triple Quadrupole 3200 QTrap. Bars represent molar fraction of total lipid, normalised to the wild-type. Error bars show standard error of normalised values. WT (Wild-Type) n=3, *NPCI<sup>-/-</sup>* n=2, *LPINI<sup>-/-</sup>* n=4, DKO (Double Knock-out aka *NPCI<sup>-/-</sup>LPINI<sup>-/-</sup>*) n=4. \*\*\*p<0.005, Student's t-test versus appropriate wild-type.

LacCer is suspected to have multiple cholesterol homeostatic effects, with inhibition of lactosylceramide synthase influencing expression of SREBP2 and cholesterol efflux agents (Furukawa et al., 2015), which offers the possibility that elevated LacCer may be involved in cholesterol dysregulation. Inability to generate lactosylceramide is embryonically lethal; fetal growth is delayed by a day and death occurs due to suspected failure of placenta or cardiac development at E10.5 (Kumagai et al., 2009). Elevated LacCer levels persist into adulthood in the *Npc1<sup>-/-</sup>* mouse (te Vrugte et al., 2004).

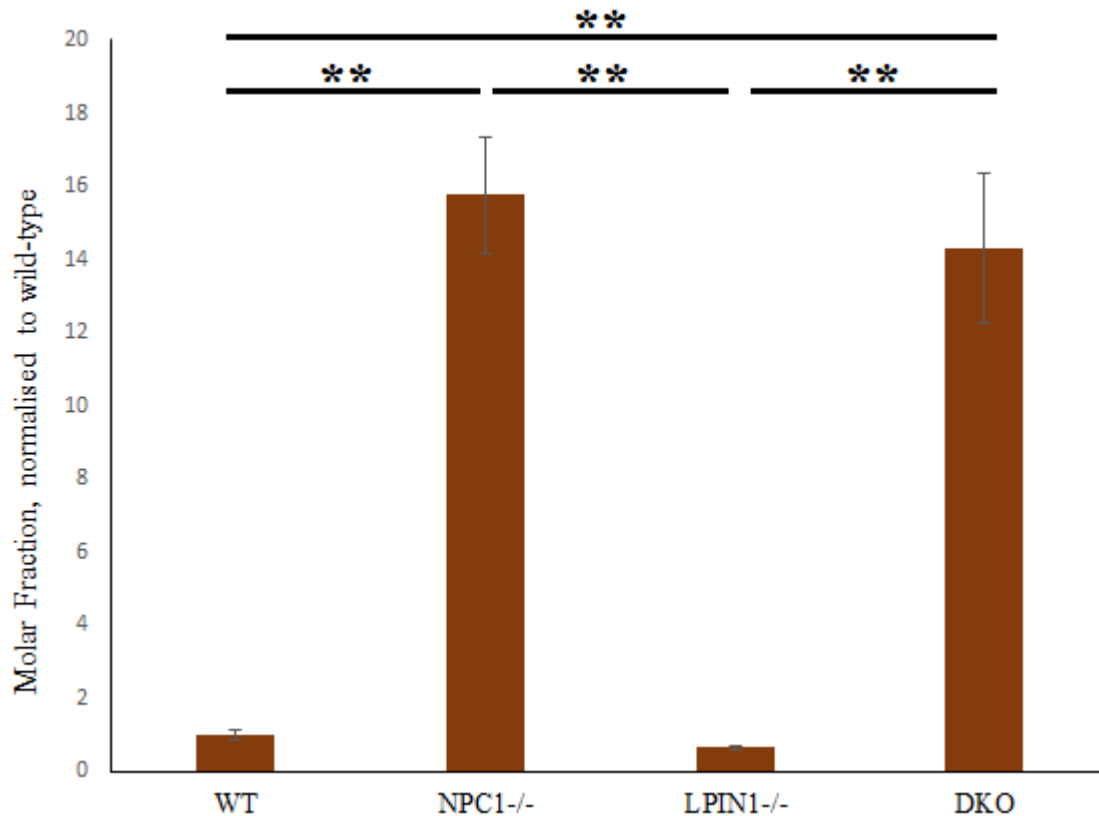


**Figure 20: Loss of *Npc1* results in 15-fold increase in LacCer in mouse liver, *Lpin1* loss does not modify lactosylceramide profile.** LacCer quantification by normal-phase HPLC with Applied Biosystems Triple Quadrupole 3200 QTrap. Bars represent molar fraction of total lipid, normalised to the wild-type. Error bars show standard error of normalised values. WT (Wild-Type) n=3, *Npc1*<sup>-/-</sup> n=2, *Lpin1*<sup>-/-</sup> n=4, DKO (Double Knock-out aka *Npc1*<sup>-/-</sup>*Lpin1*<sup>-/-</sup>) n=4. \*\*p<0.01, Student's t-test versus indicated group.

### 2.3.10 Sphingolipid homeostasis is not altered by *Lpin1* deletion in *Npc1*<sup>-/-</sup> mice in the brain

Detectable accumulation of GM3 has been reported in the NP-C disease human brain as early as 3 months from birth (Vanier, 1999), but does not differ in the P0 mouse (Fig. 22). GM3 makes up less than 1% of murine gangliosides, so minor changes may be difficult to detect, and the nature of GM3 and GM2 accumulation is not identical between mice and humans (Walkley & Vanier, 2009). Although dihydrosphingomyelin (dhSM) and



dihydroceramide (dhCer) visually appear to have been reduced by loss of *Npc1*<sup>-/-</sup>, this is not supported by t-test, nor is the spike in LacCer in the *Npc1*<sup>-/-</sup> mouse brain.

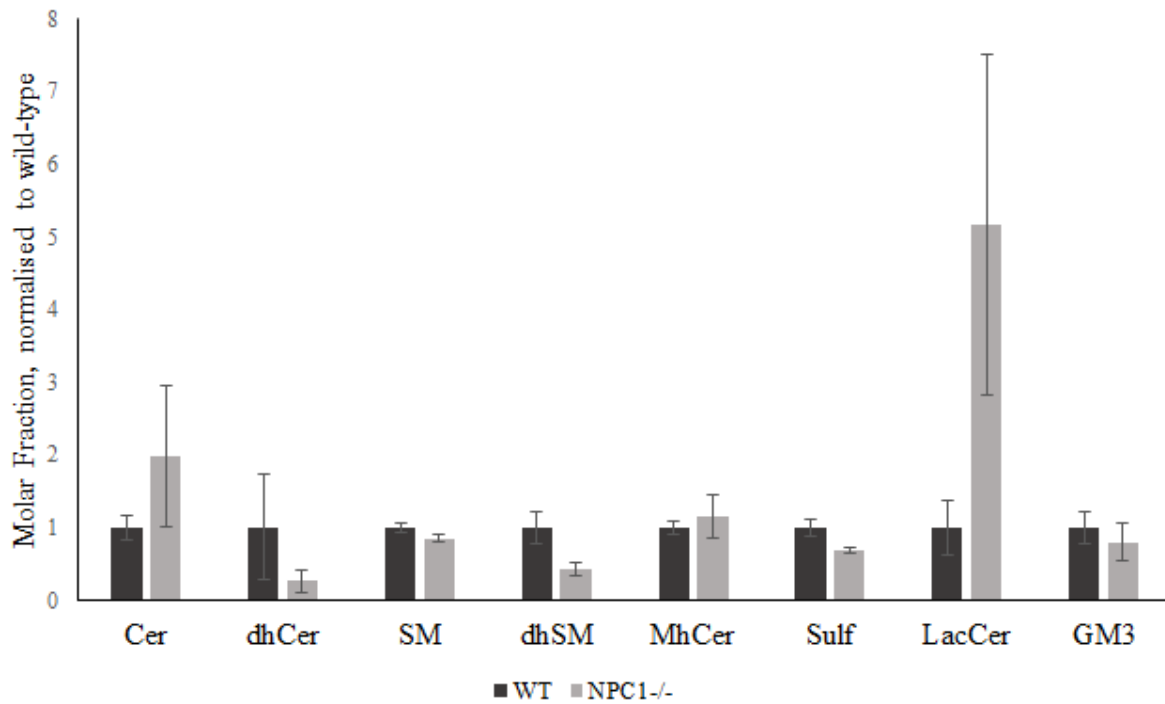


**Figure 21: Sphingolipid profile not significantly altered by loss of *Npc1* in mouse brain.** Cer: ceramide, dhCer: dihydroceramide, SM: sphingomyelin, dhSM: dihydrosphingomyelin, MhCer: monohexosylceramide, Sulf: sulfatide, LacCer: lactosylceramide. Sphingolipid quantification by normal-phase HPLC with Applied Biosystems Triple Quadrupole 3200 QTrap. Bars represent molar fraction of total lipid, normalised to the wild-type. Error bars show standard error of normalised values. WT (Wild-Type) n=3, *Npc1*<sup>-/-</sup> n=2.

Sulfatide abundance was reduced in the *Lpin1*<sup>-/-</sup> mouse (Fig.23), which has a role in maintaining organisation of nodes of Ranvier (Honke, 2013). Dysregulation of sulfatide abundance has been implicated in neurodegenerative conditions; knockout of sulfatide synthesis enzyme CST will not change the visible structure of myelinated axons, but will resoundingly impair the conduction of action potentials (Coetzee et al., 1996). *Lpin1* deletion

has also been observed to drive demyelination as a consequence of PA accumulation, although there is no clear connection between these observations. Further, the decrease in sulfatide is lost in the *Npc1<sup>-/-</sup>Lpin1<sup>-/-</sup>* mouse brain (Fig. 25). Again, although *Lpin1<sup>-/-</sup>* mice brains appear to decrease in multiple ceramides: Cer, dhCer, and LacCer, as well as dhSM, the decrease implied by the bars is not statistically supported.

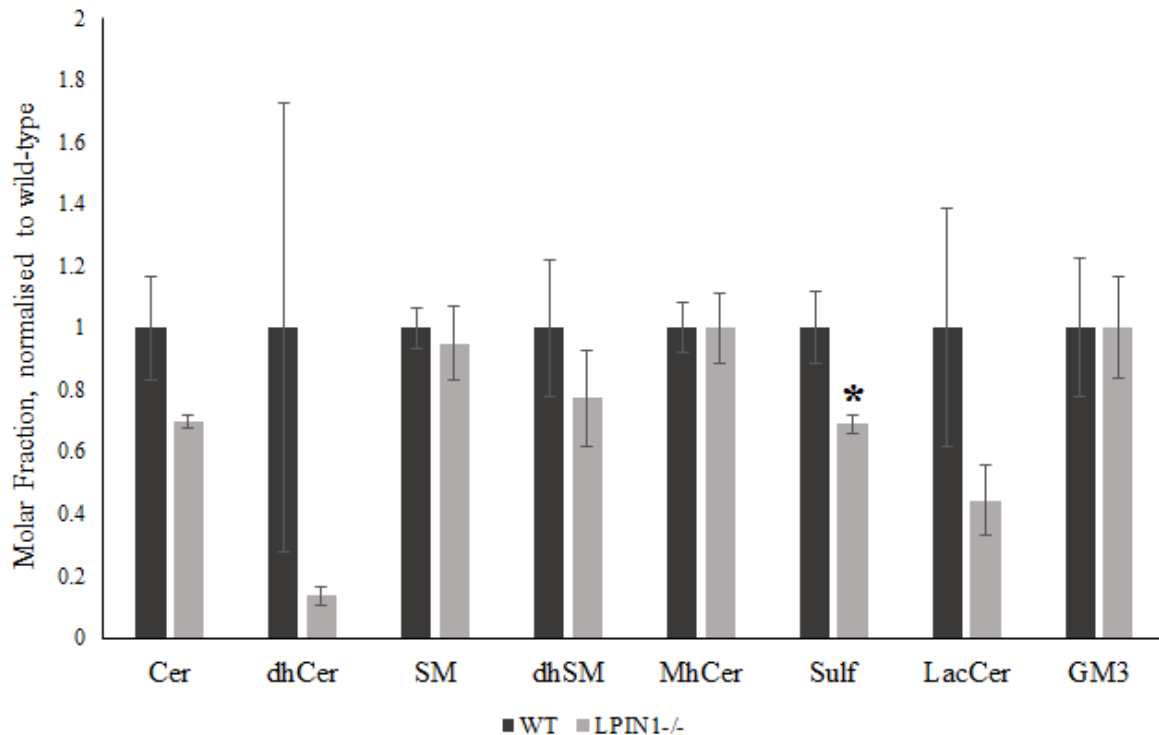


**Figure 22: Among sphingolipids, sulfatide is modestly reduced in the *Lpin1<sup>-/-</sup>* mouse brain.** Cer: ceramide, dhCer: dihydroceramide, SM: sphingomyelin, dhSM: dihydrosphingomyelin, MhCer: monohexosylceramide, Sulf: sulfatide, LacCer: lactosylceramide. Sphingolipid quantification by normal-phase HPLC with Applied Biosystems Triple Quadrupole 3200 QTrap. Bars represent molar fraction of total lipid, normalised to the wild-type. Error bars show standard error of normalised values. WT (Wild-Type) n=3, *Lpin1<sup>-/-</sup>* n=4. \*p<0.05, Student's t-test versus appropriate wild-type.

The *Npc1<sup>-/-</sup>Lpin1<sup>-/-</sup>* mouse sees a significant increase in SM and monohexosylceramide (MhCer) in the brain (Fig.24). SM is a biochemical hallmark of NP-C disease, which in humans

accumulate in the spleen and liver from birth, and accumulates in the brain later on in disease progression (Vanier & Millat, 2003).

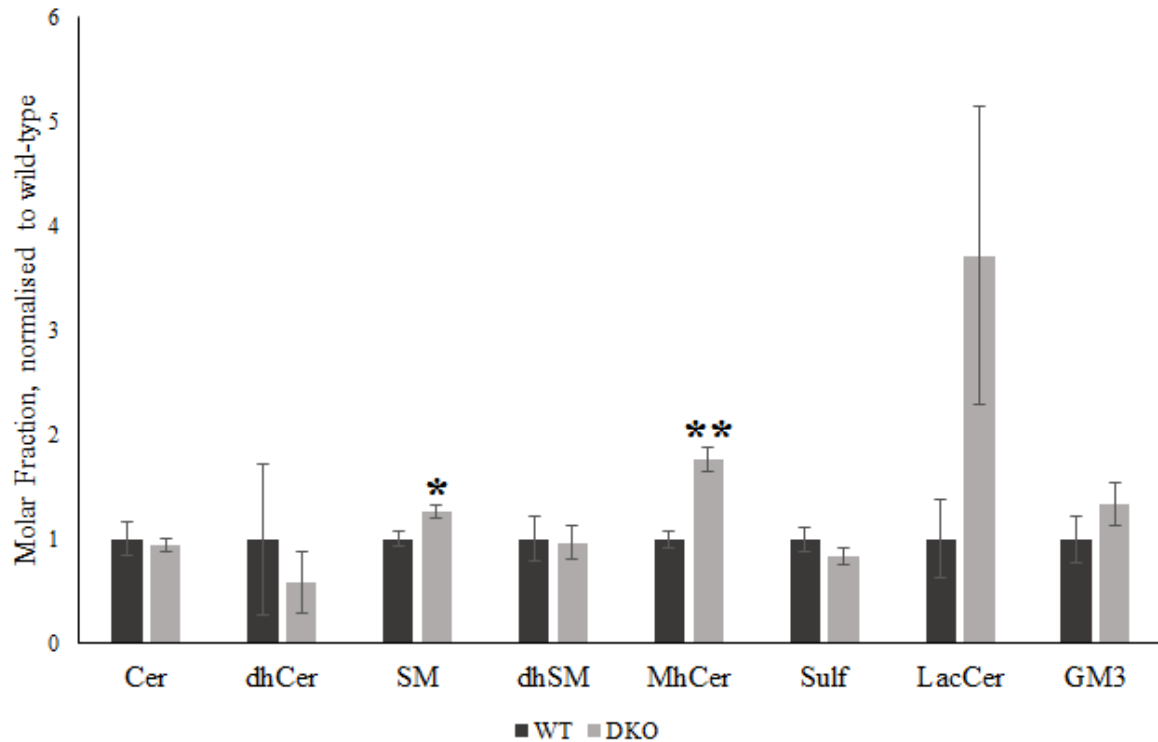


**Figure 23: SM and MhCer increased in *Npc1<sup>-/-</sup>Lpin1<sup>-/-</sup>* mouse brain.** Cer: ceramide, dhCer: dihydroceramide, SM: sphingomyelin dhSM: dihydrosphingomyelin, MhCer: monohexosylceramide, Sulf: sulfatide, LacCer: lactosylceramide. Sphingolipid quantification by normal-phase HPLC with Applied Biosystems Triple Quadrupole 3200 QTrap. Bars represent molar fraction of total lipid, normalised to the wild-type. Error bars show standard error of normalised values. WT (Wild-Type) n=3, DKO (Double Knock-out aka *Npc1<sup>-/-</sup>Lpin1<sup>-/-</sup>*) n=4. \*p<0.05, \*\*p<0.01, Student's t-test versus appropriate wild-type.

The p value for the difference in MhCer between *Npc1<sup>-/-</sup>* and *Npc1<sup>-/-</sup>Lpin1<sup>-/-</sup>* mice (Student's two-tailed t-test) is p = 0.0996, and between *Lpin1<sup>-/-</sup>* and *Npc1<sup>-/-</sup>Lpin1<sup>-/-</sup>* mice, p<0.01 (Fig.25). If MhCer was confirmed to be increased in *Npc1<sup>-/-</sup>Lpin1<sup>-/-</sup>* specifically, the effect could be regarded as epistatic. A 2015 study identified mouse alkaline ceramidase 3 (ACER3)

as a protective agent in the brain, hydrolysing age-associated ceramides including MhCer (K. Wang et al., 2015). *Acer3* knockout resulted in Purkinje cell loss and an insidious alteration in the brain sphingolipid profile. This suggests both that MhCer accumulation is a potential indicator of poor prognosis, and if so, that ceramidase manipulation may be beneficial.

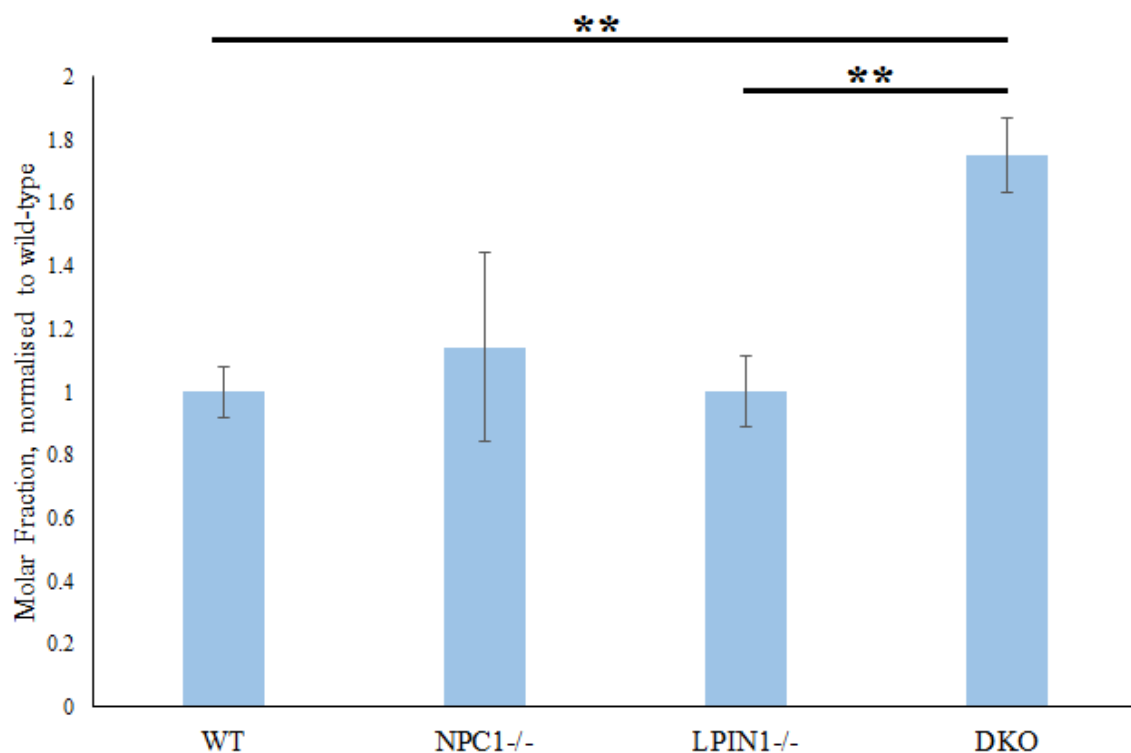


**Figure 24: MhCer accumulates in the *Npc1*<sup>-/-</sup>*Lpin1*<sup>-/-</sup> mouse brain.** MhCer quantification by normal-phase HPLC with Applied Biosystems Triple Quadrupole 3200 QTrap. Bars represent molar fraction of total lipid, normalised to the wild-type. Error bars show standard error of normalised values. WT (Wild-Type) n=3, *Npc1*<sup>-/-</sup> n=2 *Lpin1*<sup>-/-</sup> n=4, DKO (Double Knock-out aka *Npc1*<sup>-/-</sup>*Lpin1*<sup>-/-</sup>) n=4. \*\*p<0.01, Student's t-test versus indicated group. Student's t-test between *Npc1*<sup>-/-</sup> and *Npc1*<sup>-/-</sup>*Lpin1*<sup>-/-</sup> mice: p=0.10.

In the P0 mouse, brain LacCer was more abundant by 5-fold in *Npc1*<sup>-/-</sup> and 4-fold in *Npc1*<sup>-/-</sup>*Lpin1*<sup>-/-</sup> mice than in *Lpin1*<sup>-/-</sup> mice (Fig. 26). The wild-type mouse could not be said to

have a statistically different quantity of LacCer to the *Npc1*<sup>-/-</sup>, *Lpin1*<sup>-/-</sup> or *Npc1*<sup>-/-</sup>*Lpin1*<sup>-/-</sup> groups. LacCer is therefore increased in both the liver and brain with loss of *Npc1*<sup>-/-</sup>, at least compared to *Lpin1*<sup>-/-</sup> mice.

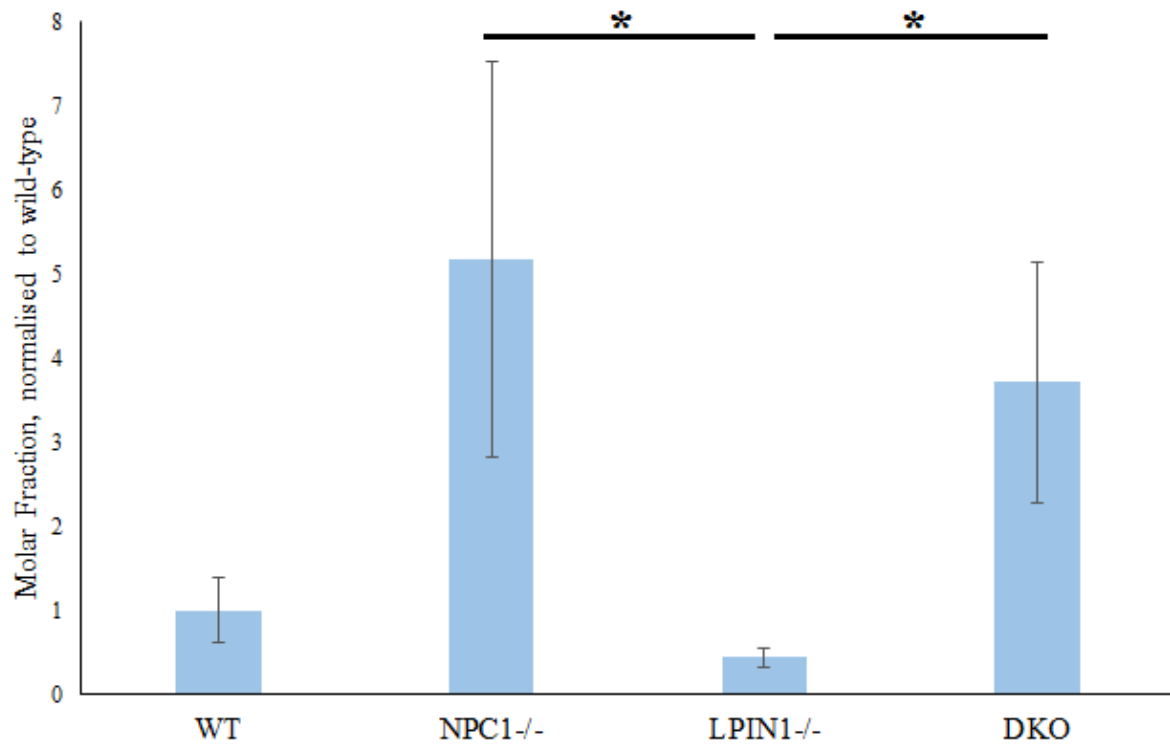


**Figure 25: LacCer accumulates with loss of *Npc1*, which is not modified by loss of *Lpin1* in mouse brain.**

Lactosylceramide quantification by normal-phase HPLC with Applied Biosystems Triple Quadrupole 3200 QTrap. Bars represent molar fraction of total lipid, normalised to the wild-type. Error bars show standard error of normalised values. WT (Wild-Type) n=3, *Npc1*<sup>-/-</sup> n=2, *Lpin1*<sup>-/-</sup> n=4, DKO (Double Knock-out aka *Npc1*<sup>-/-</sup>*Lpin1*<sup>-/-</sup>) n=4. \*p<0.05, Student's t-test versus indicated group.

### 2.3.11 Phospholipid homeostasis is regulated unexpectedly in the liver of *Npc1*<sup>-/-</sup> *Lpin1*<sup>-/-</sup> mice

Loss of *Npc1* resulted in a 60% reduction on phosphatidylserine (PS) and a 40% reduction in phosphatidylglycerol (PG) (Fig. 27). PC, phosphatidylethanolamine (PE) and

phosphatidylinositol (PI) all remained unaffected by loss of Lpin1 ( $p = 0.99$ ,  $0.14$  and  $0.12$ , respectively). For PA however, with a statistical score of ( $p = 0.055$ ), it is probable that there was a genuine reduction in *Npc1*<sup>-/-</sup> mice.

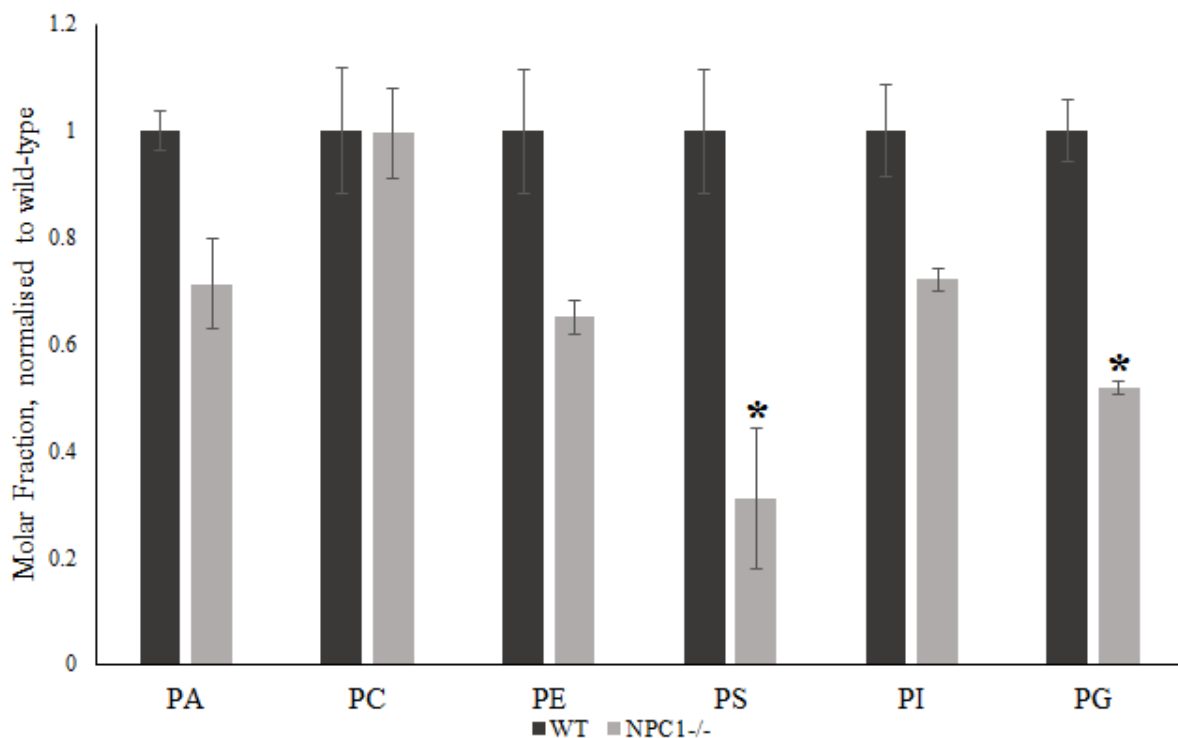


**Figure 26: PS and PG reduced in *Npc1*<sup>-/-</sup> mouse liver.** PA: Phosphatidic acid, PC: Phosphatidylcholine, PE: Phosphatidylethanolamine, PS: Phosphatidylserine, PI: Phosphatidylinositol, PG: Phosphatidylglycerol. Phospholipid quantification by normal-phase HPLC with Applied Biosystems Triple Quadrupole 3200 QTrap. Bars represent molar fraction of total lipid, normalised to the wild-type. Error bars show standard error of normalised values. WT (Wild-Type)  $n=3$ , *Npc1*<sup>-/-</sup>  $n=2$ . \* $p<0.05$ , Student's t-test versus appropriate wild-type.

*Lpin1*<sup>-/-</sup> mice showed no upheavals in phospholipid levels (Fig. 28), ( $p = 0.819$ ) which was astonishing, the PAP activity of the LPIN1 enzyme converts PA to DAG (Donkor et al., 2007), and intuitively, loss of *Lpin1*<sup>-/-</sup> would result in reduced metabolism of PA, resulting in its accumulation. This suggests PA levels are kept at a regular level *in utero* and in the neonatal stage of life, perhaps due to the placental connection to the *Npc1*<sup>+/-</sup>*Lpin1*<sup>+/-</sup> mother.

Alternatively, PA may be readily consumed in non-LPIN1 pathways for the generation of various glycerolipids (Athenstaedt & Daum, 1999). The demand for PA during embryonic development may prevent a toxic accumulation of PA until post-partum.

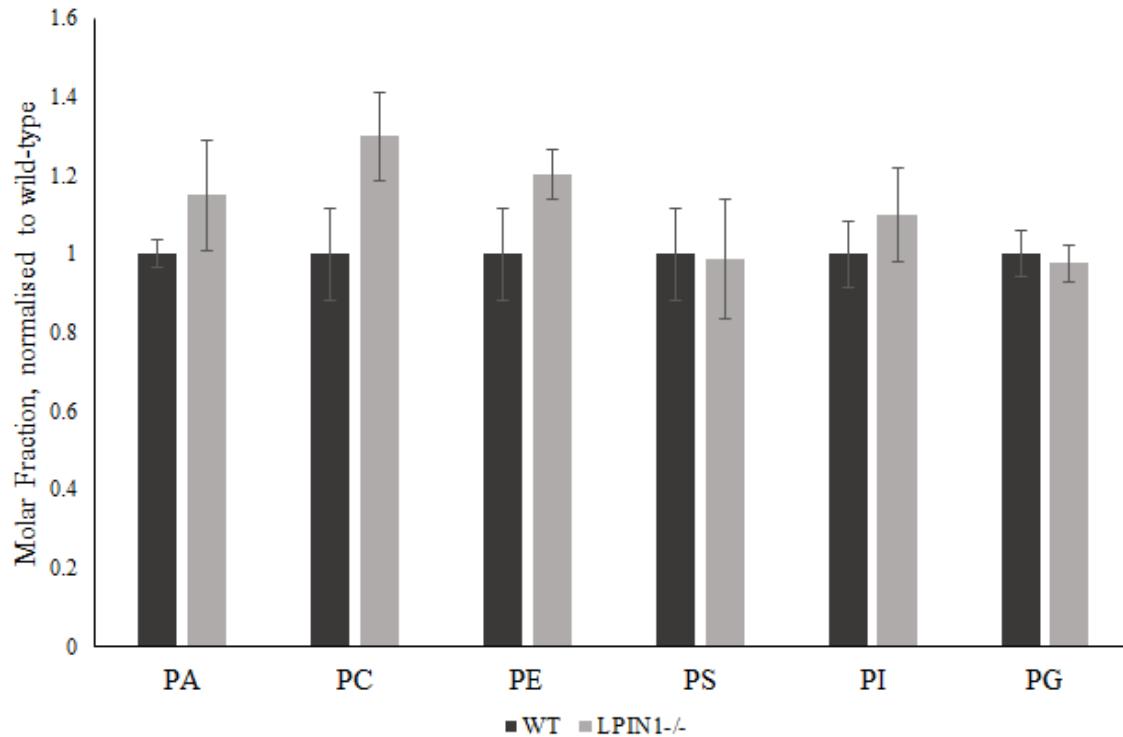


**Figure 27: Abundance of investigated phospholipids unaltered by deletion of *Lpin1* in mouse liver.** PA: Phosphatidic acid, PC: Phosphatidylcholine, PE: Phosphatidylethanolamine, PS: Phosphatidylserine, PI: Phosphatidylinositol, PG: Phosphatidylglycerol. Phospholipid quantification by normal-phase HPLC with Applied Biosystems Triple Quadrupole 3200 QTrap. Bars represent molar fraction of total lipid, normalised to the wild-type. Error bars show standard error of normalised values. WT (Wild-Type) n=3, *Lpin1*<sup>-/-</sup> n=4.

Between wild-type mice and *Npc1*<sup>-/-</sup>*Lpin1*<sup>-/-</sup> mice, liver PG was decreased ( $p = 0.019$ ). (Fig.30) The differences in quantified hepatic PA and PE between wild-type and *Npc1*<sup>-/-</sup>*Lpin1*<sup>-/-</sup> liver were not significant ( $p = 0.051$  and  $p = 0.064$ , respectively), but were close enough to the threshold of significance that it is probable that they could be identified as significant if this experiment was repeated with a greater sample size. Typically, the *Npc1*<sup>-/-</sup>*Lpin1*<sup>-/-</sup> mouse lipid

profile reflects the *Npc1*<sup>-/-</sup> profile. From this it could be interpreted that the impact of *Lpin1* knockout is of a lesser magnitude, or is downstream of, the effects that result from *Npc1* knockout.

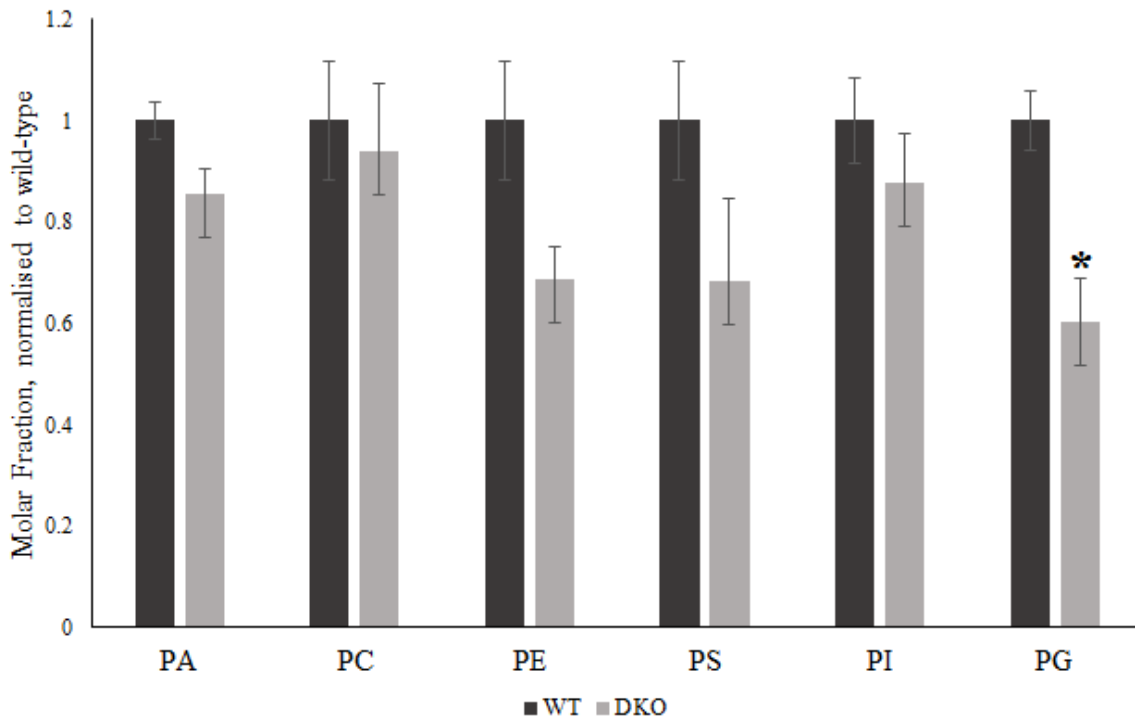


**Figure 28: PE and PG reduced in *Npc1*<sup>-/-</sup>*Lpin1*<sup>-/-</sup> mouse liver.** PA: Phosphatidic acid, PC: Phosphatidylcholine, PE: Phosphatidylethanolamine, PS: Phosphatidylserine, PI: Phosphatidylinositol, PG: Phosphatidylglycerol. Phospholipid quantification by normal-phase HPLC with Applied Biosystems Triple Quadrupole 3200 QTrap. Bars represent molar fraction of total lipid, normalised to the wild-type. Error bars show standard error of normalised values. WT (Wild-Type) n=3, DKO (aka *Npc1*<sup>-/-</sup>*Lpin1*<sup>-/-</sup> n=4. \*p<0.05, Student's t-test versus appropriate wild-type.

By examination of the PE variants, the plasmalogen forms reported similar statistics to their non-plasmalogen counterparts (Fig. 30); PE and PEp both exist in statistically higher concentrations in *Lpin1*<sup>-/-</sup> mice compared to *Npc1*<sup>-/-</sup> and *Npc1*<sup>-/-</sup>*Lpin1*<sup>-/-</sup> mice, although PE is consistently 4 times as abundant as PEp. The abundance of LPEp in the *Npc1*<sup>-/-</sup>*Lpin1*<sup>-/-</sup> group is striking (p = 0.00038, p = 0.010 and p = 0.00020 against wild-type, *Npc1*<sup>-/-</sup> mouse and *Lpin1*<sup>-/-</sup>, respectively). LPEp is a plasmalogen that has an important role in the thymus as a self-



antigen for natural killer T cells (Ni et al., 2014). Plasmalogens in general also will imbed in cell membranes (particularly neural membranes) and serve an antioxidant protective role (Hoffman-Kuczynski & Reo, 2005), however the more salient concern is synthesis rather than function, for LPEp along with all other plasmalogens are manufactured in a convoluted process that occurs at the liver (Nagan & Zoeller, 2001). However, once synthesised, plasmalogens are typically transported from the liver, with the liver typically having the lowest plasmalogen levels among organs (Braverman & Moser, 2012), the large spike in the *Npc1<sup>-/-</sup>Lpin1<sup>-/-</sup>* liver could suggest upregulated LPEp, or failure of a transport mechanism.

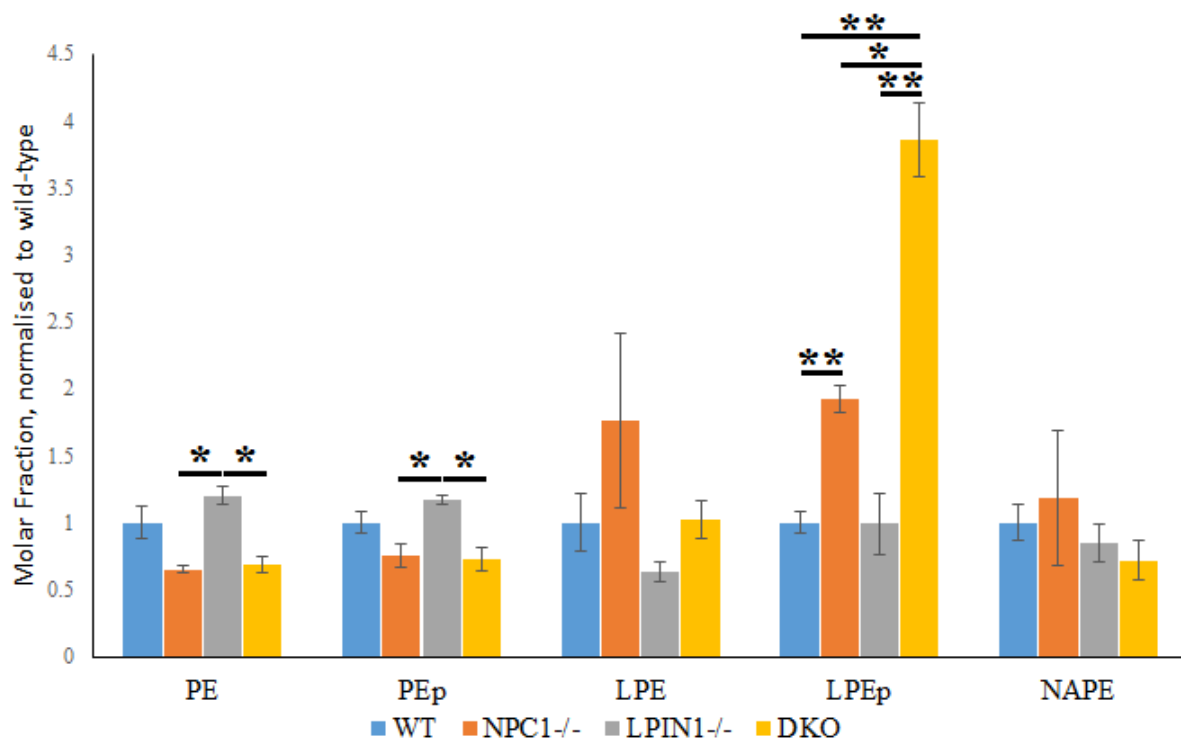


**Figure 29: Mouse liver profile of PE and variations.** PE: Phosphatidylethanolamine, Pep: Plasmalogen phosphatidylethanolamine, LPE: Lysophosphatidylethanolamine, LPEp: Plasmalogen phosphatidylethanolamine, NAPE: N-Acyl phosphatidylethanolamine. Phospholipid quantification by normal-phase HPLC with Applied Biosystems Triple Quadrupole 3200 QTrap. Bars represent molar fraction of total lipid, normalised to the wild-type. Error bars show standard error of normalised values. WT (Wild-Type) n=3, *Npc1<sup>-/-</sup>* n=2, *Lpin1<sup>-/-</sup>* n=4, DKO (aka *Npc1<sup>-/-</sup>Lpin1<sup>-/-</sup>* n=4. \*p<0.05, \*\*p<0.01, Student's t-test versus appropriate wild-type.

PC, Ether phosphatidylcholine (PCe) and Lysophosphatidylcholine (LPC) are unperturbed by loss of *Npc1* or *Lpin1* (Fig. 31). Ether lysophosphatidylcholine (LPCe) levels, however, are reduced in the *Lpin1*<sup>-/-</sup> mouse compared to wild-type.

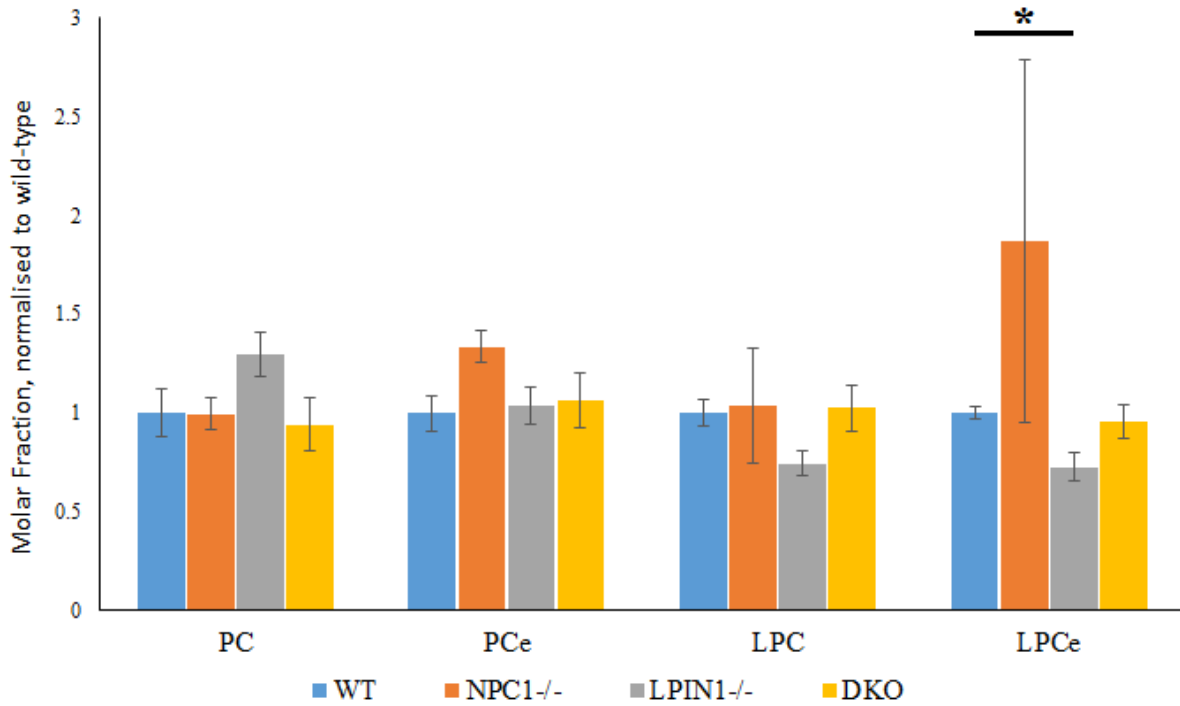


**Figure 30: Mouse liver profile of PC and variations.** PC: Phosphatidylcholine, PCe: Ether phosphatidylcholine, LPC: Lysophosphatidylcholine, LPCe: Ether lysophosphatidylcholine. Phospholipid quantification by normal-phase HPLC with Applied Biosystems Triple Quadrupole 3200 QTrap. Bars represent molar fraction of total lipid, normalised to the wild-type. Error bars show standard error of normalised values. WT (Wild-Type) n=3, *Npc1*<sup>-/-</sup> n=2, *Lpin1*<sup>-/-</sup> n=4, DKO (aka *Npc1*<sup>-/-</sup>*Lpin1*<sup>-/-</sup> n=4. \*p<0.05, Student's t-test versus appropriate wild-type.

The *Npc1*<sup>-/-</sup> liver stores a reduced level of PS compared to the wild-type mouse (p = 0.046), while the *Lpin1*<sup>-/-</sup> and *Npc1*<sup>-/-</sup>*Lpin1*<sup>-/-</sup> livers are not statistically distinguishable from the wild-type. Lysophosphatidylserine (LPS) is increased in the *Npc1*<sup>-/-</sup> mouse compared to the wild-type and *Lpin1*<sup>-/-</sup> liver. The *Lpin1*<sup>-/-</sup> mouse does not accumulate irregular LPS levels. N-Acyl phosphatidylserine (NAPS) appears unperturbed with the deletion of *Npc1* or *Lpin1*, however the large error in the wild-type group may mask a potential interaction. The *Npc1*<sup>-/-</sup>

*Lpin1*<sup>-/-</sup> mouse has a near-significant difference in NAPS compared to the *Npc1*<sup>-/-</sup> and *Lpin1*<sup>-/-</sup> groups (p = 0.054 and p = 0.065, respectively).

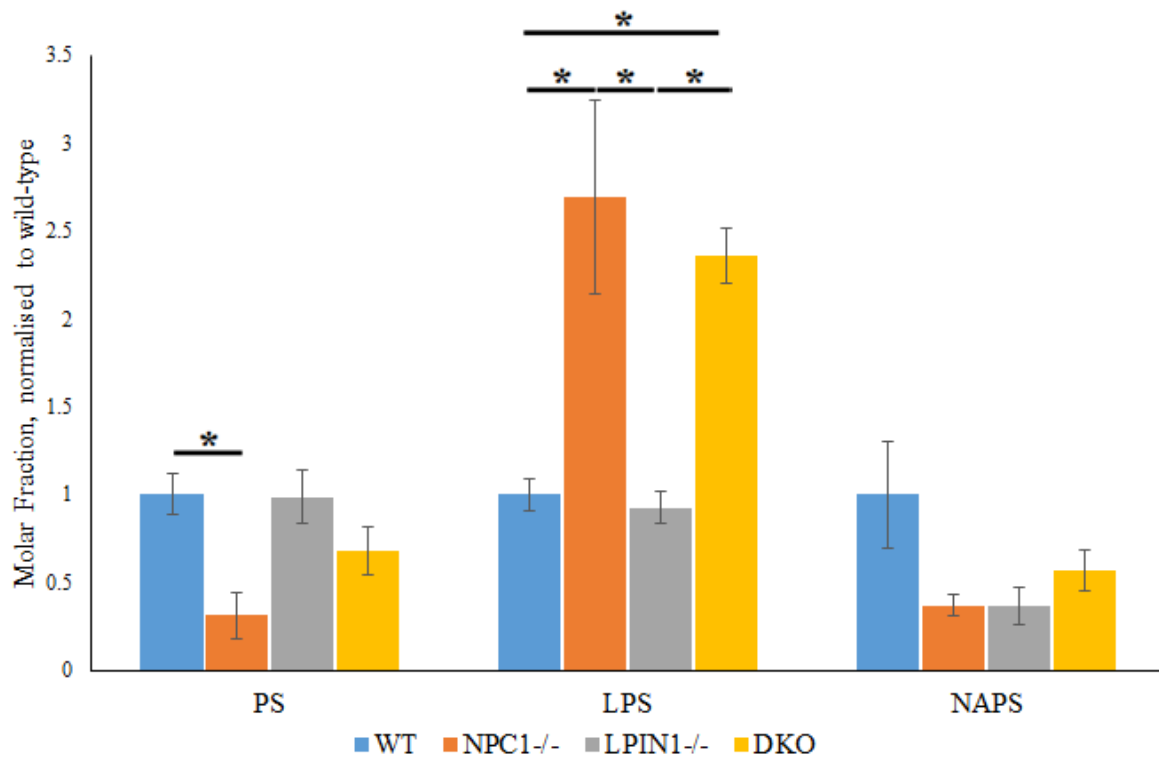


**Figure 31: Mouse liver profile of PS and variations.** PS: Phosphatidylserine, LPS: Lysophosphatidylserine, NAPS: N-Acyl phosphatidylserine. Phospholipid quantification by normal-phase HPLC with Applied Biosystems Triple Quadrupole 3200 QTrap. Bars represent molar fraction of total lipid, normalised to the wild-type. Error bars show standard error of normalised values. WT (Wild-Type) n=3, *Npc1*<sup>-/-</sup> n=2, *Lpin1*<sup>-/-</sup> n=4, DKO (aka *Npc1*<sup>-/-</sup>*Lpin1*<sup>-/-</sup> n=4. \*p<0.05, Student's t-test versus appropriate wild-type.

Unlike PI, lysophosphatidylinositol (LPI) is increased 6-fold in the *Npc1*<sup>-/-</sup> mouse, and 4-fold in the *Npc1*<sup>-/-</sup>*Lpin1*<sup>-/-</sup> mouse (Fig. 33). LPI interacts with the GPR55 receptor, an interaction which is still poorly understood, but has been thought to involve diverse metabolic processes, with links to cannabinoid receptors, obesity, pancreatic function, and the small intestine (Henstridge, Brown, & Waldhoer, 2016).

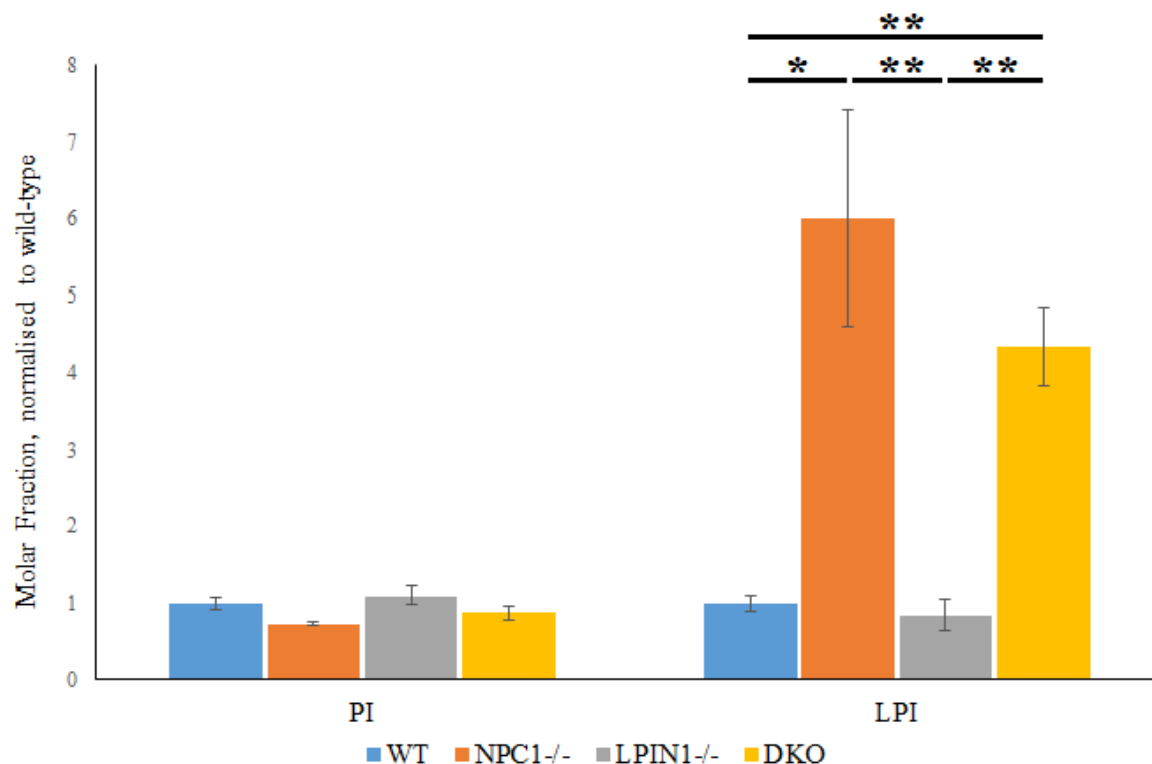


**Figure 32: Mouse liver profile of PI and LPI.** PI: phosphatidylinositol, LPI: lysophosphatidylinositol. Phospholipid quantification by normal-phase HPLC with Applied Biosystems Triple Quadrupole 3200 QTrap. Bars represent molar fraction of total lipid, normalised to the wild-type. Error bars show standard error of normalised values. WT (Wild-Type) n=3, *Npc1*<sup>-/-</sup> n=2, *Lpin1*<sup>-/-</sup> n=4, DKO (aka *Npc1*<sup>-/-</sup>*Lpin1*<sup>-/-</sup> n=4. \*p<0.05, \*\*p<0.01, Student's t-test versus appropriate wild-type.

BMP is a particularly interesting lipid to examine, as accumulation has been established as an indicator of lysosomal trafficking defects in CHO cells, and has been observed to resolve with positive *in vitro* treatments that reduced accumulation (Devlin et al., 2010; Mesens et al., 2012). With our groups we see a >5-fold increase in BMP in the *Lpin1*<sup>-/-</sup> mouse and >6-fold increase in the *Npc1*<sup>-/-</sup>*Lpin1*<sup>-/-</sup> (p = 0.018 and p = 0.0072, respectively) (Fig. 34). Although the low sample size and huge error in the *Npc1*<sup>-/-</sup> group is suspect, the p value is high (p = 0.14), however we can state that the *Npc1*<sup>-/-</sup>*Lpin1*<sup>-/-</sup> and the *Lpin1*<sup>-/-</sup> P0 mouse liver shows this established phenotype early on in development. T-test for AcylPG accumulation in *Npc1*<sup>-/-</sup> liver versus wild-type is p = 0.079.

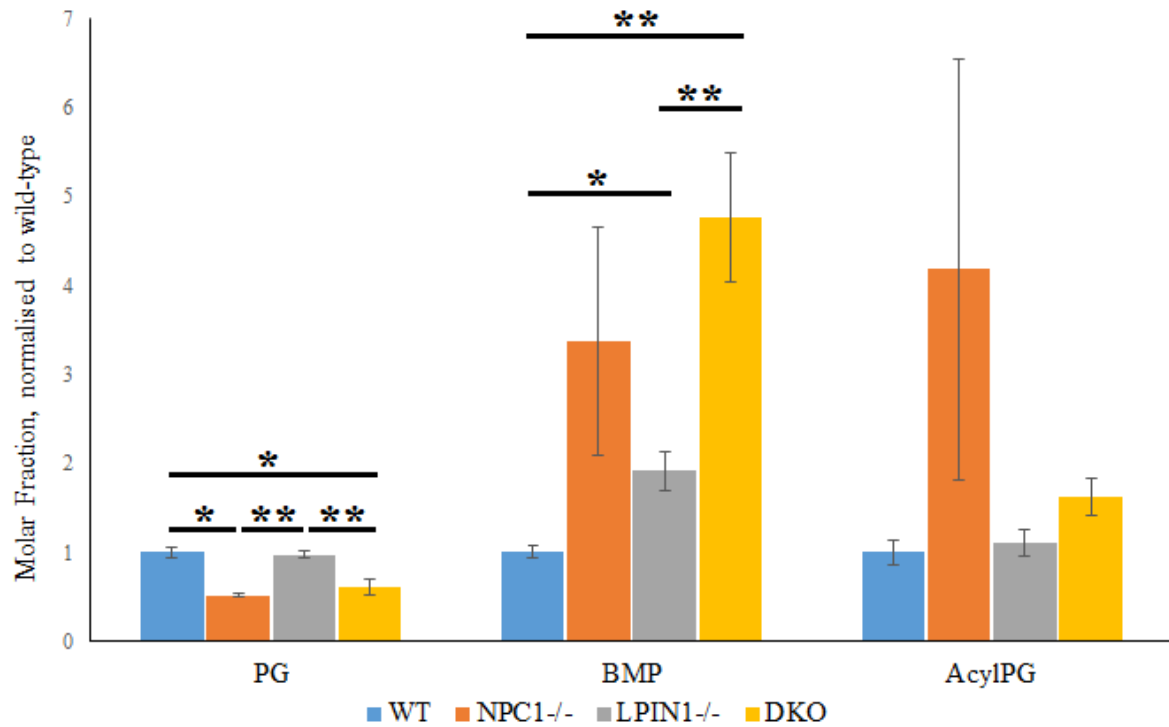


**Figure 33: Mouse liver profile of PG and variations.** PG: Phosphatidylglycerol, BMP: Bis(monoacylglycero)phosphate AcylPG: Acyl phosphatidylglycerol. Phospholipid quantification by normal-phase HPLC with Applied Biosystems Triple Quadrupole 3200 QTrap. Bars represent molar fraction of total lipid, normalised to the wild-type. Error bars show standard error of normalised values. WT (Wild-Type) n=3, *Npc1*<sup>-/-</sup> n=2, *Lpin1*<sup>-/-</sup> n=4, DKO (aka *Npc1*<sup>-/-</sup>*Lpin1*<sup>-/-</sup> n=4. \*p<0.05, \*\*p<0.01, Student's t-test versus appropriate wild-type.

### 2.3.12 Phospholipid homeostasis is not disrupted in the brain of *Npc1*<sup>-/-</sup> *Lpin1*<sup>-/-</sup> mice

All phospholipid species investigated in wild-type and *Npc1*<sup>-/-</sup> mice (Fig. 35) were consistent between the two groups (p>0.3 in each comparison). Although average PG appears to be reduced in *Npc1*<sup>-/-</sup> mice, the variability of wild-type PG levels negates this (p = 0.32).

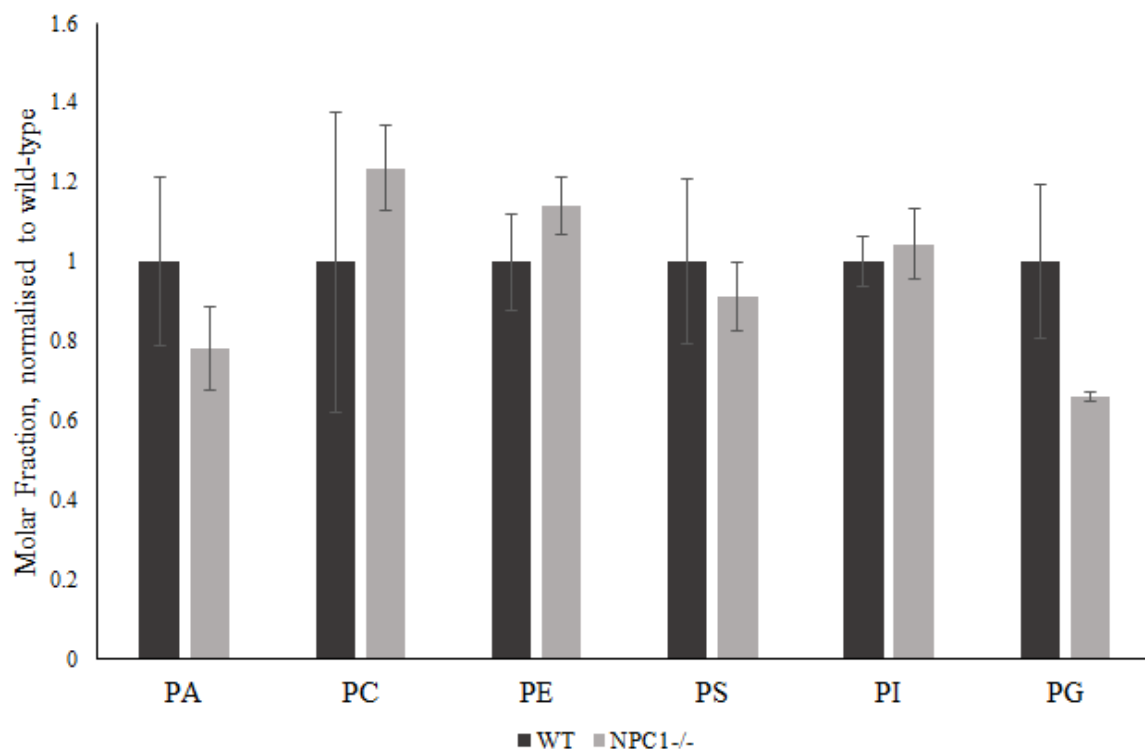


**Figure 34: Phospholipid profile of *Npc1*<sup>-/-</sup> mouse brain similar to wild-type.** PA: Phosphatidic acid, PC: Phosphatidylcholine, PE: Phosphatidylethanolamine, PS: Phosphatidylserine, PI: Phosphatidylinositol, PG: Phosphatidylglycerol. Phospholipid quantification by normal-phase HPLC with Applied Biosystems Triple Quadrupole 3200 QTrap. Bars represent molar fraction of total lipid, normalised to the wild-type. Error bars show standard error of normalised values. WT (Wild-Type) n=3, *Npc1*<sup>-/-</sup> n=2.

As in the *Lpin1*<sup>-/-</sup> liver (Fig. 28), PA in the *Lpin1*<sup>-/-</sup> brain was robustly unaltered compared to wild-type ( $p = 0.817$ ) (Fig. 36). This is perplexing as LPIN1 converts PA to DAG, and its deficiency should intuitively result in an increase in PA. Further, PA accumulation is reported in the brains of adult *Lpin1*<sup>-/-</sup> mice, and subsequent myelination failure and neurodegeneration is attributed to this accumulation (Nadra et al., 2008). As suggested previously, it is possible that PA levels are kept at a regular level *in utero* in spite of the *Lpin1* deficiency of the pup, which persists into the neonatal stage of life. This might be due to interaction from the placenta, or the developmental conditions and requirement for extensive biosynthesis in the new born pup.

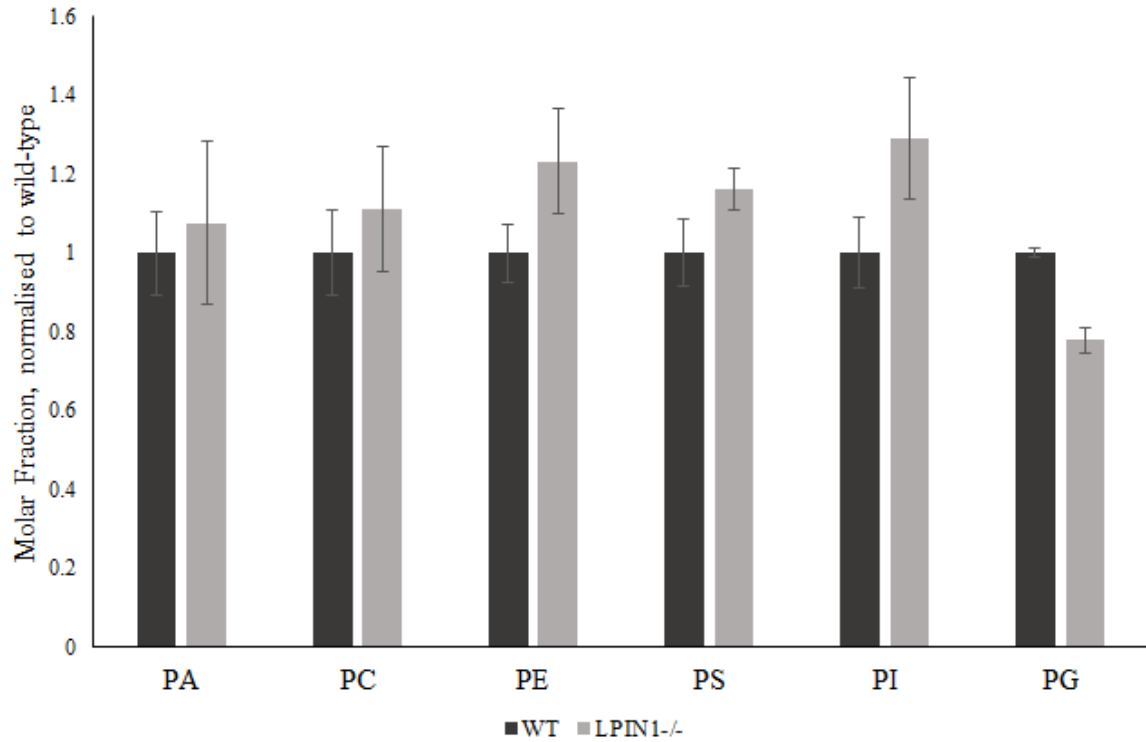


**Figure 35: Measured phospholipids not affected by deletion of *Lpin1* in mouse brain.** PA: Phosphatidic acid, PC: Phosphatidylcholine, PE: Phosphatidylethanolamine, PS: Phosphatidylserine, PI: Phosphatidylinositol, PG: Phosphatidylglycerol. Phospholipid quantification by normal-phase HPLC with Applied Biosystems Triple Quadrupole 3200 QTrap. Bars represent molar fraction of total lipid, normalised to the wild-type. Error bars show standard error of normalised values. WT (Wild-Type) n=3, *Lpin1*<sup>-/-</sup> n=4.

PI is increased in the *Npc1*<sup>-/-</sup>*Lpin1*<sup>-/-</sup> brain compared to wild-type (Fig. 37) but not compared to *Npc1*<sup>-/-</sup> or *Lpin1*<sup>-/-</sup> mice (Fig. 35 and Fig. 36). The other phospholipids examined in the *Npc1*<sup>-/-</sup>*Lpin1*<sup>-/-</sup> brain do not significantly deviate in abundance from wild-type levels, consistent with the *Npc1*<sup>-/-</sup> and *Lpin1*<sup>-/-</sup> data.

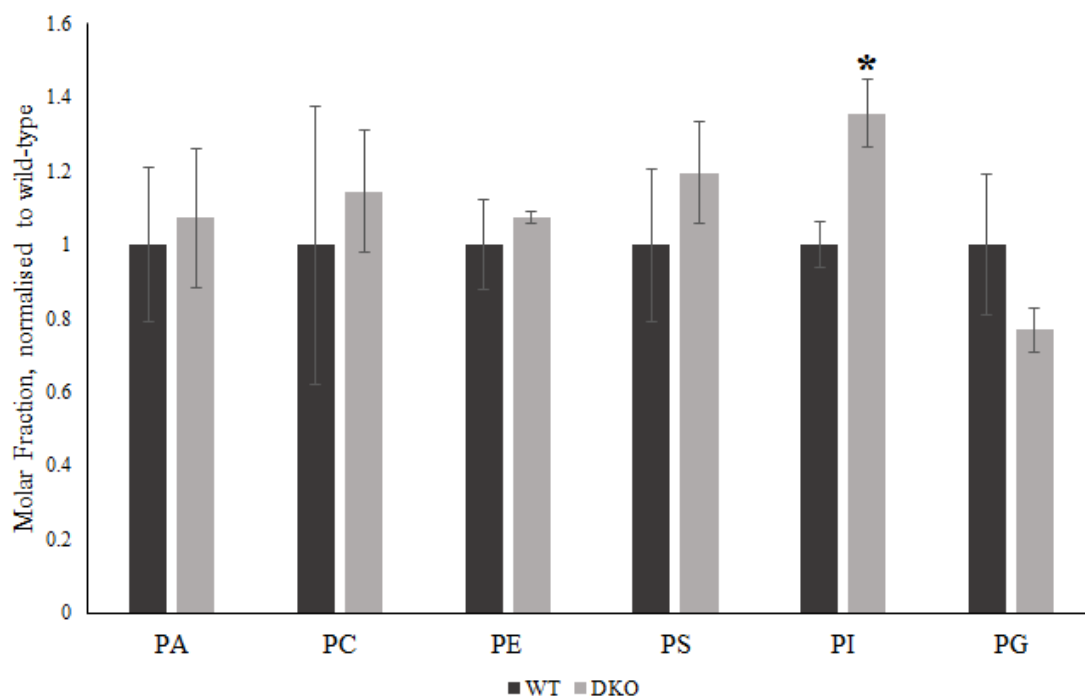


**Figure 36: PI reduced in *Npc1<sup>-/-</sup>Lpin1<sup>-/-</sup>* mouse brain.** PA: Phosphatidic acid, PC: Phosphatidylcholine, PE: Phosphatidylethanolamine, PS: Phosphatidylserine, PI: Phosphatidylinositol, PG: Phosphatidylglycerol. Phospholipid quantification by normal-phase HPLC with Applied Biosystems Triple Quadrupole 3200 QTrap. Bars represent molar fraction of total lipid, normalised to the wild-type. Error bars show standard error of normalised values. WT (Wild-Type) n=3, DKO (aka *Npc1<sup>-/-</sup>Lpin1<sup>-/-</sup>*) n=4. \*p<0.05, Student's t-test versus appropriate wild-type.

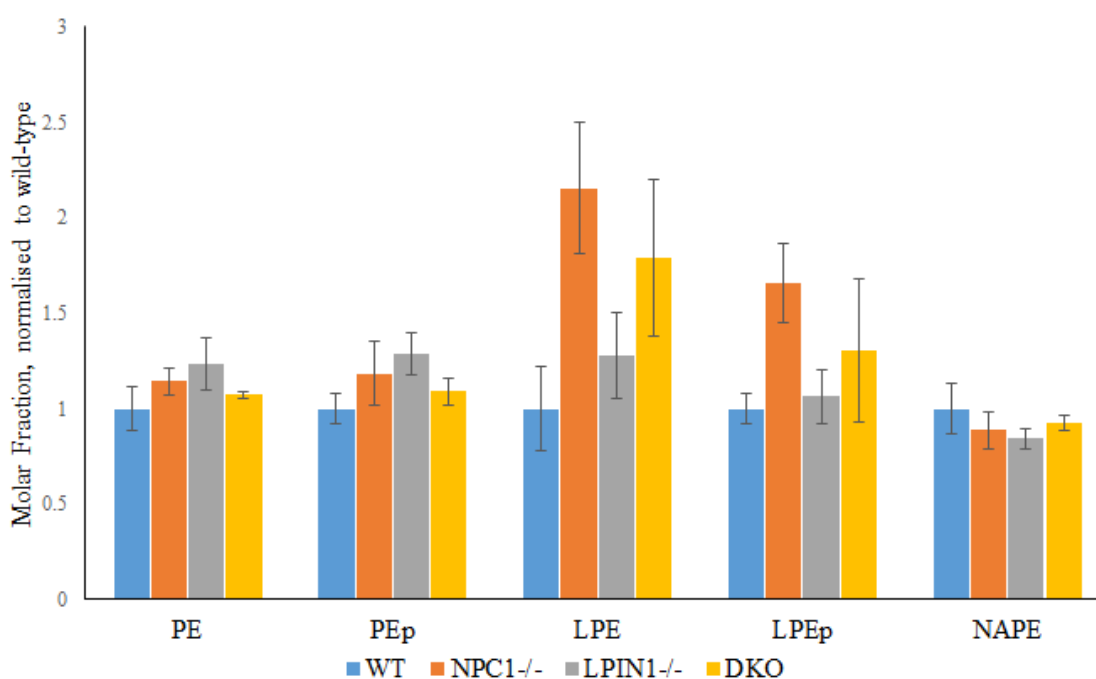




**Figure 37: Mouse brain profile of PE and variations.** PE: Phosphatidylethanolamine, PEp: Plasmalogen phosphatidylethanolamine, LPE: Lysophosphatidylethanolamine, LPEp: Plasmalogen phosphatidylethanolamine, NAPE: N-Acyl phosphatidylethanolamine. Phospholipid quantification by normal-phase HPLC with Applied Biosystems Triple Quadrupole 3200 QTrap. Bars represent molar fraction of total lipid, normalised to the wild-type. Error bars show standard error of normalised values. WT (Wild-Type) n=3, *Npc1*<sup>-/-</sup> n=2, *Lpin1*<sup>-/-</sup> n=4, DKO (aka *Npc1*<sup>-/-</sup>*Lpin1*<sup>-/-</sup>) n=4.

In the mouse brain, PE, PEp, LPE, LPEp and NAPE were measured in the *Npc1*<sup>-/-</sup> mouse, the *Lpin1*<sup>-/-</sup> mouse, the *Npc1*<sup>-/-</sup>*Lpin1*<sup>-/-</sup> mouse, and the wild-type mouse (Fig. 39). These phospholipids were found to not fluctuate significantly in between these mice groups. In regards to the *Npc1*<sup>-/-</sup>*Lpin1*<sup>-/-</sup> brain, LPCe accumulates compared to wild-type and *Lpin1*<sup>-/-</sup> mice. PA was found not to accumulate in the *Lpin1*<sup>-/-</sup> brain (Fig. 37), similarly the *Lpin1*<sup>-/-</sup> brain does not accumulate lipids downstream of PA, such as PC, PCe, and LPC.

Similar to in the liver, neural PC, PCe and LPC are consistent between genotypes investigated (Fig. 40). LPCe however is doubled in the *Npc1*<sup>-/-</sup>*Lpin1*<sup>-/-</sup> brain compared to wild-type, and *Npc1*<sup>-/-</sup> brain LPCe is increased compared to the *Lpin1*<sup>-/-</sup> brain.

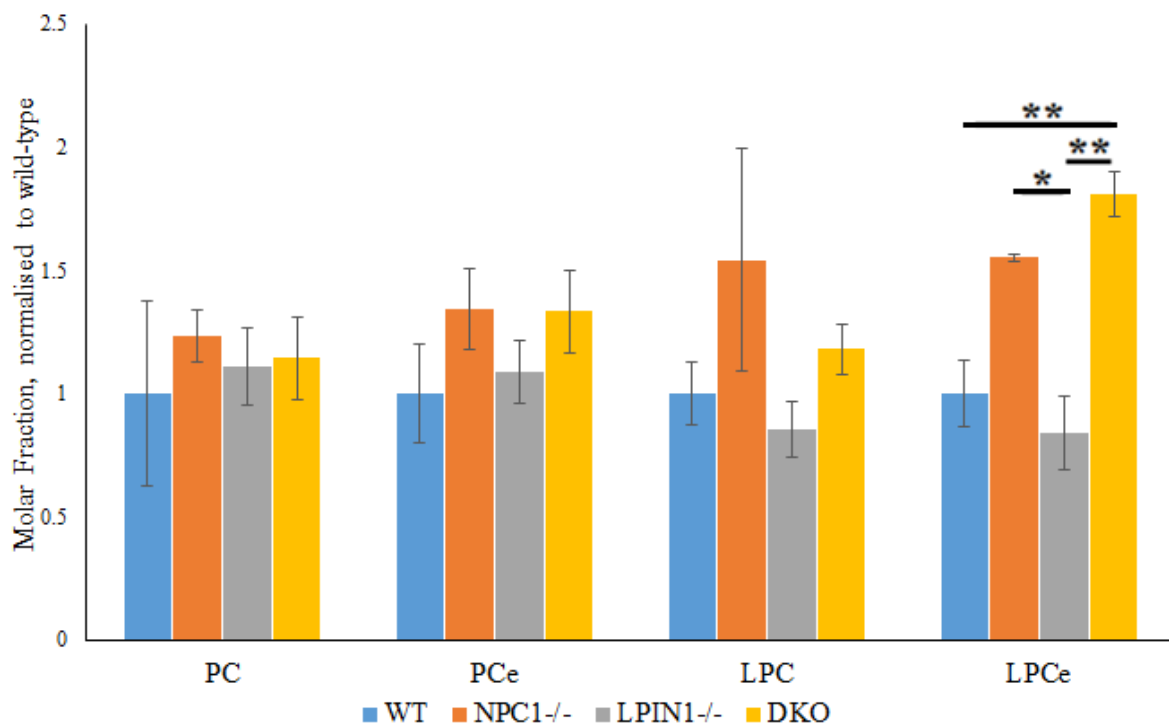


**Figure 38: Mouse brain profile of PC and variations.** PC: Phosphatidylcholine, PCe: Ether phosphatidylcholine, LPC: Lysophosphatidylcholine, LPCe: Ether lysophosphatidylcholine. Phospholipid quantification by normal-phase HPLC with Applied Biosystems Triple Quadrupole 3200 QTrap. Bars represent molar fraction of total lipid, normalised to the wild-type. Error bars show standard error of normalised values. WT (Wild-Type) n=3, *Npc1*<sup>-/-</sup> n=2, *Lpin1*<sup>-/-</sup> n=4, DKO (aka *Npc1*<sup>-/-</sup>*Lpin1*<sup>-/-</sup> n=4. \*p<0.05, Student's t-test versus appropriate wild-type.

Unlike in the liver, the neural PS values are consistent between all genotypes (Fig. 40). The brain LPS profile, however does resemble the hepatic LPS ratios (Fig. 33), once more LPS levels being heightened in the *Npc1*<sup>-/-</sup> and *Npc1*<sup>-/-</sup>*Lpin1*<sup>-/-</sup> mice compared to *Lpin1*<sup>-/-</sup>. When compared to the wild-type LPS levels, p = 0.099 versus the *Npc1*<sup>-/-</sup> brain and 0.070 versus the *Npc1*<sup>-/-</sup>*Lpin1*<sup>-/-</sup> brain.

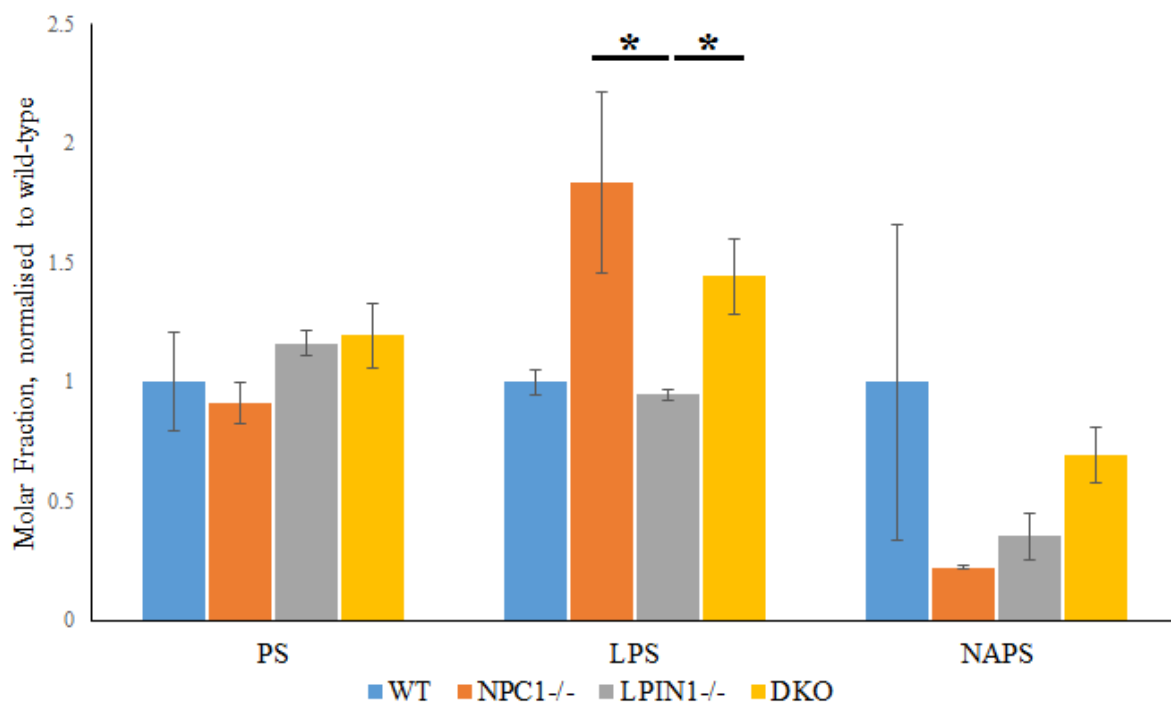


**Figure 39: Mouse brain profile of PS and variations.** PS: Phosphatidylserine, LPS: Lysophosphatidylserine, NAPS: N-Acyl phosphatidylserine. Phospholipid quantification by normal-phase HPLC with Applied Biosystems Triple Quadrupole 3200 QTrap. Bars represent molar fraction of total lipid, normalised to the wild-type. Error bars show standard error of normalised values. WT (Wild-Type) n=3, *Npc1*<sup>-/-</sup> n=2, *Lpin1*<sup>-/-</sup> n=4, DKO (aka *Npc1*<sup>-/-</sup>*Lpin1*<sup>-/-</sup> n=4. \*p<0.05, Student's t-test versus appropriate wild-type.

*Npc1<sup>-/-</sup>Lpin1<sup>-/-</sup>* mouse brains accumulate more PI than the wild-type and more LPI than wild-type as well as *Lpin1<sup>-/-</sup>* brains (Fig. 41). LPI interacts with the GPR55 receptor, which has been reported to influence axon growth and upregulates neural growth cone development (Cherif et al., 2015). The upregulation of LPI in *Npc1<sup>-/-</sup>* mice may contribute to improper neural development, or may even be protective.

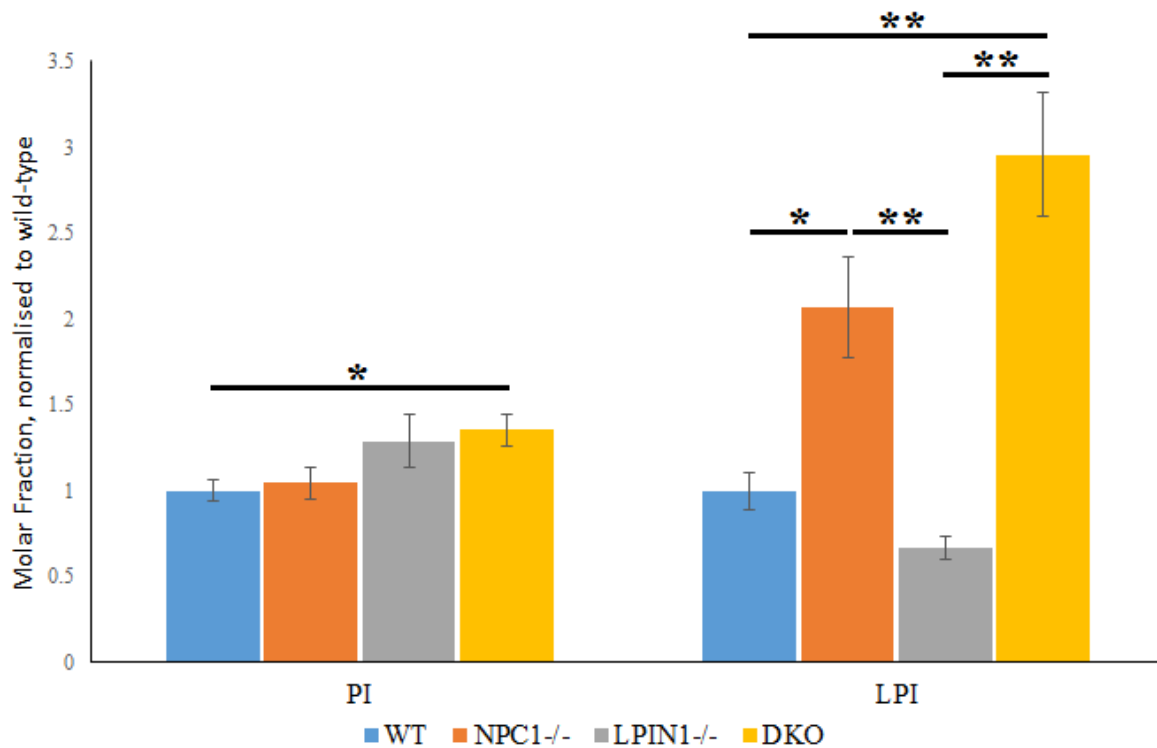


**Figure 40: Mouse brain profile of PI and LPI.** PI: phosphatidylinositol, LPI: lysophosphatidylinositol. Phospholipid quantification by normal-phase HPLC with Applied Biosystems Triple Quadrupole 3200 QTrap. Bars represent molar fraction of total lipid, normalised to the wild-type. Error bars show standard error of normalised values. WT (Wild-Type) n=3, *Npc1<sup>-/-</sup>* n=2, *Lpin1<sup>-/-</sup>* n=4, DKO (aka *Npc1<sup>-/-</sup>Lpin1<sup>-/-</sup>* n=4. \*p<0.05, \*\*p<0.01, Student's t-test versus appropriate wild-type.

PG levels are unperturbed in the brain (Fig. 42), however we see a 5-fold increase in BMP in the *Npc1*<sup>-/-</sup> brain, and a 6.5-fold increase in the *Npc1*<sup>-/-</sup>*Lpin1*<sup>-/-</sup> brain.

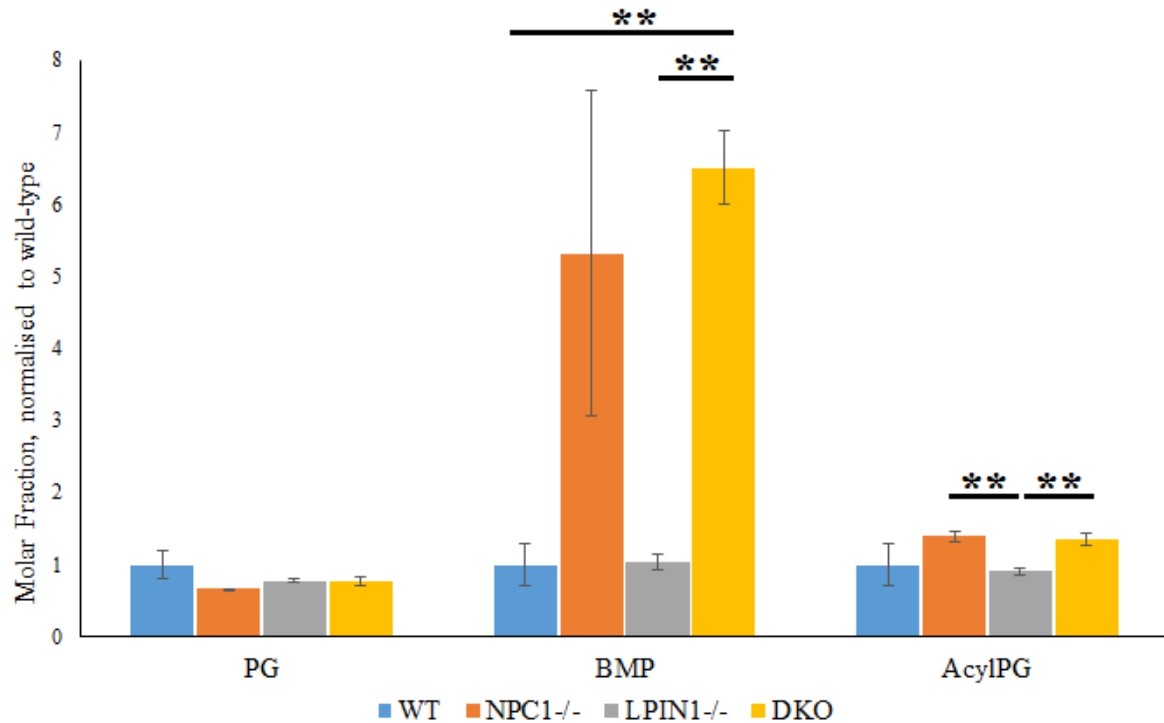


**Figure 41: Profile of PG and variations.** PG: Phosphatidylglycerol, BMP: Bis(monoacylglycerol)phosphate  
AcylPG: Acyl phosphatidylglycerol. Phospholipid quantification by normal-phase HPLC with Applied Biosystems Triple Quadrupole 3200 QTrap. Bars represent molar fraction of total lipid, normalised to the wild-type. Error bars show standard error of normalised values. WT (Wild-Type) n=3, *Npc1*<sup>-/-</sup> n=2, *Lpin1*<sup>-/-</sup> n=4, DKO (aka *Npc1*<sup>-/-</sup>*Lpin1*<sup>-/-</sup> n=4. \*\*p<0.01, Student's t-test versus appropriate wild-type.

## 2.5 Discussion

NP-C disease is a gastrointestinal and neurodegenerative disease with complex manifestations and no current adequate treatment available. In investigating the complex and incredibly variable nature of NP-C disease between patients, it seems clear that this disease, although monogenic in its inception, is notably shaped in its severity and manifestations by other interacting genes, of which our understanding is critical for the best opportunity to develop an effective therapy. This thesis therefore, followed a line of enquiry generated from the results of a yeast screen which identified genes necessary for the survival of a NP-C model in sterol starvation (Munkacsı et al., 2011). One of those identified genes was the yeast homolog of *Lpin1*. The relevance of *Lpin1* as a modifier of NP-C disease in our mouse model was the unifying sentiment that underlies the three aims set out in **1.5**: to investigate the therapeutic potential of DGK and PLD inhibition, from the perspective of preventing PA accumulation, and to identify the effect of *Lpin1* deletion on the *Npc1*<sup>-/-</sup> mouse.

The *Lpin1* gene generates a PAP enzyme of the same name that converts PA to DAG. In this project, PA levels were targeted in two ways: 1) inhibition of DGK by R59022 and 2) inhibition of PLD by FIPI. These procedures had no impact according to the metric of the filipin assay. One potential caveat is that the culture media used for these assays were not LDL-enriched, as it has been reported that enriching the media with LDL can result in an even more dramatic accumulation of cholesterol and a more intense filipin signal (Vanier & Latour, 2015). With a higher top signal, there would be a greater possibility of identifying minor changes in cholesterol storage. In general, the treatment times in other studies using R59022 were much shorter than 24 hours, and the half-life of R59022 is not known. Furthermore, even if R59022 or FIPI are not affecting cholesterol accumulation, they may be having a positive effect on the cell in a fashion that does not directly alter lysosomal accumulation of cholesterol. Assays of cell health such as MTT to measure metabolism (Ayto, 2011) or additional assays of NPC

disease progression such as the fluorescent BODIPY-lactosylceramide to investigate lipid trafficking (Sun et al., 2001) could be conducted in the future. In any case, it should be said that there is still potential that reduction in phosphatidic acid generation can be beneficial in NP-C disease, however there is not evidence to support it here.

To the best of our knowledge, this is the neonatal examination of NP-C disease in the *Npc1*<sup>-/-</sup> mouse at P0. This is the earliest post-partum lipid profile, however as the sample size of the *Npc1*<sup>-/-</sup> mouse was 2, the reported statistics cannot be asserted to have legitimate statistical significance. However, these lipid results were compared regardless, and in many cases, seem notably different to wild-type pups. In the liver and brain, *Npc1*<sup>-/-</sup> pups were seen to have a large increase in LacCer, which can drive dramatic cell changes in adhesion, migration and angiogenesis (Chatterjee & Pandey, 2008). The *Npc1*<sup>-/-</sup> liver also exhibits a near two-fold increase in LPEp a plasmalogen with a many ascribed functions, from antioxidant to immune ligand. The *Npc1*<sup>-/-</sup> liver also exhibited decreases in PS, PG and cholesterol ester, and increases in bioactive lipids LPS and LPI (Arifin & Falasca, 2016; Nagura et al., 2016).

Unfortunately, the histological examination of the cerebellum was inadequate, and histological examination of the liver was abandoned due to poor sample quality. Cerebellar histologic visualisation of the Purkinje cells was critical but not achieved, and future investigations in the *Npc1*<sup>-/-</sup>*Lpin1*<sup>-/-</sup> would need to address this. The liver of the P0 *Lpin1*<sup>-/-</sup> mouse is physically much larger than the wild-type mouse (Péterfy et al., 2001), justifying investigation for architectural change in the *Lpin1*<sup>-/-</sup> and *Npc1*<sup>-/-</sup>*Lpin1*<sup>-/-</sup> liver at P0. The autophagy investigation by western blot was also inadequate. It is likely that failure to visualise two bands was due to deaturing of LC3-I or enhanced autophagy at the neonatal stage regardless of genotype. Fresh protein extractions would need to be performed before reattempting the blot (Daniel J Klionsky et al., 2007).

The *Lpin1*<sup>-/-</sup> mouse generally portrayed less dramatic lipid perturbations next to the *Npc1*<sup>-/-</sup> and *Npc1*<sup>-/-</sup>*Lpin1*<sup>-/-</sup> mice. It is worth bearing in mind that in the liver and whole brain, *Lpin2* is also expressed in appreciable levels, and although LPIN2 PAP activity is lesser to LPIN1, its presence compensates at least partially for *Lpin1* deletion, so PAP activity is still undertaken in these organs (Csaki et al., 2013; Dwyer et al., 2012). However, much of the transcription factor roles that *Lpin1* plays is specific to itself.

There were two situations within the lipid analysis where a lipid measured in *Npc1*<sup>-/-</sup> *Lpin1*<sup>-/-</sup> tissue was seemingly different to the corresponding *Npc1*<sup>-/-</sup> and *Lpin1*<sup>-/-</sup> groups. First, MhCer extracted from the brain was significantly higher than the *Lpin1*<sup>-/-</sup> group, and between *Npc1*<sup>-/-</sup> was approaching significance ( $p = 0.0996$ ) (Fig.26). MhCer appears to have a deleterious effect on the brain, and if not maintained by *ACER3*, will accumulate and induce Purkinje cell death and contribute to detrimental lipidoses (K. Wang et al., 2015). Ceramidase manipulation or *ACER3* upregulation may be beneficial to NP-C patients. Second, the abundance of LPEp in the *Npc1*<sup>-/-</sup>*Lpin1*<sup>-/-</sup> suggests either a blockage in plasmalogen egress, or a gross overproduction of LPEp. LPEp has an important role in the thymus as a self-antigen for natural killer T cells (Ni et al., 2014). If a natural killer T cell ligand is accumulating viscally, it may have some deleterious effect on local resident immune cells, or those in the circulation. Plasmalogens in general also will imbed in cell membranes (particularly neural membranes) and serve an antioxidant protective role (Hoffman-Kuczynski & Reo, 2005).

To summarise, this thesis examined inhibition of phosphatidic acid production in a NP-C disease fibroblast model as well as investigated the interaction between the *Npc1* and *Lpin1* genes in a mouse model. The DGK inhibitor R59022 and PLD inhibitor FIPI did not reduce cholesterol in NP-C disease fibroblasts. Likewise, the lipid profile of the *Npc1*<sup>-/-</sup>*Lpin1*<sup>-/-</sup> mouse at P0 was not drastically different from the *Npc1*<sup>-/-</sup> mouse. Therefore, this thesis completed initial experiments required to test the therapeutic efficacy of targeting PA to treat NP-C

disease and also provided the first lipid analysis for a neonatal *Npc1*<sup>-/-</sup> mouse, which provides new information about the NP-C mouse model.



## **Chapter 3. References**

- Alobaidy, H. (2015). Recent advances in the diagnosis and treatment of niemann-pick disease type C in children: a guide to early diagnosis for the general pediatrician. *Int J Pediatr*, 2015, 816593. doi:10.1155/2015/816593
- Anheim, M., Lagha-Boukbiza, O., Fleury-Lesaunier, M.-C., Valenti-Hirsch, M.-P., Hirsch, E., Gervais-Bernard, H., . . . Tranchant, C. (2014). Heterogeneity and frequency of movement disorders in juvenile and adult-onset Niemann-Pick C disease. *J Neurol*, 261(1), 174-179. doi:10.1007/s00415-013-7159-9
- Aqul, A., Liu, B., Ramirez, C. M., Pieper, A. A., Estill, S. J., Burns, D. K., . . . Dietschy, J. M. (2011). Unesterified cholesterol accumulation in late endosomes/lysosomes causes neurodegeneration and is prevented by driving cholesterol export from this compartment. *J Neurosci*, 31(25), 9404-9413. doi:10.1523/jneurosci.1317-11.2011
- Arifin, S. A., & Falasca, M. (2016). Lysophosphatidylinositol Signalling and Metabolic Diseases. *Metabolites*, 6(1). doi:10.3390/metabo6010006
- Athenstaedt, K., & Daum, G. (1999). Phosphatidic acid, a key intermediate in lipid metabolism. *Eur J Biochem*, 266(1), 1-16.
- Ayto, R. M. (2011). *Investigation of the linkage between Gaucher disease and BCell disorders including multiple myeloma*. UCL (University College London).
- Beltray, E. P., Liu, B., Dietschy, J. M., & Turley, S. D. (2007). Lysosomal unesterified cholesterol content correlates with liver cell death in murine Niemann-Pick type C disease. *J Lipid Res*, 48(4), 869-881. doi:10.1194/jlr.M600488-JLR200
- Berg, T. O., Fengsrud, M., Strømhaug, P. E., Berg, T., & Seglen, P. O. (1998). Isolation and characterization of rat liver amphisomes. Evidence for fusion of autophagosomes with both early and late endosomes. *J Biol Chem*, 273(34), 21883-21892.
- Bligh EG, Dyer WJ (1959). A rapid method of total lipid extraction and purification. *Can J Biochem Physiol*, 37(8), 911-917.
- Brady, R. O., Kanfer, J. N., Mock, M. B., & Fredrickson, D. S. (1966). The metabolism of sphingomyelin. II. Evidence of an enzymatic deficiency in Niemann-Pick disease. *Proc Natl Acad Sci U S A*, 55(2), 366-369.
- Braverman, N. E., & Moser, A. B. (2012). Functions of plasmalogen lipids in health and disease. *Biochimica et Biophysica Acta (BBA)-Molecular Basis of Disease*, 1822(9), 1442-1452.
- Camina, J. P., Casabiell, X., & Casanueva, F. F. (1999). Inositol 1,4,5-trisphosphate-independent Ca(2+) mobilization triggered by a lipid factor isolated from vitreous body. *J Biol Chem*, 274(40), 28134-28141.
- Carstea, E. D., Morris, J. A., Coleman, K. G., Loftus, S. K., Zhang, D., Cummings, C., . . . Tagle, D. A. (1997). Niemann-Pick C1 disease gene: homology to mediators of cholesterol homeostasis. *Science*, 277(5323), 228-231.
- Carstea, E. D., Polymeropoulos, M. H., Parker, C. C., Detera-Wadleigh, S. D., O'Neill, R. R., Patterson, M. C., . . . Vanier, M. T. (1993). Linkage of Niemann-Pick disease type C to human chromosome 18. *Proc Natl Acad Sci U S A*, 90(5), 2002-2004.
- Chan, R. B., Oliveira, T. G., Cortes, E. P., Honig, L. S., Duff, K. E., Small, S. A., . . . Di Paolo, G. (2012). Comparative Lipidomic Analysis of Mouse and Human Brain with Alzheimer Disease. *J Biol Chem*, 287(4), 2678-2688
- Chatterjee, S., & Pandey, A. (2008). The Yin and Yang of lactosylceramide metabolism: implications in cell function. *Biochim Biophys Acta*, 1780(3), 370-382. doi:10.1016/j.bbagen.2007.08.010
- Cheng, D., Espenshade, P. J., Slaughter, C. A., Jaen, J. C., Brown, M. S., & Goldstein, J. L. (1999). Secreted site-1 protease cleaves peptides corresponding to luminal loop of sterol regulatory element-binding proteins. *J Biol Chem*, 274(32), 22805-22812.
- Cherif, H., Argaw, A., Cecyre, B., Bouchard, A., Gagnon, J., Javadi, P., . . . Bouchard, J. F. (2015). Role of GPR55 during Axon Growth and Target Innervation. *eNeuro*, 2(5). doi:10.1523/eneuro.0011-15.2015

- Choudhury, A., Dominguez, M., Puri, V., Sharma, D. K., Narita, K., Wheatley, C. L., . . . Pagano, R. E. (2002). Rab proteins mediate Golgi transport of caveola-internalized glycosphingolipids and correct lipid trafficking in Niemann-Pick C cells. *J Clin Invest*, 109(12), 1541-1550. doi:10.1172/jci15420
- Coetzee, T., Fujita, N., Dupree, J., Shi, R., Blight, A., Suzuki, K., . . . Popko, B. (1996). Myelination in the absence of galactocerebroside and sulfatide: normal structure with abnormal function and regional instability. *Cell*, 86(2), 209-219.
- Crocker, A. C. (1961). The cerebral defect in Tay-Sachs disease and Niemann-Pick disease. *J Neurochem*, 7, 69-80.
- Csaki, L. S., Dwyer, J. R., Fong, L. G., Tontonoz, P., Young, S. G., & Reue, K. (2013). Lipins, lipinopathies, and the modulation of cellular lipid storage and signaling. *Prog Lipid Res*, 52(3), 305-316. doi:10.1016/j.plipres.2013.04.001
- Davidson, C. D., Ali, N. F., Micsenyi, M. C., Stephney, G., Renault, S., Dobrenis, K., . . . Walkley, S. U. (2009). Chronic cyclodextrin treatment of murine Niemann-Pick C disease ameliorates neuronal cholesterol and glycosphingolipid storage and disease progression. *PLoS One*, 4(9), e6951. doi:10.1371/journal.pone.0006951
- Davies, J. P., & Ioannou, Y. A. (2000). Topological analysis of Niemann-Pick C1 protein reveals that the membrane orientation of the putative sterol-sensing domain is identical to those of 3-hydroxy-3-methylglutaryl-CoA reductase and sterol regulatory element binding protein cleavage-activating protein. *J Biol Chem*, 275(32), 24367-24374. doi:10.1074/jbc.M002184200
- de Chaffoy de Courcelles, D. C., Roevens, P., & Van Belle, H. (1985). R 59 022, a diacylglycerol kinase inhibitor. Its effect on diacylglycerol and thrombin-induced C kinase activation in the intact platelet. *J Biol Chem*, 260(29), 15762-15770.
- Devlin, C., Pipalia, N. H., Liao, X., Schuchman, E. H., Maxfield, F. R., & Tabas, I. (2010). Improvement in lipid and protein trafficking in Niemann-Pick C1 cells by correction of a secondary enzyme defect. *Traffic*, 11(5), 601-615. doi:10.1111/j.1600-0854.2010.01046.x
- Di Rocco, M., Dardis, A., Madeo, A., Barone, R., & Fiumara, A. (2012). Early miglustat therapy in infantile Niemann-Pick disease type C. *Pediatr Neurol*, 47(1), 40-43. doi:10.1016/j.pediatrneurol.2012.04.005
- Donkor, J., Sariahmetoglu, M., Dewald, J., Brindley, D. N., & Reue, K. (2007). Three mammalian lipins act as phosphatidate phosphatases with distinct tissue expression patterns. *J Biol Chem*, 282(6), 3450-3457. doi:10.1074/jbc.M610745200
- Du, X., Zhang, Y., Jo, S. R., Liu, X., Qi, Y., Osborne, B., . . . Yang, H. (2015). Akt activation increases cellular cholesterol by promoting the proteasomal degradation of Niemann-Pick C1. *Biochem J*, 471(2), 243-253. doi:10.1042/bj20150602
- Dvorakova, L., Sikora, J., Hrebicek, M., Hulkova, H., Bouckova, M., Stolnaja, L., & Elleder, M. (2006). Subclinical course of adult visceral Niemann-Pick type C1 disease. A rare or underdiagnosed disorder? *J Inherit Metab Dis*, 29(4), 591. doi:10.1007/s10545-006-0330-z
- Dwyer, J. R., Donkor, J., Zhang, P., Csaki, L. S., Vergnes, L., Lee, J. M., . . . Reue, K. (2012). Mouse lipin-1 and lipin-2 cooperate to maintain glycerolipid homeostasis in liver and aging cerebellum. *Proc Natl Acad Sci U S A*, 109(37), E2486-2495. doi:10.1073/pnas.1205221109
- Elleder, M., Smíd, F., Hyniová, H., Čihula, J., Zeman, J., & Macek, M. (1984). Liver findings in Niemann-Pic disease type C. *The Histochemical Journal*, 16(11), 1147-1170. doi:10.1007/bf01003441
- Elrick, M. J., & Lieberman, A. P. (2013). Autophagic dysfunction in a lysosomal storage disorder due to impaired proteolysis. *Autophagy*, 9(2), 234-235. doi:10.4161/auto.22501
- Finck, B. N., Gropler, M. C., Chen, Z., Leone, T. C., Croce, M. A., Harris, T. E., . . . Kelly, D. P. (2006). Lipin 1 is an inducible amplifier of the hepatic PGC-1alpha/PPARalpha regulatory pathway. *Cell Metab*, 4(3), 199-210. doi:10.1016/j.cmet.2006.08.005

- Finn, P. F., & Dice, J. F. (2006). Proteolytic and lipolytic responses to starvation. *Nutrition*, 22(7-8), 830-844. doi:10.1016/j.nut.2006.04.008
- Ford, C. P., Stemkowski, P. L., Light, P. E., & Smith, P. A. (2003). Experiments to test the role of phosphatidylinositol 4,5-bisphosphate in neurotransmitter-induced M-channel closure in bullfrog sympathetic neurons. *J Neurosci*, 23(12), 4931-4941.
- Furukawa, K., Ohmi, Y., Kondo, Y., Ohkawa, Y., Tajima, O., & Furukawa, K. (2015). Regulatory function of glycosphingolipids in the inflammation and degeneration. *Arch Biochem Biophys*, 571, 58-65. doi:10.1016/j.abb.2015.02.007
- Gévry, N., Schoonjans, K., Guay, F., & Murphy, B. D. (2008). Cholesterol supply and SREBPs modulate transcription of the Niemann-Pick C-1 gene in steroidogenic tissues. *J Lipid Res*, 49(5), 1024-1033. doi:10.1194/jlr.M700554-JLR200
- Goldstein, J. L., & Brown, M. S. (1987). Regulation of low-density lipoprotein receptors: implications for pathogenesis and therapy of hypercholesterolemia and atherosclerosis. *Circulation*, 76(3), 504-507.
- Greer, W. L., Riddell, D. C., Gillan, T. L., Girouard, G. S., Sparrow, S. M., Byers, D. M., . . . Neumann, P. E. (1998). The Nova Scotia (type D) form of Niemann-Pick disease is caused by a G3097-->T transversion in NPC1. *Am J Hum Genet*, 63(1), 52-54. doi:10.1086/301931
- Gu, J. Z., Carstea, E. D., Cummings, C., Morris, J. A., Loftus, S. K., Zhang, D., . . . Rosenfeld, M. A. (1997). Substantial narrowing of the Niemann-Pick C candidate interval by yeast artificial chromosome complementation. *Proc Natl Acad Sci U S A*, 94(14), 7378-7383.
- Hara, T., Nakamura, K., Matsui, M., Yamamoto, A., Nakahara, Y., Suzuki-Migishima, R., . . . Mizushima, N. (2006). Suppression of basal autophagy in neural cells causes neurodegenerative disease in mice. *Nature*, 441(7095), 885-889. doi:10.1038/nature04724
- Henstridge, C. M., Brown, A. J., & Waldhoer, M. (2016). GPR55: Metabolic Help or Hindrance? *Trends Endocrinol Metab*. doi:10.1016/j.tem.2016.04.012
- Higashi, Y., Murayama, S., Pentchev, P., & Suzuki, K. (1993). Cerebellar degeneration in the Niemann-Pick type C mouse. *Acta neuropathologica*, 85(2), 175-184.
- Higgins, M. E., Davies, J. P., Chen, F. W., & Ioannou, Y. A. (1999). Niemann-Pick C1 is a late endosome-resident protein that transiently associates with lysosomes and the trans-Golgi network. *Mol Genet Metab*, 68(1), 1-13. doi:10.1006/mgme.1999.2882
- Hoffman-Kuczynski, B., & Reo, N. V. (2005). Administration of Myo-inositol Plus Ethanolamine Elevates Phosphatidylethanolamine Plasmalogen in the Rat Cerebellum. *Neurochemical Research*, 30(1), 47-60. doi:10.1007/s11064-004-9685-4
- Honke, K. (2013). Biosynthesis and biological function of sulfoglycolipids. *Proc Jpn Acad Ser B Phys Biol Sci*, 89(4), 129-138.
- Hua, X., Nohturfft, A., Goldstein, J. L., & Brown, M. S. (1996). Sterol resistance in CHO cells traced to point mutation in SREBP cleavage-activating protein. *Cell*, 87(3), 415-426.
- Imrie, J., Heptinstall, L., Knight, S., & Strong, K. (2015). Observational cohort study of the natural history of Niemann-Pick disease type C in the UK: a 5-year update from the UK clinical database. *BMC Neurol*, 15, 257. doi:10.1186/s12883-015-0511-1
- Infante, R. E., Abi-Mosleh, L., Radhakrishnan, A., Dale, J. D., Brown, M. S., & Goldstein, J. L. (2008). Purified NPC1 protein. I. Binding of cholesterol and oxysterols to a 1278-amino acid membrane protein. *J Biol Chem*, 283(2), 1052-1063. doi:10.1074/jbc.M707943200
- Kaptzan, T., West, S. A., Holicky, E. L., Wheatley, C. L., Marks, D. L., Wang, T., . . . Pagano, R. E. (2009). Development of a Rab9 transgenic mouse and its ability to increase the lifespan of a murine model of Niemann-Pick type C disease. *Am J Pathol*, 174(1), 14-20. doi:10.2353/ajpath.2009.080660
- Karten, B., Vance, D. E., Campenot, R. B., & Vance, J. E. (2002). Cholesterol accumulates in cell bodies, but is decreased in distal axons, of Niemann-Pick C1-deficient neurons. *J Neurochem*, 83(5), 1154-1163.

- Klionsky, D. J., Abeliovich, H., Agostinis, P., Agrawal, D. K., Aliev, G., Askew, D. S., . . . Deter, R. L. (2008). Guidelines for the use and interpretation of assays for monitoring autophagy in higher eukaryotes. *Autophagy*, 4(2), 151-175.
- Klionsky, D. J., Cuervo, A. M., & Seglen, P. O. (2007). Methods for monitoring autophagy from yeast to human. *Autophagy*, 3(3), 181-206.
- Komatsu, M., Wang, Q. J., Holstein, G. R., Friedrich, V. L., Iwata, J.-i., Kominami, E., . . . Yue, Z. (2007). Essential role for autophagy protein Atg7 in the maintenance of axonal homeostasis and the prevention of axonal degeneration. *Proc Natl Acad Sci U S A*, 104(36), 14489-14494. doi:10.1073/pnas.0701311104
- Kruth, H. S., Comly, M. E., Butler, J. D., Vanier, M. T., Fink, J. K., Wenger, D. A., . . . Pentchev, P. G. (1986). Type C Niemann-Pick disease. Abnormal metabolism of low density lipoprotein in homozygous and heterozygous fibroblasts. *J Biol Chem*, 261(35), 16769-16774.
- Kuma, A., Hatano, M., Matsui, M., Yamamoto, A., Nakaya, H., Yoshimori, T., . . . Mizushima, N. (2004). The role of autophagy during the early neonatal starvation period. *Nature*, 432(7020), 1032-1036. doi:10.1038/nature03029
- Kumagai, T., Tanaka, M., Yokoyama, M., Sato, T., Shinkai, T., & Furukawa, K. (2009). Early lethality of beta-1,4-galactosyltransferase V-mutant mice by growth retardation. *Biochem Biophys Res Commun*, 379(2), 456-459. doi:10.1016/j.bbrc.2008.12.078
- Kurimasa, A., Ohno, K., & Oshimura, M. (1993). Restoration of the cholesterol metabolism in 3T3 cell lines derived from the sphingomyelinosis mouse (spm/spm) by transfer of a human chromosome 18. *Hum Genet*, 92(2), 157-162.
- Kwon, H. J., Abi-Mosleh, L., Wang, M. L., Deisenhofer, J., Goldstein, J. L., Brown, M. S., & Infante, R. E. (2009). Structure of N-terminal domain of NPC1 reveals distinct subdomains for binding and transfer of cholesterol. *Cell*, 137(7), 1213-1224. doi:10.1016/j.cell.2009.03.049
- Liao, G., Yao, Y., Liu, J., Yu, Z., Cheung, S., Xie, A., . . . Bi, X. (2007). Cholesterol accumulation is associated with lysosomal dysfunction and autophagic stress in Npc1 <sup>-/-</sup> mouse brain. *Am J Pathol*, 171(3), 962-975. doi:10.2353/ajpath.2007.070052
- Loftus, S. K., Morris, J. A., Carstea, E. D., Gu, J. Z., Cummings, C., Brown, A., . . . Pavan, W. J. (1997). Murine Model of Niemann-Pick C Disease: Mutation in a Cholesterol Homeostasis Gene. *Science*, 277(5323), 232-235. doi:10.1126/science.277.5323.232
- Lombardi, D., Soldati, T., Riederer, M. A., Goda, Y., Zerial, M., & Pfeffer, S. R. (1993). Rab9 functions in transport between late endosomes and the trans Golgi network. *EMBO J*, 12(2), 677-682.
- Lopez, J. M., Bennett, M. K., Sanchez, H. B., Rosenfeld, J. M., & Osborne, T. F. (1996). Sterol regulation of acetyl coenzyme A carboxylase: a mechanism for coordinate control of cellular lipid. *Proc Natl Acad Sci U S A*, 93(3), 1049-1053.
- Lopez, M. E., Klein, A. D., Dimbil, U. J., & Scott, M. P. (2011). Anatomically defined neuron-based rescue of neurodegenerative Niemann-Pick type C disorder. *J Neurosci*, 31(12), 4367-4378. doi:10.1523/jneurosci.5981-10.2011
- Madra, M., & Sturley, S. L. (2010). Niemann-Pick type C pathogenesis and treatment: from statins to sugars. *Clinical lipidology*, 5(3), 387-395. doi:10.2217/clp.10.19
- Matsuo, M., Togawa, M., Hirabaru, K., Mochinaga, S., Narita, A., Adachi, M., . . . Ohno, K. (2013). Effects of cyclodextrin in two patients with Niemann-Pick Type C disease. *Mol Genet Metab*, 108(1), 76-81. doi:10.1016/j.ymgme.2012.11.005
- Maue, R. A., Burgess, R. W., Wang, B., Wooley, C. M., Seburn, K. L., Vanier, M. T., . . . Erickson, R. P. (2012). A novel mouse model of Niemann-Pick type C disease carrying a D1005G-Npc1 mutation comparable to commonly observed human mutations. *Hum Mol Genet*, 21(4), 730-750. doi:10.1093/hmg/ddr505
- Medina, J. M., Vicario, C., Juanes, M., & Fernández, E. (1992). Biochemical adaptations to early extrauterine life *Perinatal biochemistry* (pp. 233-258): CRC Press Boca Raton, FL.
- Meikle, P. J., Hopwood, J. J., Clague, A. E., & Carey, W. F. (1999). Prevalence of lysosomal storage disorders. *JAMA*, 281(3), 249-254.

- Mesens, N., Desmidt, M., Verheyen, G. R., Starckx, S., Damsch, S., De Vries, R., . . . Lammens, L. (2012). Phospholipidosis in rats treated with amiodarone: serum biochemistry and whole genome micro-array analysis supporting the lipid traffic jam hypothesis and the subsequent rise of the biomarker BMP. *Toxicol Pathol*, 40(3), 491-503. doi:10.1177/0192623311432290
- Millat, G., Chikh, K., Naureckiene, S., Sleat, D. E., Fensom, A. H., Higaki, K., . . . Vanier, M. T. (2001). Niemann-Pick disease type C: spectrum of HE1 mutations and genotype/phenotype correlations in the NPC2 group. *Am J Hum Genet*, 69(5), 1013-1021. doi:10.1086/324068
- Millat, G., Marçais, C., Rafi, M. A., Yamamoto, T., Morris, J. A., Pentchev, P. G., . . . Vanier, M. T. (1999). Niemann-Pick C1 disease: the I1061T substitution is a frequent mutant allele in patients of Western European descent and correlates with a classic juvenile phenotype. *Am J Hum Genet*, 65(5), 1321-1329. doi:10.1086/302626
- Morell, P., & Jurevics, H. (1996). Origin of cholesterol in myelin. *Neurochem Res*, 21(4), 463-470.
- Munkacsí, A. B., Chen, F. W., Brinkman, M. A., Higaki, K., Gutiérrez, G. D., Chaudhari, J., . . . Sturley, S. L. (2011). An "exacerbate-reverse" strategy in yeast identifies histone deacetylase inhibition as a correction for cholesterol and sphingolipid transport defects in human Niemann-Pick type C disease. *J Biol Chem*, 286(27), 23842-23851. doi:10.1074/jbc.M111.227645
- Munkacsí, A. B., Pentchev, P. G., & Sturley, S. L. (2009). Spreading the wealth: Niemann-Pick type C proteins bind and transport cholesterol. *Cell Metab*, 10(1), 3-4. doi:10.1016/j.cmet.2009.06.007
- Nadra, K., de Preux Charles, A.-S., Médard, J.-J., Hendriks, W. T., Han, G.-S., Grès, S., . . . Chrast, R. (2008). Phosphatidic acid mediates demyelination in Lpin1 mutant mice. *Genes Dev*, 22(12), 1647-1661. doi:10.1101/gad.1638008
- Nagan, N., & Zoeller, R. A. (2001). Plasmalogens: biosynthesis and functions. *Progress in lipid research*, 40(3), 199-229.
- Nagura, Y., Tsuno, N. H., Kano, K., Inoue, A., Aoki, J., Hirowatari, Y., . . . Okazaki, H. (2016). Regulation of the lysophosphatidylserine and sphingosine 1-phosphate levels in autologous whole blood by the pre-storage leukocyte reduction. *Transfus Med*. doi:10.1111/tme.12326
- Naureckiene, S., Sleat, D. E., Lackland, H., Fensom, A., Vanier, M. T., Wattiaux, R., . . . Lobel, P. (2000). Identification of HE1 as the second gene of Niemann-Pick C disease. *Science*, 290(5500), 2298-2301. doi:10.1126/science.290.5500.2298
- Ni, G., Li, Z., Liang, K., Wu, T., De Libero, G., & Xia, C. (2014). Synthesis and evaluation of immunostimulant plasmalogen lysophosphatidylethanolamine and analogues for natural killer T cells. *Bioorg Med Chem*, 22(11), 2966-2973. doi:10.1016/j.bmc.2014.04.012
- Pacheco, C. D., Elrick, M. J., & Lieberman, A. P. (2009). Tau deletion exacerbates the phenotype of Niemann-Pick type C mice and implicates autophagy in pathogenesis. *Hum Mol Genet*, 18(5), 956-965. doi:10.1093/hmg/ddn423
- Pacheco, C. D., Kunkel, R., & Lieberman, A. P. (2007). Autophagy in Niemann-Pick C disease is dependent upon Beclin-1 and responsive to lipid trafficking defects. *Hum Mol Genet*, 16(12), 1495-1503. doi:10.1093/hmg/ddm100
- Patterson, M. C., Hendriks, C. J., Walterfang, M., Sedel, F., Vanier, M. T., Wijburg, F., & Group, N.-C. G. W. (2012). Recommendations for the diagnosis and management of Niemann-Pick disease type C: an update. *Mol Genet Metab*, 106(3), 330-344. doi:10.1016/j.ymgme.2012.03.012
- Patterson, M. C., Vecchio, D., Prady, H., Abel, L., & Wraith, J. E. (2007). Miglustat for treatment of Niemann-Pick C disease: a randomised controlled study. *Lancet Neurol*, 6(9), 765-772. doi:10.1016/s1474-4422(07)70194-1
- Pearson, K. (1900). X. On the criterion that a given system of deviations from the probable in the case of a correlated system of variables is such that it can be reasonably supposed to have arisen from random sampling. *The London, Edinburgh, and Dublin Philosophical Magazine and Journal of Science*, 50(302), 157-175.
- Pentchev, P. G. (2004). Niemann-Pick C research from mouse to gene. *Biochim Biophys Acta*, 1685(1-3), 3-7. doi:10.1016/j.bbalip.2004.08.005

- Pentchev, P. G., Boothe, A. D., Kruth, H. S., Weintroub, H., Stivers, J., & Brady, R. O. (1984). A genetic storage disorder in BALB/C mice with a metabolic block in esterification of exogenous cholesterol. *J Biol Chem*, 259(9), 5784-5791.
- Pentchev, P. G., Comly, M. E., Kruth, H. S., Patel, S., Proestel, M., & Weintroub, H. (1986). The cholesterol storage disorder of the mutant BALB/c mouse. A primary genetic lesion closely linked to defective esterification of exogenously derived cholesterol and its relationship to human type C Niemann-Pick disease. *J Biol Chem*, 261(6), 2772-2777.
- Pentchev, P. G., Comly, M. E., Kruth, H. S., Tokoro, T., Butler, J., Sokol, J., . . . Patel, S. (1987). Group C Niemann-Pick disease: faulty regulation of low-density lipoprotein uptake and cholesterol storage in cultured fibroblasts. *FASEB J*, 1(1), 40-45.
- Pentchev, P. G., Comly, M. E., Kruth, H. S., Vanier, M. T., Wenger, D. A., Patel, S., & Brady, R. O. (1985). A defect in cholesterol esterification in Niemann-Pick disease (type C) patients. *Proc Natl Acad Sci U S A*, 82(23), 8247-8251.
- Péterfy, M., Phan, J., Xu, P., & Reue, K. (2001). Lipodystrophy in the fld mouse results from mutation of a new gene encoding a nuclear protein, lipin. *Nat Genet*, 27(1), 121-124. doi:10.1038/83685
- Peterson, T. R., Sengupta, S. S., Harris, T. E., Carmack, A. E., Kang, S. A., Balderas, E., . . . Sabatini, D. M. (2011). mTOR complex 1 regulates lipin 1 localization to control the SREBP pathway. *Cell*, 146(3), 408-420. doi:10.1016/j.cell.2011.06.034
- Pinto, R., Caseiro, C., Lemos, M., Lopes, L., Fontes, A., Ribeiro, H., . . . Sa Miranda, M. C. (2004). Prevalence of lysosomal storage diseases in Portugal. *Eur J Hum Genet*, 12(2), 87-92. doi:10.1038/sj.ejhg.5201044
- Platt, F. M., Wassif, C., Colaco, A., Dardis, A., Lloyd-Evans, E., Bembi, B., & Porter, F. D. (2014). Disorders of cholesterol metabolism and their unanticipated convergent mechanisms of disease. *Annu Rev Genomics Hum Genet*, 15, 173-194. doi:10.1146/annurev-genom-091212-153412
- Radhakrishnan, A., Sun, L.-P., Kwon, H. J., Brown, M. S., & Goldstein, J. L. (2004). Direct binding of cholesterol to the purified membrane region of SCAP: mechanism for a sterol-sensing domain. *Mol Cell*, 15(2), 259-268. doi:10.1016/j.molcel.2004.06.019
- Ravikumar, B., Sarkar, S., Davies, J. E., Futter, M., Garcia-Arencibia, M., Green-Thompson, Z. W., . . . Rubinsztein, D. C. (2010). Regulation of mammalian autophagy in physiology and pathophysiology. *Physiol Rev*, 90(4), 1383-1435. doi:10.1152/physrev.00030.2009
- Sakai, J., Rawson, R. B., Espenshade, P. J., Cheng, D., Seegmiller, A. C., Goldstein, J. L., & Brown, M. S. (1998). Molecular identification of the sterol-regulated luminal protease that cleaves SREBPs and controls lipid composition of animal cells. *Mol Cell*, 2(4), 505-514.
- Sarkar, S. (2013). Regulation of autophagy by mTOR-dependent and mTOR-independent pathways: autophagy dysfunction in neurodegenerative diseases and therapeutic application of autophagy enhancers. *Biochem Soc Trans*, 41(5), 1103-1130. doi:10.1042/bst20130134
- Sarkar, S., Carroll, B., Buganim, Y., Maetzel, D., Ng, A. H. M., Cassady, J. P., . . . Jaenisch, R. (2013). Impaired autophagy in the lipid-storage disorder Niemann-Pick type C1 disease. *Cell Rep*, 5(5), 1302-1315. doi:10.1016/j.celrep.2013.10.042
- Sato, R., Yang, J., Wang, X., Evans, M. J., Ho, Y. K., Goldstein, J. L., & Brown, M. S. (1994). Assignment of the membrane attachment, DNA binding, and transcriptional activation domains of sterol regulatory element-binding protein-1 (SREBP-1). *J Biol Chem*, 269(25), 17267-17273.
- Schneider, E. L., Pentchev, P. G., Hibbert, S. R., Sawitsky, A., & Brady, R. O. (1978). A new form of Niemann-Pick disease characterised by temperature-labile sphingomyelinase. *J Med Genet*, 15(5), 370-374.
- Sechi, A., Dardis, A., Zampieri, S., Rabacchi, C., Zanoni, P., Calandra, S., . . . Bembi, B. (2014). Effects of miglustat treatment in a patient affected by an atypical form of Tangier disease. *Orphanet J Rare Dis*, 9, 143. doi:10.1186/s13023-014-0143-3

- Shimano, H., Horton, J. D., Hammer, R. E., Shimomura, I., Brown, M. S., & Goldstein, J. L. (1996). Overproduction of cholesterol and fatty acids causes massive liver enlargement in transgenic mice expressing truncated SREBP-1a. *J Clin Invest*, 98(7), 1575-1584. doi:10.1172/jci118951
- Singh, R., Kaushik, S., Wang, Y., Xiang, Y., Novak, I., Komatsu, M., . . . Czaja, M. J. (2009). Autophagy regulates lipid metabolism. *Nature*, 458(7242), 1131-1135. doi:10.1038/nature07976
- Sleat, D. E., Wiseman, J. A., El-Banna, M., Price, S. M., Verot, L., Shen, M. M., . . . Lobel, P. (2004). Genetic evidence for nonredundant functional cooperativity between NPC1 and NPC2 in lipid transport. *Proc Natl Acad Sci U S A*, 101(16), 5886-5891. doi:10.1073/pnas.0308456101
- Smulan, L. J., Ding, W., Freinkman, E., Gujja, S., Edwards, Y. J., & Walker, A. K. (2016). Cholesterol-Independent SREBP-1 Maturation Is Linked to ARF1 Inactivation. *Cell Rep*, 16(1), 9-18. doi:10.1016/j.celrep.2016.05.086
- Solomon, D., Winkelman, A. C., Zee, D. S., Gray, L., & Büttner-Ennever, J. (2005). Niemann-Pick type C disease in two affected sisters: ocular motor recordings and brain-stem neuropathology. *Ann N Y Acad Sci*, 1039, 436-445. doi:10.1196/annals.1325.041
- Sovadinova, I., Babica, P., Böke, H., Kumar, E., Wilke, A., Park, J.-S., . . . Upham, B. L. (2015). Phosphatidylcholine Specific PLC-Induced Dysregulation of Gap Junctions, a Robust Cellular Response to Environmental Toxicants, and Prevention by Resveratrol in a Rat Liver Cell Model. *PLoS One*, 10(5), e0124454. doi:10.1371/journal.pone.0124454
- Su, W., Yeku, O., Olepu, S., Genna, A., Park, J. S., Ren, H., . . . Frohman, M. A. (2009). 5-Fluoro-2-indolyl des-chlorohalopemide (FIPI), a phospholipase D pharmacological inhibitor that alters cell spreading and inhibits chemotaxis. *Mol Pharmacol*, 75(3), 437-446. doi:10.1124/mol.108.053298
- Sun, X., Marks, D. L., Park, W. D., Wheatley, C. L., Puri, V., O'Brien, J. F., . . . Snow, K. (2001). Niemann-Pick C variant detection by altered sphingolipid trafficking and correlation with mutations within a specific domain of NPC1. *Am J Hum Genet*, 68(6), 1361-1372. doi:10.1086/320599
- Surmeli-Onay, O., Yakarisik, S., Korkmaz, A., Akcoren, Z., Yuce, A., Runz, H., . . . Yurdakok, M. (2013). Prenatal-onset Niemann-Pick type C disease with nonimmune hydrops fetalis. *Pediatr Neonatol*, 54(5), 344-347. doi:10.1016/j.pedneo.2013.01.015
- Tanaka, J., Nakamura, H., & Mlyawaki, S. (1988). Cerebellar Involvement in Murine Sphingomyelinosis: A New Model of Niemann-Pick Disease. *Journal of Neuropathology & Experimental Neurology*, 47(3), 291-300. doi:10.1097/00005072-198805000-00008
- Tanaka, Y., Yamada, Y., Ishitsuka, Y., Matsuo, M., Shiraishi, K., Wada, K., . . . Irie, T. (2015). Efficacy of 2-Hydroxypropyl- $\beta$ -cyclodextrin in Niemann-Pick Disease Type C Model Mice and Its Pharmacokinetic Analysis in a Patient with the Disease. *Biol Pharm Bull*, 38(6), 844-851. doi:10.1248/bpb.b14-00726
- te Vruchte, D., Lloyd-Evans, E., Veldman, R. J., Neville, D. C., Dwek, R. A., Platt, F. M., . . . Sillence, D. J. (2004). Accumulation of glycosphingolipids in Niemann-Pick C disease disrupts endosomal transport. *J Biol Chem*, 279(25), 26167-26175. doi:10.1074/jbc.M311591200
- Terry, R. D., Sperry, W. M., & Brodoff, B. (1954). Adult lipidosis resembling Niemann-Pick's disease. *Am J Pathol*, 30(2), 263-285.
- Tooze, J., Hollinshead, M., Ludwig, T., Howell, K., Hoflack, B., & Kern, H. (1990). In exocrine pancreas, the basolateral endocytic pathway converges with the autophagic pathway immediately after the early endosome. *J Cell Biol*, 111(2), 329-345.
- Vanier, M. T. (1983). Biochemical studies in Niemann-Pick disease. I. Major sphingolipids of liver and spleen. *Biochim Biophys Acta*, 750(1), 178-184.
- Vanier, M. T. (1999). Lipid changes in Niemann-Pick disease type C brain: personal experience and review of the literature. *Neurochem Res*, 24(4), 481-489.
- Vanier, M. T. (2010). Niemann-Pick disease type C. *Orphanet J Rare Dis*, 5, 16. doi:10.1186/1750-1172-5-16



- Vanier, M. T. (2015). Complex lipid trafficking in Niemann-Pick disease type C. *J Inherit Metab Dis*, 38(1), 187-199. doi:10.1007/s10545-014-9794-4
- Vanier, M. T., Duthel, S., Rodriguez-Lafrasse, C., Pentchev, P., & Carstea, E. D. (1996). Genetic heterogeneity in Niemann-Pick C disease: a study using somatic cell hybridization and linkage analysis. *Am J Hum Genet*, 58(1), 118-125.
- Vanier, M. T., & Latour, P. (2015). Laboratory diagnosis of Niemann-Pick disease type C: the filipin staining test. *Methods Cell Biol*, 126, 357-375. doi:10.1016/bs.mcb.2014.10.028
- Vanier, M. T., & Millat, G. (2003). Niemann-Pick disease type C. *Clin Genet*, 64(4), 269-281.
- Vanier, M. T., Rodriguez-Lafrasse, C., Rousson, R., Mandon, G., Boué, J., Choiset, A., . . . Pentchev, P. G. (1992). Prenatal diagnosis of Niemann-Pick type C disease: current strategy from an experience of 37 pregnancies at risk. *Am J Hum Genet*, 51(1), 111-122.
- Walkley, S. U., & Vanier, M. T. (2009). Secondary lipid accumulation in lysosomal disease. *Biochim Biophys Acta*, 1793(4), 726-736. doi:10.1016/j.bbamcr.2008.11.014
- Walter, M., Davies, J. P., & Ioannou, Y. A. (2003). Telomerase immortalization upregulates Rab9 expression and restores LDL cholesterol egress from Niemann-Pick C1 late endosomes. *J Lipid Res*, 44(2), 243-253. doi:10.1194/jlr.M200230-JLR200
- Wang, K., Xu, R., Schrandt, J., Shah, P., Gong, Y. Z., Preston, C., . . . Mao, C. (2015). Alkaline Ceramidase 3 Deficiency Results in Purkinje Cell Degeneration and Cerebellar Ataxia Due to Dyshomeostasis of Sphingolipids in the Brain. *PLoS Genet*, 11(10), e1005591. doi:10.1371/journal.pgen.1005591
- Wang, X., Sato, R., Brown, M. S., Hua, X., & Goldstein, J. L. (1994). SREBP-1, a membrane-bound transcription factor released by sterol-regulated proteolysis. *Cell*, 77(1), 53-62.
- Wijburg, F. A., Sedel, F., Pineda, M., Hendriksz, C. J., Fahey, M., Walterfang, M., . . . Kolb, S. A. (2012). Development of a suspicion index to aid diagnosis of Niemann-Pick disease type C. *Neurology*, 78(20), 1560-1567. doi:10.1212/WNL.0b013e3182563b82
- Winsor, E. J., & Welch, J. P. (1978). Genetic and demographic aspects of Nova Scotia Niemann-Pick disease (type D). *Am J Hum Genet*, 30(5), 530-538.
- Wortmann, S. B., Vaz, F. M., Gardeitchik, T., Vissers, L. E. L. M., Renkema, G. H., Schuurs-Hoeijmakers, J. H. M., . . . de Brouwer, A. P. M. (2012). Mutations in the phospholipid remodeling gene SERAC1 impair mitochondrial function and intracellular cholesterol trafficking and cause dystonia and deafness. *Nat Genet*, 44(7), 797-802. doi:10.1038/ng.2325
- Wouters, S., De Meirleir, L., Campforts, E., & Lampo, A. (2014). Psychosis in an adolescent girl: a common manifestation in Niemann-Pick Type C disease. *Child Adolesc Psychiatry Ment Health*, 8, 20. doi:10.1186/1753-2000-8-20
- Wraith, J. E., Baumgartner, M. R., Bembi, B., Covanis, A., Levade, T., Mengel, E., . . . Patterson, M. C. (2009). Recommendations on the diagnosis and management of Niemann-Pick disease type C. *Mol Genet Metab*, 98(1-2), 152-165. doi:10.1016/j.ymgme.2009.06.008
- Yang, J., Sato, R., Goldstein, J. L., & Brown, M. S. (1994). Sterol-resistant transcription in CHO cells caused by gene rearrangement that truncates SREBP-2. *Genes Dev*, 8(16), 1910-1919.
- Yang, R., Tan, D., Wang, Y., Ye, J., Han, L., Qiu, W., . . . Zhang, H. (2015). [Three Chinese children with Niemann-Pick disease type C with neonatal cholestasis as initial presentation]. *Zhonghua Er Ke Za Zhi*, 53(1), 57-61.
- Zervas, M., Dobrenis, K., & Walkley, S. U. (2001). Neurons in Niemann-Pick disease type C accumulate gangliosides as well as unesterified cholesterol and undergo dendritic and axonal alterations. *J Neuropathol Exp Neurol*, 60(1), 49-64.
- Zhang, P., Verity, M. A., & Reue, K. (2014). Lipin-1 regulates autophagy clearance and intersects with statin drug effects in skeletal muscle. *Cell Metab*, 20(2), 267-279. doi:10.1016/j.cmet.2014.05.003